ABSTRACT

Title of Thesis: HYDROTHERMALLY ALTERED BASALT AS A SOURCE FOR INDIUM IN ORE DEPOSITS

John Walter Hollingsworth, Master of Science, 2018

Thesis Directed by: Research Scientist Philip Piccoli and Professor Philip Candela
Department of Geology

Indium is an element integral to various emerging technologies. Despite the demand for indium, little is known about its geochemical behavior in hydrothermal systems that generate economic deposits. The aim of this study is to estimate the efficiency with which indium can be removed from basalt during hydrothermal alteration in order to develop better exploration vectors. This can be accomplished by studying how indium partitions between an aqueous solution and the products of hydrothermal alteration. To evaluate the magnitude of this efficiency, two sets of experiments were performed. The first set used a low initial pH, indium+HCl-bearing aqueous solution, whereas the second used a higher initial pH, indium+sulfur-bearing seawater solution. The water/rock mass ratio ranged from 1-10. Experiments were performed at 500°C and 50 MPa for 2-8 weeks. Water/rock was found to have the greatest affect on the partition coefficient of indium between the altered basalt and the aqueous solution.

HYDROTHERMALLY ALTERED BASALT AS A SOURCE FOR INDIUM IN ORE DEPOSITS

by

John Walter Hollingsworth

Thesis submitted to the Faculty of the Graduate School of the
University of Maryland, College Park in partial fulfillment
of the requirements for the degree of
Master of Science
2018

Advisory Committee:
Dr. Philip Piccoli, Chair
Professor Philip Candela
Professor Sarah Penniston-Dorland

© Copyright by John Walter Hollingsworth
2018

Acknowledgments

I would first like to thank my advisors, Dr. Philip Piccoli and Dr. Philip Candela for all of their time and assistance. I greatly appreciate their dedication to developing me as a young scientist. Second, I would like to thank Austin Gion, my lab mate, for all the help and advice he gave me over the past two years. Third, I would like to thank Dr. Sarah Penniston-Dorland for being a member of my committee and discussing various concepts with me. I would also like to thank Dr. James Farquhar for helping me work through the water/rock calculations that are found in the last chapter of my thesis and Phillip Goodling for his help in collecting the seawater. Additionally, I would like to thank my family for all the love and encouragement they provided me throughout my graduate career. Lastly, I acknowledge funding from NSF grant EAR 1348010.

Table of Contents

Acknowledgments ii
Table of Contents iii
List of Figures v
List of Tables vi
List of Abbreviations viii
Overview 1
1. Introduction 2
1.1 Motivation 2
1.2 Background 4
1.3 Aqueous Geochemistry 5
2. Previous Work in Hydrothermal Systems 9
2.1 Hydrothermal Alteration of Basalts 9
2.2 Metal Partitioning in Hydrothermal Systems 10
3. Low Initial pH, HCl-bearing Experiments 14
3.1 Methods 14
3.2 Results: Mineralogy and Geochemistry 20
3.3 Discussion 28
3.4 Conclusions 40
4. High Initial pH, Sulfur-bearing Seawater Experiments 42
4.1 Methods 43
4.2 Mineralogy 45
4.3 Geochemistry 47
4.4 Discussion 55
4.5 Conclusions 63
5. Implications 65
5.1 Application to Mineral Exploration 65
5.2 $\delta^{18}O$ as a Tool for Exploration Potential 68
6. Appendices 81
Appendix A. Methods for Creating Starting HCl-bearing Aqueous Solutions 81
Appendix B. Experimental Conditions for Low Initial pH, HCl-bearing Experiments 82
Appendix C. Method for Calculating Modes 83
Appendix D. Long Valley Moat Basalt Composition 88
Appendix E. Major and Trace Element Data 91
Appendix F. Method 2 Methodology, Results, and Discussion 101
Appendix G. Data Comparison Between Method 1 and Method 2 117
Appendix H. Estimating Volumes of the Interior and Rim 120
Appendix I. EPMA Methodology 120

Appendix J. Experimental Conditions for the High Initial pH, Sulfur-bearing Seawater Experiments 124
Appendix K. Major Element and Indium Concentrations in the High Initial pH, Sulfur-bearing Seawater Experiments 124
Appendix L. Method for Calculating Area of Plagioclase and Altered Glass 132
Appendix M. Mosaics of BSE Images 133
7. References 144

List of Figures

Figure 1. Criticality matrix of various elements 3
Figure 2. World production of indium over the past three decades 3
Figure 3. Configuration of the experimental charge 16
Figure 4. BSE image of the starting basalt 18
Figure 5. Mosaic of BSE images of JH-B4, displaying the strongly altered rim and the weakly altered interior 20
Figure 6. BSE image of an altered olivine 22
Figure 7. Partition coefficients for indium between the altered matrix and aqueous solution in the interior, rim, and the total matrix versus water/rock 33
Figure 8. Matrix/aqueous solution partition coefficients as a function of water/rock 34
Figure 9. Plot of efficiencies of removal for experiments with water/rock = 1 and water/rock = 2 35
Figure 10. Efficiencies of removal calculated using indium data from (1) the interior and the rim of the altered basalt and (2) the rim only 38
Figure 11. Schematic depicting the formation of a volcanogenic massive sulfide deposit 43
Figure 12. A mosaic of BSE images from JH-S1 with plagioclase veins and crystals colored in red 46
Figure 13. ACF diagram for the interior fine-grained altered basaltic glass 48
Figure 14. ACF diagram for the rim fine-grained altered basaltic glass 49
Figure 15. Model of mineralogy versus water/rock during the hydrothermal alteration of basalt by seawater 52
Figure 16. A mosaic of BSE images from experiment JH-S8. 54
Figure 17. Partition coefficients for the altered glass or plagioclase and the aqueous solution 58
Figure 18. $D_{In}^{ag+plag/aqueous}$ for each experiment plotted versus water/rock 59
Figure 19. Efficiencies of removal for the seawater experiments. 60
Figure 20. Efficiency of removal model 66
Figure 21. Calculated scenarios for δ_{rock}^{f} as a function of water/rock 70
Figure 22. Water/rock vs. δ_{rock}^{f} plot for the Corbet deposit 75
Figure 23. Plot of water/rock vs. δ_{rock}^{f} for the Thalanga deposit 77
Figure 24. Plot of water/rock vs. tonnage of various hydrothermal ore deposit types 79
Figure 25. Plot of temperature vs. tonnage of various hydrothermal ore deposit types 80
Figure 26. BSE image of experiment JH-B4 Region E 84
Figure 27. BSE image of experiment JH-B4 Region E after filtering with ImageJ 86
Figure 28. BSE image of experiment JH-B4 Region E after filtering with ImageJ.. 87
Figure 29. BSE image of the groundmass in JH-B4, depicting the grain size of the altered matrix 104
Figure 30. Plot of the partition coefficient of indium between the altered interior matrix and the aqueous fluid calculated using Method 1 and 2 106

List of Tables

Table 1. Experimental conditions for analyzed experiments 16
Table 2. Indium analyses of alteration phases 28
Table 3. Partition coefficients for the interior, rim, and total matrix 33
Table 4. Efficiencies of removal calculated using only the indium data from the rim. 37
Table 5. Independent variables for seawater experiments. 44
Table 6. Average indium concentrations in various regions of the altered basalt 54
Table 7. Partition coefficients calculated for each region in the altered basalt 57
Table 8. Hydrothermal deposits, water/rock, temperatures of formation and estimated tonnages 71
Table 9. Data used for calculating the water/rock of the Corbet and Thalanga deposits 73
Table 10. Mineral fractionation factors used in determining $\Delta_{r\text{-}w}$ 74
Table 11. Experimental conditions for HCl-bearing experiments 82
Table 12. Composition of the starting basalt matrix and phenocrysts 88
Table 13. Major element data for the altered matrices found in the interior and the rim of the experimental run products 91
Table 14. Major element data for talc and smectite alteration products found in experiment JH-B16 98
Table 15. Indium analyses of the interior and rim of the run products 99
Table 16. Comparison of indium concentrations and partition coefficients obtained using Method 1 and 2 105
Table 17. Modal abundance of phenocrysts and matrix regions 106
Table 18. Major and trace element data for Region 1 in the starting basalt and run products 108
Table 19. Major and trace element data for Region 2 in the starting basalt and run products 111
Table 20. Major and trace element data for Region 3 in the starting basalt and run products 114
Table 21. Data comparison for major elements and indium between Methods 1 and 2 117
Table 22. EPMA conditions used for major element and trace element analyses 121
Table 23. Standards used in WDS analyses in the low initial pH, HCl-bearing experiments. 122
Table 24. Standards used in WDS analyses of the altered glass in the high initial pH, sulfur-bearing seawater experiments. 122
Table 25. Standards used in WDS analyses of the plagioclase in the high pH, sulfur-bearing seawater experiments. 123
Table 26. Experimental conditions for seawater experiments 124
Table 27. Composition of the Juan de Fuca MORB 124
Table 28. Major element and indium concentrations in the interior of the altered basaltic glass 125
Table 29. Major element and indium concentrations in the rim of the altered basaltic glass 127

Table 30. Major element and indium concentrations in the plagioclase veins and crystals 130

List of Abbreviations

Abbreviations: low initial pH, HCl-bearing aqueous solution experiments

$D_{In}^{rim/aqueous}$	Partition coefficient of indium between the matrix in the rim and the aqueous solution.
$D_{In}^{int/aqueous}$	Partition coefficient of indium between the matrix in the interior (int) and the aqueous solution.
$D_{In}^{rim+int/aqueous}$	Partition coefficient of indium between the total matrix (both rim and interior) and the aqueous solution. Calculated based on volume proportions of the rim and interior.
$D_{In}^{xl/aqueous}$	Partition coefficient of indium between the phenocrysts (xl) and microphenocrysts and the aqueous solution.
$D_{In}^{rim+int+xl/aqueous}$	Partition coefficient of indium between the entire bulk basalt and the aqueous solution. Calculated based on volume proportions of the rim, interior, and (micro)phenocrysts.

Abbreviations: high initial pH, sulfur-bearing aqueous solution experiments

$D_{In}^{ag/aqueous}$	Partition coefficient of indium between the altered glass (ag) and the aqueous solution.
$D_{In}^{plag/aqueous}$	Partition coefficient of indium between plagioclase and the aqueous solution.
$D_{In}^{ag+plag/aqueous}$	Partition coefficient of indium between the bulk basalt (glass and plagioclase) and the aqueous solution. Calculated based on area proportions of the glass and plagioclase and appropriate Ds.

Overview

This thesis comprises five chapters. The first will focus on introducing the reader to indium, including its demand, its various uses and its known geochemical behavior. The second chapter will discuss hydrothermal alteration of basalts and the geochemical behavior of metals within hydrothermal systems. The next two chapters will discuss two sets of experiments that were performed in order to determine how indium partitions between basalt and aqueous solution during hydrothermal alteration. By understanding how indium partitions in hydrothermal environments, we can better understand how an indium-bearing ore fluid is formed and which phases sequester indium. Phases that sequester indium prevent indium from partitioning into the ore fluid and can therefore be thought as poison in the ore system.

Analytical problems can arise from experimentally stripping indium from natural basalt, as the concentration of indium is much too low to analyze with the electron probe microanalyzer. Analyzing the basalt with LA-ICP-MS would allow us to have lower detection limits, however, it does not give us the same spatial resolution as the EPMA. Lastly, analyzing the final aqueous solution with ICP-MS is problematic because upon termination of a given experiment, the run product is quenched and results in the precipitation of many metastable phases that may contain indium. Therefore, the experiments in this study use aqueous solution that is doped with indium. By doing so, the amount of indium in the system is dramatically increased, such that indium partitioning into the basalt is detectable with the EPMA. The third chapter will discuss the first set of experiments, which consist of the hydrothermal alteration of basalt by a

low initial pH, HCl-bearing aqueous solution in order to examine how indium partitions in highly acidic hydrothermal systems. The fourth chapter describes the second set of experiments, which utilize a high initial pH, sulfur-bearing seawater aqueous solution to hydrothermally alter volcanic glass in order to examine how indium behaves in volcanogenic massive sulfide (VMS) systems. The fifth and last chapter develops the implications of the results of this thesis with further discussion and modeling applications.

1. Introduction

1.1 Motivation

Indium is used in many emerging technologies, including liquid crystal displays (LCD), light-emitting diodes (LED), thin-film solar cell technology, nuclear control rods, and infrared cameras. Despite the widespread use of these emerging technologies, the U.S. Department of Energy classified indium as at near-critical risk based on its importance to alternative energy sources and its supply risk in their 2011 Critical Materials Strategy report (Figure 1). In part, this risk is due a potential supply disruption associated with China's large control of indium production (55.8% of world production) and the increased trade restrictions that have recently been made by China (Silberglitt et al., 2013). Despite the risk of supply disruption, the demand for indium has greatly increased with the advent of various emerging technologies and, consequently, indium production increased by 1000% since 1980 (U.S. Dept. of Energy, 2011) (Figure 2). Due to the increased demand for indium, coupled with the supply risk of indium and its

importance to both alternative energy sources and emerging technologies, it is essential to create new exploration vectors for the discovery and assessment of indium deposits.

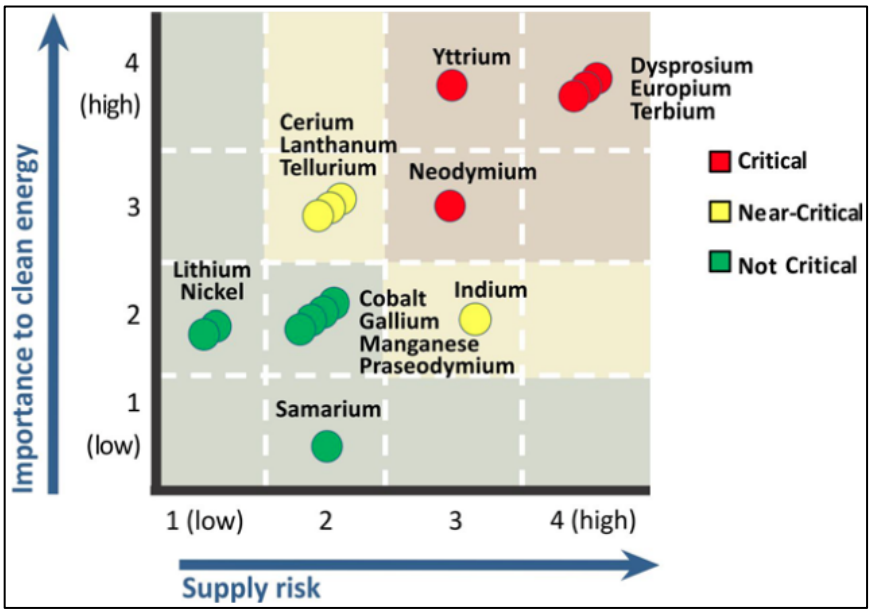

Figure 1. Criticality matrix of various elements from *U.S. D.O.E. 2011 Critical Materials Strategy*.

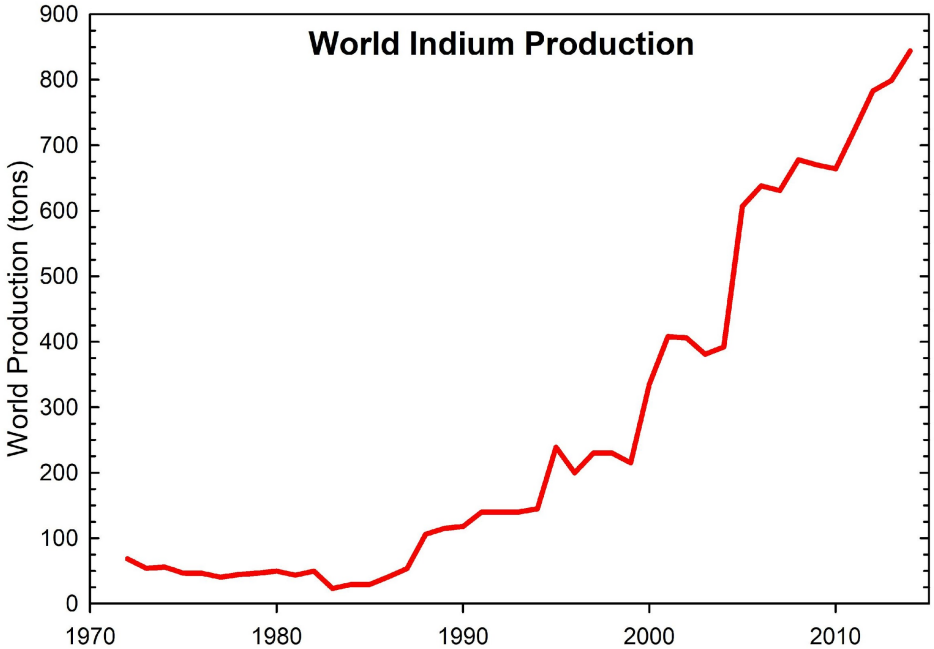

Figure 2. World production of indium over the past three decades (data from Kelly and Mathos, 2014).

1.2 Background

Despite its high demand, not much is understood about the geochemical behavior of indium. Indium is relatively incompatible in mantle melting (McDonough and Sun, 1995; Yi et al., 2000) and is not concentrated above the ppb level in any major earth reservoir. The bulk silicate earth contains ~11 ppb indium, whereas oceanic basalts (both OIBs and MORBs) contain 50-100 ppb indium (McDonough and Sun, 1995; Yi et al., 2000) and the continental crust contains ~52 ppb indium (Rudnick and Gao, 2003). Indium cations have a 3+ oxidation state and an ionic radius ranging from 0.62 Å in tetrahedral coordination to 0.80 Å in octahedral coordination (Shannon, 1976). Consequently, indium frequently substitutes for Fe^{3+}, Fe^{2+}, and Mg^{2+} and preferentially partitions into ferromagnesian phases. Indium concentrations can be, therefore, relatively low in felsic to intermediate rocks, which typically have a low abundance of these phases (Gion et al., 2016; Shaw, 1952; Wager et al., 1958). Indium can also behave as a chalcophile trace element (Hertogen et al., 1980; Shaw, 1952; Wager et al., 1958) and is enriched in sulfide minerals such as sphalerite, chalcopyrite, cassiterite, and stannite. There are no major ore minerals that contain indium as a primary constituent; however, roquesite ($CuInS_2$) forms a solid solution with sphalerite (Cook et al., 2011; Paradis, 2015) but does not commonly occur in high enough abundance to be of economic significance. 95% of indium is mined as a byproduct of zinc mining (Paradis, 2015) given that the technology for indium recovery does not make it economically viable to be mined as the primary product (U.S. Dept. of Energy, 2011). Indium is mostly extracted from volcanogenic massive sulfide (VMS) deposits, epithermal vein-breccia-stockwork

deposits, hydrothermal base metal vein deposits, granite-related Sn-base metal deposits, and skarn deposits (Paradis, 2015; Schwarz-Schampera and Herzig, 1997). In addition, Paradis (2015) and Cook et al. (2009) note that indium appears to be more abundant in higher temperature base-metal deposits, indicating that elevated temperatures may play an important role in indium-bearing ore deposition. Because indium is frequently associated with hydrothermal deposits, it is essential to understand how indium behaves in these systems by identifying the phases that sequester indium and characterizing the conditions that maximize the potential for an indium-bearing ore-forming fluid to form.

1.3 Aqueous Geochemistry

Complexation in aqueous solution is an important, if not essential, aspect of ore formation because it can enhance the solubility of a given mineral. Wood and Samson (1998) note that, "solubility refers to the sum on the concentrations of all dissolved forms of a given metal in a hydrothermal solution in equilibrium with a mineral containing that metal". Therefore, the complexation of metal ions and ligands is essential in order to reach solubilities high enough for ore deposition to occur.

Indium is classified as a hard acid and will tend to complex with hard bases, such as OH^- and F^- (Pearson, 1963). However, indium is geochemically unique from other similar hard acids (i.e. Ga, Ge, Sc) in that soft bases, such as HS^- may also be an important ligand (Wood and Samson, 2006). Additionally, indium contains a full 10 d–electron valence shell, resulting in higher tendency to form covalent bonds with ligands such as Cl^-, which in aqueous solutions are called coordination complexes (Wood and Samson, 1998; Wood and Samson, 2006).

Thermodynamic data reviewed by Wood and Samson (2006) indicate that at 25°C and 1 bar, $In(OH)_3$ will be the dominant aqueous species in near neutral solutions, but at lower pH ranges and when the molality of chloride is close to unity (i.e. $\log a_{Cl^-} \sim 1$), $InCl_3^0$ becomes the dominant species. Seward et al. (2000) note the number of Cl^- bound to indium(III) increases with increasing temperature. At hydrothermal temperatures (350°C), Seward et al. (2000) observed that more than 95% of the indium in an aqueous 0.1-3 M HCl solution complexed with Cl^- to form $InCl_4^-$; however, other studies suggest this aqueous species is relatively unstable and will only complex in high concentrations of chloride (Schufle et al., 1951; Kondziela and Biernat, 1975). Based on these data, indium will mostly complex with Cl^- in an acidic chloride-bearing aqueous solution, whereas indium will mostly complex with OH^-, Cl^-, and may even form polynuclear species (i.e. $InClOH^+$) in alkaline chloride-bearing aqueous solutions (Seward et al., 2000). However, it should be noted that the behavior of indium in aqueous solution is highly variable and is dependent on various physical conditions (Wood and Samson, 2006).

The fact that indium(III) can complex to form multiple chloride species increases the solubility of indium-bearing minerals and permits indium to be mobilized from the altered rock into aqueous solution. For example, if indium silicate ($In_2Si_2O_7$) is placed in an acidic aqueous solution at elevated temperature and pressure, it can result in the formation of quartz + water + aqueous In^{3+} (i.e. $In_2Si_2O_7 + 6H^+_{aq} = 2In^{3+}_{aq} + 2SiO_2 + 3H_2O^0_{aq}$). Two situations can be described, one with chloride and one without chloride, in order to evaluate the effect of chloride on the solubility of indium silicate.

Example 1: Acidic non-chloride bearing aqueous solution

Solubility = $\sum In = [In^{3+}]$

Example 2: Acidic chloride-bearing aqueous solution

Solubility = $\sum In = [In^{3+}] + [InCl^{2+}] + [InCl_2^+] + [InCl_3^0] + [InCl_4^-]$

In both examples, OH^- will complex with indium in negligible quantities because of the high acidity of the aqueous solution. Therefore, in example 1, the only indium-bearing species will be In^{3+}. $[In^{3+}]$ can be calculated by determining the equilibrium constant (K):

$$K = \frac{\left(a_{In3+}^{aq}\right)^2 \left(f_{H2O}^{aq}\right)^3}{\left(a_{H+}^{aq}\right)^6} \quad (1)$$

where a is activity and f_{H2O} is the fugacity of water. Here, we can assume the indium silicate and silica are pure phases and their activity ~1. The concentration of In^{3+} can then be found by the equation:

$$(a_{In3+}^{aq})^2 = (\gamma_{In3+}^{aq})^2 [In^{3+}]^2 \quad (2)$$

where γ is the activity coefficient. In Example 2, Cl^- is a readily available ligand, which will complex with indium to form various indium-chloride species (i.e. $InCl^{2+}$, $InCl_2^+$, $InCl_3^0$, $InCl_4^-$). Assuming pH, the activity of SiO_2, and fugacity of H_2O are constant between example 1 and 2, $[In^{3+}]$ will also be constant. Consequently, the additional complexing of indium with chloride will increase the concentration of indium in the aqueous solution, thereby increasing the solubility of indium silicate. Unfortunately, there are no thermodynamic data on indium silicates to quantify this solubility. Despite the lack of data, this example is simply meant to aid in the conceptualization and qualification of

the effect of metal-ligand complexation on mineral solubility and the mobilization of metals, such as indium, into aqueous solution.

2. Previous Work in Hydrothermal Systems

2.1 Hydrothermal Alteration of Basalts

Most previous experimental studies on the hydrothermal alteration of basalt focus on hydrothermal seawater-basalt interactions because they occur ubiquitously on the ocean floor at convergent and divergent boundaries. The exchange of Mg^{2+} in seawater for Ca^{2+} in the basalt is one of the most significant reactions and involves the formation of chlorite from the alteration of Ca-rich clinopyroxene and volcanic glass (Hajash, 1975; Mottl, 1983; Mottl and Holland, 1978; Nakamura et al., 2007; Seyfried and Bischoff, 1977; Seyfried and Mottl, 1982). High-temperature hydrothermal alteration (>300°C) of basalt results in greenschist facies-type alteration (albite + chlorite + epidote + actinolite-tremolite); the reacting aqueous fluid becomes more reduced and acidic with increased concentrations of Ca^{2+}, Si^{4+}, K^{+}, and base metals, decreased Mg^{+}, SO_4^{2-}, and (at water/rock ratios (W/R; mass of aqueous solution/mass of rock) > 5) Na^{+} (Bischoff and Dickerson, 1975; Hajash, 1975; Humphris and Thompson, 1978a; James et al., 2003; Mottl, 1983; Mottl and Holland, 1978; Nakamura et al., 2007; Seyfried and Bischoff, 1977).

The degree of alteration in high-temperature (>300°C) hydrothermal systems is affected by water/rock (Mottl and Holland, 1978). Hydrothermal alteration of basalts by seawater can generally be divided into two categories: chlorite-rich and epidote-rich. Epidote can form when Ca^{2+} is released upon the albitization of plagioclase and the alteration of pyroxene and volcanic glass. However, because Ca^{2+} is the primary cation

that is exchanged for Mg^{2+} in the seawater, Ca^{2+} will be depleted at higher water/rock, which will result in the formation of chlorite. In a series of experiments, Mottl (1983) quantified this relationship between water/rock and chlorite- vs. epidote-rich hydrothermal alteration. When water/rock < 10, the altered basalts were actinolite + epidote-rich and chlorite + quartz-poor. Alternatively, when water/rock > 10, the altered basalts tended to be chlorite + quartz-rich and actinolite + epidote-poor. These experimental data have been supported by observations made in the field. For example, Shikazono et al. (1995) noted that epidote formed in the Furutobe district of the Kuroko mine, Japan at water/rock < 2, whereas chlorite formed at water/rock as high as 40. Additionally, Seyfried et al. (1978) noticed that plagioclase + olivine, found within ocean floor spilites, was altered to actinolite + quartz in the interior of the rock, whereas it was altered to chlorite + epidote in the rim. Because the rim of the spilite interacts with a larger proportion of the hydrothermal fluid than the interior, it effectively has a higher water/rock (also known as effective water/rock ratio) and is therefore altered to an assemblage associated with higher water/rock ratios (i.e. has abundant chlorite).

2.2 Metal Partitioning in Hydrothermal Systems

Various experimental and field studies have focused on the behavior of metals during the hydrothermal alteration of basalts. Base metals, such as Cu, Zn, Fe, and Mn, in aqueous solution increase in concentration with increasing temperature (Hajash, 1975; Humphris and Thompson, 1978b; Mottl et al., 1979; Seewald and Seyfried, 1990; Seyfried and Janecky, 1985; Wolery, 1978), indicating these metals partition from their primary phases into the aqueous solution. Other metals, such as Al, V, Ti, and Cr, are

typically immobile in hydrothermal systems (Berger et al., 1987; Hajash, 1975; Humphris and Thompson, 1978b; MacLean and Kranidiotis, 1987; Reed, 1983; Seyfried and Bischoff, 1977; Staudigel and Hart, 1983; Wolery, 1978) and do not readily partition into aqueous solution. However, it is not always straightforward to determine which metals will partition into aqueous solution within a given system. For example, Nakamura et al. (2007) examined rocks at the SW Indian Ridge in the Indian Ocean and noticed that Mn and Zn were enriched in the basalt, whereas Cr, Co, and Ni were depleted due to the hydrothermal breakdown of clinopyroxene, olivine, and spinel. The Mn-enrichment in the basalt was likely due to the formation of chlorite at this location. Therefore, whether or not metals will partition into the aqueous solution is related to the physical conditions of the hydrothermal system (i.e. temperature, pressure, acidity, etc.) and the phases in which they are hosted. Phases that do not breakdown readily and form secondary phases will retain their initial chemistry, whereas phases that do breakdown easily will release their metals into aqueous solution.

However, as in cases such as the SW Indian Ridge example described above, the formation of secondary minerals can sequester metals released upon the destruction of the primary phases. For example, Humphris and Thompson (1978b) plotted metal concentration versus H_2O in hydrothermally altered oceanic basalts in order to examine metal behavior. They found that metals, such as Fe, Mn, Ni, Co, and Cu partitioned into solution (i.e. released from their primary phase) within submarine hydrothermal systems. Yet, other than Cu and Mn, all other metals partitioned into secondary phases in the rim of the altered basalt. Therefore, Fe, Ni, and Co were not removed efficiently from the basalt and were consequently unavailable to a potential ore-forming fluid. Thus, in order

to understand the potential of a metal to partition into an ore-forming fluid via hydrothermal alteration, it is important to evaluate the alteration phases that sequester it.

Increases in pressure tend to decrease the partitioning of metals into aqueous solution, whereas, increases in temperature tend to increase metal the partitioning (Hajash, 1975; Hemley and Hunt, 1992; Humphris and Thompson, 1978b; Mottl et al., 1979; Nakamura et al., 2007; Seewald and Seyfried, 1990; Seyfried and Janecky, 1985; Wolery, 1978) (Note: a few of these papers incorrectly used the phrase 'metal solubility', which is only correct if a metal phase, such as pure Cu, exists in a system. If the metal is hosted within a mineral phase, you may either discuss the mineral solubility or the partitioning of the metal from one phase into another, which is related to the mineral solubility). At temperatures >350°C, increases in temperature and decreases in pressure help to lower fluid pressure, which in turn lowers the pH of the fluid (Seyfried and Janecky, 1985). Consequently, acidity is perhaps the primary factor in the partitioning of metals from a primary phase into the aqueous solution.

In the hydrothermal alteration of basalt by seawater, acidic conditions must be generated in order to efficiently partition metals into hydrothermal seawater solutions. This can be accomplished through Mg-hydrolysis, which results in the generation of H^+ and the formation of a hydrated mineral, such as Mg-smectite or chlorite (Seyfried and Janecky, 1985). For example, $2FeMgSi_2O_6 + 2Mg^{2+} + 6H_2O = Mg_4Fe_2Si_4O_{10}(OH)_8 + 4H^+$. However, H^+ is also consumed in silicate hydrolysis reactions, such as talc production from enstatite alteration: $4MgSiO_3 + 2H^+ = Mg_3Si_4O_{10}(OH)_2 + Mg^{2+}$. That is, there are two competing sets of reactions affecting the concentration of H^+ in the reacting seawater (Bischoff and Dickson, 1975; Mottl and Seyfried, 1980; Mottl, 1983; Reed,

1983; Seyfried and Bischoff, 1977; Seyfried and Mottl, 1982). Once Mg^{2+} in the seawater has been reduced to levels wherein aqueous magnesium concentrations are controlled by the aqueous solubility of mineral phases, Mg-hydrolysis ceases. Silicate hydrolysis may continue to consume the H^+ such that the acidic conditions are not maintained. Therefore, water/rock can influence the acidity because as water/rock increases, more Mg^{2+} is available for Mg-hydrolysis. The water/rock at which the system is able to produce more H^+ than is consumed is at the transition between rock- and water-dominated systems. This transition occurs around water/rock $\geq 50 \pm 5$ and involves the removal of Mg^{2+} from seawater to levels controlled by mineral solubility (Bischoff and Dickson, 1975; Mottl and Seyfried, 1980; Mottl, 1983; Seyfried and Bischoff, 1977; Seyfried and Mottl, 1982). Once water/rock is high enough such that the system becomes water-dominated, acidic conditions can be maintained. Basalts in submarine water-dominated systems (water/rock > 50) have lower concentrations of metals, such as Fe, Mn, and Zn, than in rock-dominated systems (water/rock < 50) (Mottl and Seyfried, 1980; Seyfried and Mottl, 1982; Seyfried et al., 1978), thus indicating that water-dominated systems remove metals more efficiently from the source rock.

3. Low Initial pH, HCl-bearing Experiments

The purpose of the experiments performed in this chapter of this study is to examine the geochemical behavior of indium under acidic hydrothermal conditions. Certain ore deposits, such as epithermal, Cu-porphyry, VMS, and iron oxide copper-gold (IOCG), can exhibit advanced argillic alteration. Advanced argillic alteration is characterized by extremely low pH and may range significantly in the concentration or fugacity of sulfur. Deposits low in sulfur are mostly associated with metals that complex readily with chloride, whereas deposits high in sulfur are associated with metals that readily complex with sulfur (Kreiner and Barton, 2017). Because indium may readily complex with either chloride or sulfur, these experiments are designed to gain insights into how indium partitions in highly acidic environments.

3.1 Methods

Experimental Design

Each experiment consisted of an experimental charge loaded into a René 41 cold-seal pressure vessel, which was subsequently placed into a near-horizontal furnace inclined at 8°. The experimental charge included an aqueous solution containing 0.1 M or 1 M HCl + indium ± 0.5 M NaCl ± 0.5 M KCl (see Appendix A for methods involving making the starting aqueous solution) and an approximately equant ~4 mm diameter piece of basalt sealed within a 5 mm outer diameter platinum capsule with a 0.15 mm wall thickness, which was about 1.8 cm in length (Figure 3). Starting aqueous solutions had a pH of about 0-1 at 25°C. Initial indium concentrations varied between 345 ± 0.5

and 503 ± 0.5 ppm (as measured by ICP-MS) depending on the aqueous solution used in a given experiment. Water/rock ratios were 1-3, which are consistent with values suggested for subaerial geothermal systems, although regions of the oceanic crust can attain water/rock well over 100 (Mottl and Holland, 1978; Mottl 1983; Schardt et al., 2006). Experimental charges were then placed in an oven at ~150°C in order to ensure the charge was properly sealed prior to being placed in a furnace (Table 1, Appendix B). Experiments were performed at 500°C and 50 MPa. In part, this was by design to remove the variability of temperature and its effect on mineral solubility and the variation of mineral-aqueous solution partition coefficients. Neutral pH at 500°C and 50 MPa is ~8 (Barnes, 2015), whereas the pH of the 1 M HCl-bearing aqueous solution at this temperature and pressure was less than 4 (Johnson et al., 1992).

Run times varied between 2 and 8 weeks, upon which the experiments were quenched. After which, the experimental charges were removed from the René 41 cold-seal vessels and weighed. Many experiments either gained or lost mass. This change in mass was caused by aqueous solution entering or leaving the experimental charge through a rupture in the Pt capsule. This rupture most likely occurs at one of two times: (1) when the system undergoes an increase in pressure or (2) when the system is quenched and pressure rapidly drops. Thus far, there is no reason to suspect the former in any of the analyzed experiments reported in this study because indium was found in concentrations above the detection limit within the altered basalt in every case. The timing is important because if the capsule ruptured, the indium-bearing solution would be flushed from the capsule and strongly diluted by the water used to pressurize the René 41 vessel.

Table 1. Experimental conditions for analyzed experiments. Experiments with solutions that contained added chlorides contained 345 ± 0.5 ppm In, whereas other experiments listed contained 368 ± 0.5 ppm In.

	Time (weeks)	W/R	HCl (M)	NaCl + KCl (M)	NaCl wt% eq.	In (ppm) in solution
JH-B1	2	1	1	0	3.6%	368
JH-B2	2	2	1	0	3.6%	368
JH-B4	2	2	1	0	3.6%	368
JH-B6	2	2	1	0.5+0.5 M	10.5%	345
JH-B7	2	1	1	0.5+0.5 M	10.5%	345
JH-B8	4	1	1	0	3.6%	368
JH-B9	4	2	1	0	3.6%	368
JH-B10	4	1	1	0.5+0.5 M	10.5%	345

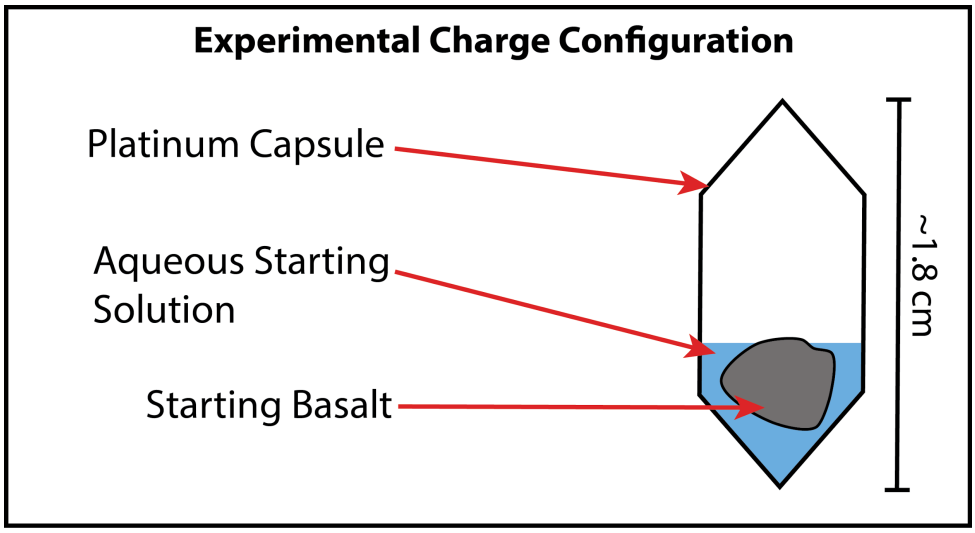

Figure 3. Configuration of the experimental charge, where aqueous solution and rounded fresh basalt are sealed within a Pt capsule.

Starting Basalt

The basalt used in this study is from one of the eight pyroclastic units, which, along with 26 lava flows, constitute the moat basalt sequence in Long Valley, California (Eichelberger et al., 1988). Phenocryst contents range from 11.7% to completely aphyric with an average phenocryst content of ~2.5% (Vogel et al., 1994). Backscatter electron (BSE) images of the starting basalt groundmass (altered matrix + microphenocrysts)

reveal plagioclase, olivine, and pyroxene microphenocrysts. Microphenocrysts are by definition smaller than phenocrysts but larger than the grains that make up the matrix (i.e. the rest of the groundmass) (Barker, 1983). ImageJ was used to determine that the modal proportion of microphenocrysts and phenocrysts is ~35 ± 4% (see Appendix C for procedure). Additionally, the volcanic matrix exhibits a herringbone pattern with three noticeably distinct regions (Figure 4). Region 1 is interpreted to be volcanic glass, which is characterized by relatively low concentrations of FeO (5.5 wt%) and relatively high concentrations of Na_2O (~4.7 wt%), K_2O (3.5 wt%), and SiO_2 (58.4 wt%). Region 2 is interpreted to be small, elongate grains of pyroxene, which have an Mg# of 49 ± 2.3. Given that these grains are the same size as the grains that make up the matrix, they are not considered microphenocrysts. Lastly, Region 3 is characterized by small (<1 μm) light grains (in BSE) with high concentrations of FeO and typically forms on the grain boundaries of microphenocrysts. It is difficult to characterize this phase by its chemical composition due to its small size. Given that these small grains are smaller than the beam of the electron probe microanalyzer (EPMA) (1 μm), other regions in the matrix are clipped, which means the wavelength dispersive spectroscopy (WDS) data on this region are not entirely accurate.

The unaltered matrix consists mostly of Regions 1 and 2 with low (<1 %) abundance of Region 3. Mineral phases present include abundant plagioclase microphenocrysts (~An_{68}), variable amounts of olivine (Fo# = 81.5 ± 0.6) and augite (Mg# = 77.9 ± 0.4) microphenocrysts, minor chromium spinel (typically hosted within olivine microphenocrysts), and trace occurrences of barite. Major oxide and trace element data for these phases and the matrix were collected by using WDS via EPMA and are

listed in Appendix D. Lastly, ImageJ was utilized in order to determine the modal abundances of these regions (see Appendix C for methods involving the calculation of modes), which was used in order to determine if the modal proportions changed after alteration occurred.

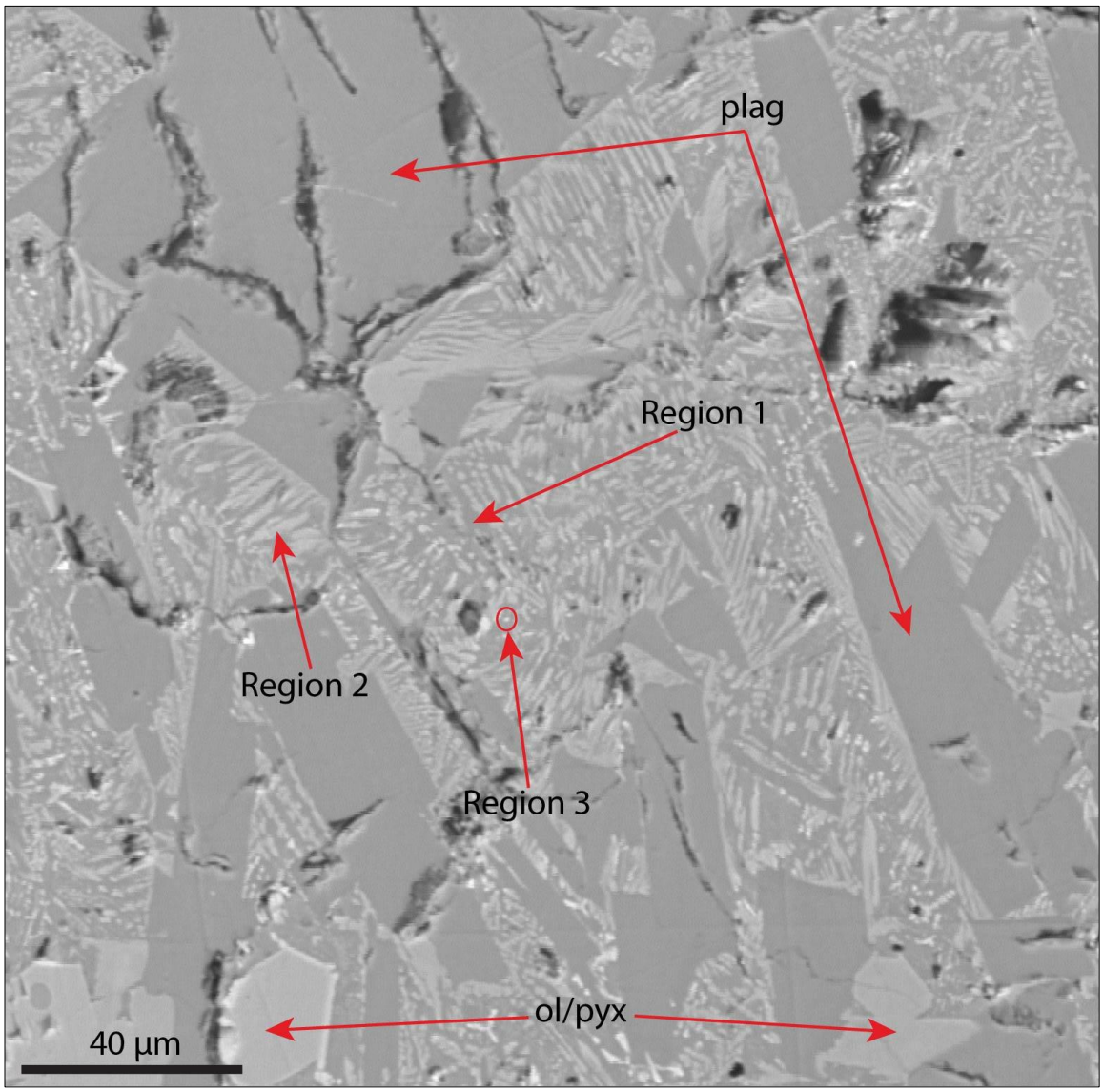

Figure 4. BSE image of the starting basalt with phenocrysts/microphenocrysts and matrix regions labeled. Region 3 can be identified as very bright, small grains in the image.

Analytical Methods

Upon quench, the altered basalt run products were removed from the capsule and mounted in epoxy and subsequently polished for EPMA use. Samples JH-B1 through JH-B10 were analyzed using energy dispersive spectrometry (EDS) and BSE images were collected in order to aid in the determination of alteration phases. Additionally, major element and indium concentrations were determined by using wavelength dispersive spectrometry (WDS) (See Appendix I for more information). The beam size for WDS analyses was 10 μm.

Given that each of the three regions in the starting basalt are characterized by grain sizes smaller than 2 μm, the analyses collected with this method represent a sampling of the bulk composition of these three regions within the altered matrix. Each data point was scrutinized in the following ways: First, in order to filter out regions that were not part of the altered matrix (i.e. microphenocrysts such as plagioclase), qualitative EDS analyses were performed. Regions that contained Ca, Al, Si, Mg, K, and Fe were considered to be potential regions of altered matrix simply because they could not only be pyroxene, olivine, or plagioclase. After WDS quantitative data was collected, mineral formulas were calculated in order to determine whether or not the data point resembled a mineral formula of a single microphenocryst phase. Because the altered matrix comprised fine-grained (~1-2 μm) alteration phases, a 10 μm beam should not record a composition consistent with a mineral formula for only one phase. Any analyses that had a formula consistent with a microphenocryst phase were subsequently disregarded in the analysis of the data.

3.2 Results: Mineralogy and Geochemistry

Microphenocryst Mineralogy

All run products displayed two domains: (1) a weakly altered interior and (2) a strongly altered rim (Figure 5). The degree of alteration displayed in these two domains is a function of the interaction of the basalt with the aqueous solution. Consequently, the rim of the basalt has a high effective water/rock. On the other hand, the interior has a low effective water/rock because the aqueous solution can only reach the interior of the basalt by transport via grain boundaries, vesicles, fractures, etc. Differences in the effective water/rock result in different alteration mineralogies.

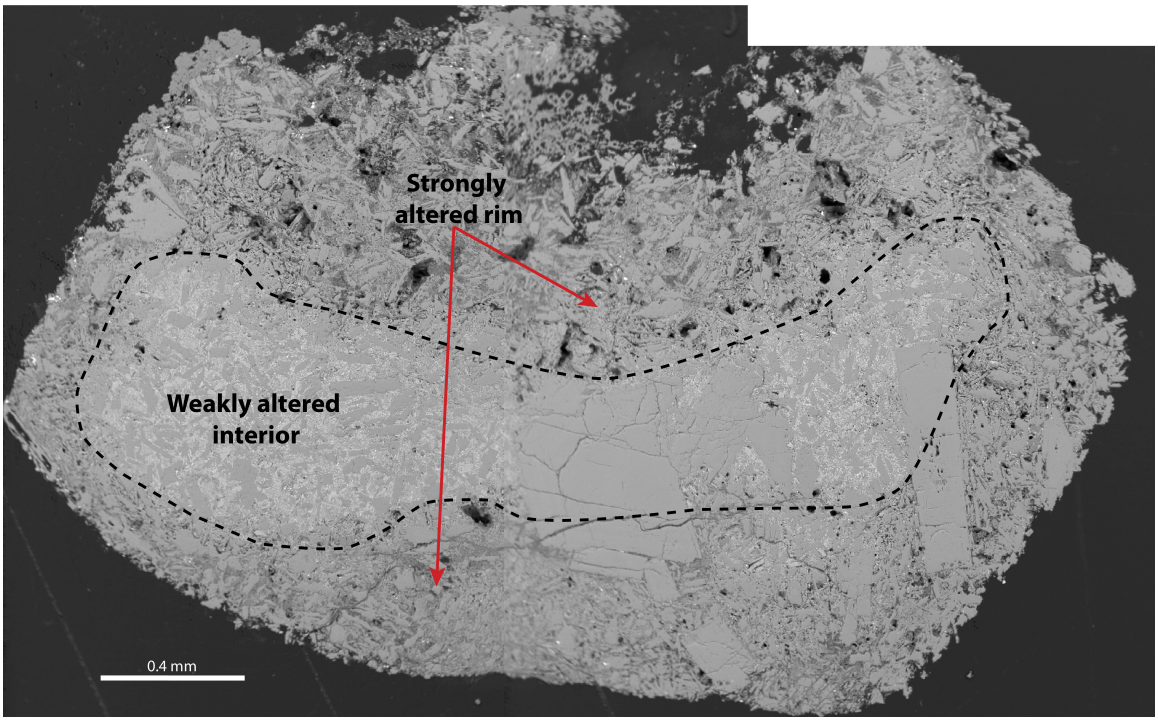

Figure 5. Mosaic of BSE images of JH-B4, displaying the strongly altered rim and the weakly altered interior.

Olivine was readily altered in all experiments and typically was most altered along grain boundaries and fractures (Figure 6). The alteration along the grain boundaries

and fractures is characterized by the growth of magnetite and talc. This can be expressed by the serpentinization of olivine to form serpentine and magnetite, subsequently followed by the alteration of serpentine to form talc, i.e.:

$$10Fe_{0.33}Mg_{1.67}SiO_4 + 8H_2O + 4H^+_{(aq)} + ½O_{2\,(aq)},$$

$$\rightarrow Fe_3O_4 + 5Mg_3Si_2O_5(OH)_4 + 0.33Fe^{2+}_{(aq)} + 1.67Mg^{2+}_{(aq)}$$

and

$$Mg_3Si_2O_5(OH)_4 + 2SiO_2 \rightarrow Mg_3Si_4O_{10}(OH)_2 + H_2O.$$

The aqueous silica is sourced from the alteration of crystalline material and volcanic glass. The fact that talc is present in these experiments and serpentine is not indicates that silica concentrations in the aqueous solution are high enough such that serpentine is not stable. Results of 4 WDS analyses are consistent with talc having high FeO wt% (~5%), which may be due to the analysis interacting with fine-grained magnetite in the surrounding area. Distinct grains of olivine were not identified in the strongly altered rim except for large phenocrysts that are almost completely altered. Additionally, in the weakly altered interior of experiment JH-B16, entire phenocrysts of olivine were completely altered to talc. This is likely due to the long run time of the experiment and the relatively high water/rock (run time = 4 weeks and water/rock = 3). In short, olivine does not persist for very long in this acidic, high-temperature hydrothermal environment. The fact that secondary magnetite also disappears in the strongly altered rim indicates that it too is an ephemeral phase, meaning that if experiments ran to a time of infinity, there would be little to no olivine and magnetite. Similarly, augite persists in the weakly altered interior but its decreased abundance/disappearance in the strongly altered rim may

suggest it is not stable in regions of high degrees of alteration and/or regions with high effective water/rock.

Plagioclase microphenocrysts altered along grain boundaries, especially in the strongly altered rim of the basalt, but were otherwise unaltered. Chromite was highly resistant to alteration and maintained its euhedral grain boundaries in all experiments with rare exception. One of the chromite grains in JH-B17 (run time = 8 weeks) appeared to be slightly altered. This could indicate that eventually chromite would break down but in the course of these experiments, chromite should be considered unaltered.

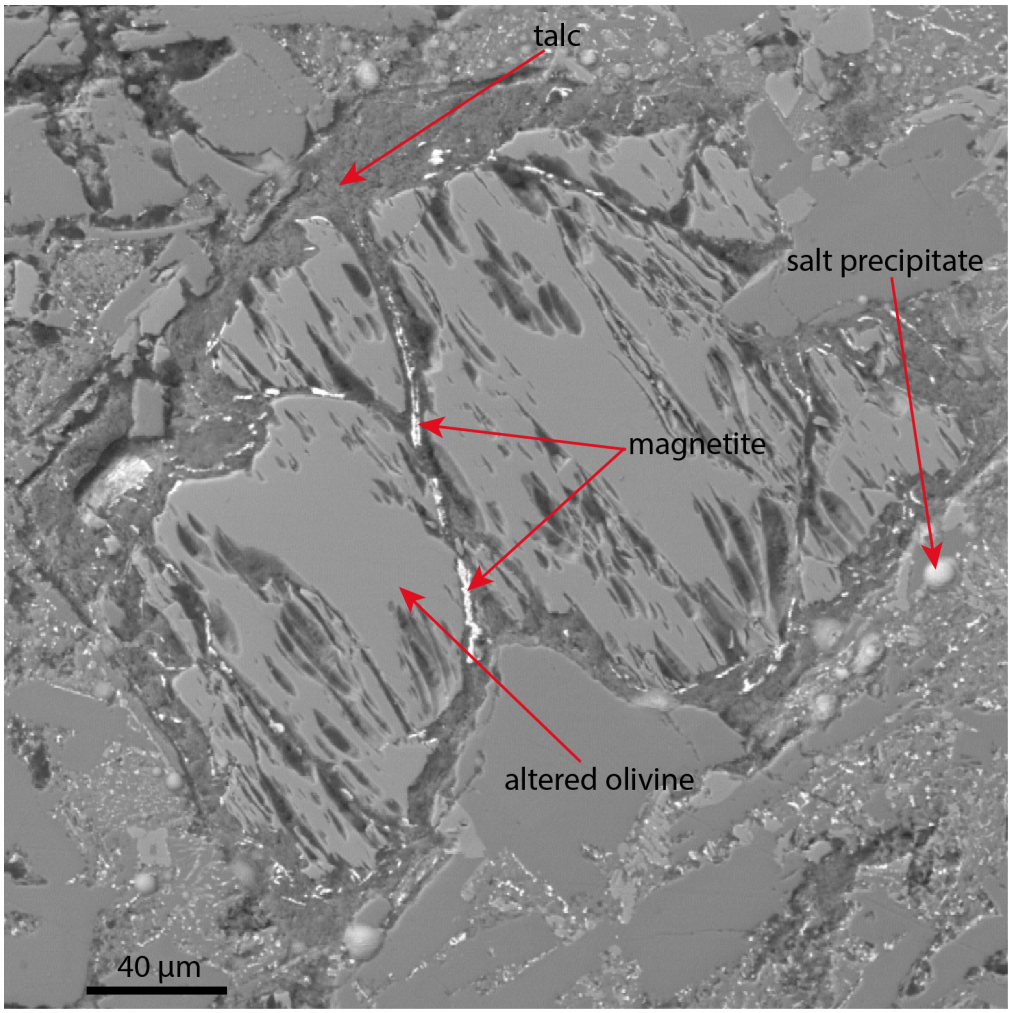

Figure 6. BSE image of an olivine microphenocryst altered along grain boundaries and fractures to form magnetite and talc within experiment JH-B4.

Chlorine-rich apatite formed in several experiments and tends to be in higher abundance in the higher water/rock experiments. The apatite likely incorporated Cl^- from the aqueous solution, CaO from the breakdown of augite, and P_2O_5 from the altered glass. Apatite was only found on the outside of the strongly altered rim, which is consistent with CaO and P_2O_5 diffusing down their concentration gradient into the aqueous solution on the exterior of the basalt. The apatite then formed when a change in pH, temperature, or pressure occurred, most likely upon quench. Similarly, thin, long (<60 μm) ilmenite grains were found on the outside rim of experiments (JH-B14, JH-B15, and JH-B17). Additionally, JH-B17 contained anhedral ilmenite grains in pore spaces of the altered basalt. This likely indicates that ilmenite formed in the aqueous solution both outside and inside of the basalt. This in turn suggests that TiO_2 and FeO were leached from the groundmass into aqueous solution in both the interior and rim of the basalt.

A smectite-like mineral forms as thin, platy crystals along the outside rim of the altered basalt, where there is a higher degree of water-rock interaction, and contains variable amounts of SiO_2, MgO, Al_2O_3, MgO, FeO, and CaO with low totals (Appendix E, Table 14). Due to low and variable totals, which are likely due to the small grain size and the fact that the samples do not polish well, this mineral is difficult to positively identify. Assuming we are not analyzing adjacent phases, the chemistry is consistent with a smectite mineral and will henceforth be discussed as smectite. Mottl and Holland (1978) found that metastable Mg-smectite formed in their experiments instead of chlorite and attributed this to issues with kinetics. Although smectite formed instead of chlorite, the authors note that the solution chemistry responded similarly to natural systems (Mottl,

1983). Therefore, it is possible that the smectite formed in this study may have formed chlorite under natural conditions.

Smectite appears to be slightly more abundant in the experiments with longer run times and those at higher water/rock. Due to these factors, the basalt experiences higher degrees of alteration and allows more Mg mobilization to occur, thus allowing for the potential for smectite to form. The altered basalt in these experiments should be smectite/chlorite-poor due to the low water/rock of these experiments and the fact that seawater is not used in these experiments, which adds Mg to the system. Consequently, smectite forms in low abundance in these experiments and mostly forms along the outside rim, where the effective water/rock is the highest. Lastly, quartz was present in experiments along the outside of the basalt and within vesicles throughout the basalt. In one instance it appeared as if an olivine/pyroxene phenocryst was entirely replaced by quartz. The presence of talc and the lack of serpentine is consistent with appreciable amounts of SiO_2 being mobilized within the rock, i.e. $Mg_3Si_2O_5(OH)_4 + 2SiO_2 \rightarrow Mg_3Si_4O_{10}(OH)_4 + H_2O$, whereas the presence of quartz outside of the basalt may indicate that some precipitated upon quench.

Altered Matrix Mineralogy and Geochemistry

Analyzing the mineralogy and major element chemistry within the altered volcanic matrix was a complicated task for multiple reasons. First, like the starting matrix, the altered matrix had three regions of varying chemical composition (Figure 4). Region 1 represents the altered volcanic glass and may even be palagonite, which is metastable hydrated basaltic glass (Wolery, 1978). Across all analyzed experiments, there

was no consistent trend for any major oxides in Region 1. This may suggest that the volcanic glass is altering to form a fine-grained mineralogy that is highly variable in composition across the altered matrix. Region 1 became more abundant in the altered basalt (61.2 ± 2.4 modal%) when compared to Region 1 in the starting basalt. Region 2 appears to grow larger in grain size and become more rounded than elongate when compared to the starting basalt but also decrease in modal abundance (35.7 ± 1.7 modal%). Grains in Region 2 are still interpreted to be pyroxenes with an Mg# of 47 ± 3 between analyzed experiments. Region 3 exhibits small (<1 μm) grains, however, they are slightly larger and more abundant in the run products by about a factor of 2 (3.1 ± 0.4 modal%). Additionally, Region 2 remains FeO- and TiO_2-rich but is typically less enriched in FeO but more enriched in TiO_2 compared to the starting Region 3. All three regions are present in the weakly altered interior. However, in the strongly altered rims, sometimes only Region 1 persists. This suggests that Region 2 is unstable at higher effective water/rock.

Second, the presence of microphenocrysts makes it challenging to analyze the altered matrix exclusively. Zeng et al. (2014) recognized that plagioclase microphenocrysts alter to different phases and at different rates than volcanic glass. The authors identified up to four types of alteration in the volcanic glass and five in the plagioclase microphenocrysts. In this work, the phases in the groundmass alter at different rates and by different mechanisms, which has made it difficult to determine the regions that only comprise the altered matrix.

Third, analytical totals were variable and often low in the strongly altered rim. The low totals likely reflect the prevalence of hydrated minerals, which do not polish

well, and increased pore space due to extensive alteration. As a result of the large range of analytical totals, it has been difficult to determine the mineralogy of the altered matrix within the rim. In order to determine the mineralogy of the rim, x-ray diffraction (XRD) analyses were completed at the University of Maryland, College Park at the X-ray Crystallographic Center. However, these analyses did not yield any useful insights into the matrix mineralogy. Two phases that may be good candidates for making up the altered matrix are talc and smectite. They are both stable in these experiments and have been identified elsewhere in the altered basalt. Due to the variability of the chemical analyses of the matrix, it is hard to generalize how the chemical composition changes with degree of alteration, where the starting basalt is unaltered, the interior is less altered, and the rim is the most altered. The only evident change is as degree of alteration increases is the standard deviations of the data get larger.

Indium

Altered matrix: All analyzed run products (JH-B1 to JH-B10) have regions within the altered matrix that contain indium concentrations above the detection limit (25 ppm) (Appendix E). In the experiments performed in this study, water/rock was found to have the greatest influence on the concentration of indium in the altered matrix. The altered matrices within experiments that had a water/rock = 1 had mean indium concentrations ranging from 30 to 140 ppm (three of the four experiments had mean concentrations above 105 ppm). On the other hand, the altered matrices within experiments that had a water/rock = 2 had mean indium concentrations ranging from 31 to 83 ppm. Additionally, indium concentrations within the weakly altered interior matrix differed from the strongly

altered rim matrix. The concentrations within the rim tended to have a much larger range than in the interior, suggesting there might be more heterogeneity in the rim than the interior, which could be influenced by the mineralogy in the rim. Nonetheless, indium concentrations throughout the entire altered matrix are highly heterogeneous and may be related to the ability of the aqueous solution to reach certain locations within the basalt.

Alteration Phases: Some of the alteration products other than the altered matrix contained indium in concentrations above the detection limit (Table 2). Indium concentrations in smectite were analyzed in experiments JH-B16 and JH-B17. Smectite analyses yielded indium concentrations below detection in experiment JH-B16, whereas in JH-B17 indium concentrations ranged from 40-199 ppm (average 112 ppm). Talc was analyzed in experiment JH-B16 and indium concentrations ranged from 48 to 155 ppm. When indium partitions into talc, it is likely that In^{3+} is substituting for Mg^{2+}, for example:

$$2In^{3+} + Mg_3Si_4O_{10}(OH)_2 \rightarrow \square In_2Si_4O_{10}(OH)_2 + 3Mg^{2+}$$

Therefore, smectite and talc could be important sources of indium sequestration if abundant. Additionally, two ilmenite analyses in experiment JH-B17 yielded indium concentrations of below detection and 56 ppm. Indium concentrations within apatite were below the detection limit. Ephemeral phases, such as magnetite, were not analyzed because they are not long-term sources of indium sequestration. All other crystalline phenocryst phases present in the starting basalt (i.e. olivine, plagioclase, pyroxene, etc.) had indium concentrations below the detection limit.

Table 2. Indium analyses of alteration phases. For analyses with indium concentrations below detection (bd), rather than quantify the analyses at 0 ppm or at 25 ppm, I chose the midpoint (12.5 ppm). From this point on, all indium concentrations below detection will be set to half the detection limit. Uncertainty of a given analysis represents the analytical error. SD is the standard deviation of the mean (1σ) of the concentrations in a given experiment.

Mineral	Experiment	In (ppm)
Smectite	JH-B16	bd
		bd
		bd
	JH-B17	140 ± 16
		70 ± 15
		108 ± 17
		41 ± 21
		199 ± 18

	Avg. ± SD	***74 ± 24***
Talc	JH-B16	155 ± 16
		91 ± 16
		124 ± 16
		48 ± 18

	Avg. ± SD	***105 ± 23***
Ilmenite	JH-B17	bd
		56 ± 25

	Avg. ± SD	***34 ± 22***

3.3 Discussion

Indium has an affinity for magmatic ferromagnesian phases, such as hornblende, olivine, pyroxene and biotite (Gion et al., 2016; Shaw, 1952; Wager et al., 1958). The hydrothermal breakdown of these ferromagnesian phases allows for the formation of secondary ferromagnesian phases, such as chlorite, to form and may be important sites for indium sequestration. Olivine and pyroxene were the only ferromagnesian phases present in the starting basalt. Their subsequent breakdown during hydrothermal alteration enables indium that is hosted within these phases to be mobilized either into secondary

phases or the aqueous solution. However, in igneous rocks with a dearth of primary ferromagnesian phases, indium is likely hosted in the volcanic glass, as indium is relatively incompatible with the other phases in the rock. Volcanic glass is, by definition, thermodynamically unstable and thus is readily altered in a hydrothermal setting (Fisher and Schmincke, 1984). This is significant because the breakdown of volcanic glass will result in the release of indium, which will then be concentrated in alteration phases, pre-existing phases that persist in the assemblage, or the aqueous solution.

For the experiments performed as a part of this study, the only phases other than the altered matrix that were identified and that contained indium were ilmenite, smectite, and talc. Ilmenite contains fairly low concentrations of indium and makes up a low modal percentage of the altered basalt (<<1%). Therefore, ilmenite is not considered to play a significant role in the sequestration of indium in these experiments. Similarly, smectite forms only in low abundances within these experiments (<1%). Therefore, despite the fact that smectite contains up to 200 ppm indium in these experiments, it only has a small effect on indium sequestration. It is possible that smectite could be a major phase that sequesters indium, especially at higher water/rock where we might expect it to be a more abundant phase. Lastly, talc, which replaces olivine, is the most abundant phase that sequesters indium. Olivine is a minor constituent in the starting basalt (around 5 modal%), which suggests talc plays an important but minor role in the sequestration of indium in these experiments. However, in cases where olivine is more prevalent, talc could play a major role in the sequestration of indium. This sequestration of indium by phases such as smectite and talc would inhibit the ability of indium to partition into a potential ore-forming fluid.

Partition Coefficients and Efficiency of Removal

Data on the concentration of indium in various phases were used to calculate the partition coefficient of indium between constituents of the altered rock and the aqueous fluid ($D_{In}^{phase/aqueous} = \frac{[In_{phase}]}{[In_{aqueous}]}$) (Table 3). First, partition coefficients were determined for the interior and the rim separately. Then by multiplying the volume proportions (Appendix H) of each region (i.e. interior and rim) by their partition coefficient, the $D_{In}^{rim+int/aqueous}$ was determined (i.e. $D_{In}^{rim+int/aqueous} = V\%_{rim} * D_{In}^{rim/aqueous_{rim}} + V\%_{interior} * D_{In}^{int/aqueous}$) (Appendix H). This calculation assumes the densities of the materials are similar. In all experiments, $D_{In}^{rim+int/aqueous}$ indicates that indium preferentially partitions into the aqueous solution relative to the altered matrix (i.e. $D_{In}^{rim+int/aqueous} < 1$). For experiments with a water/rock = 1, $D_{In}^{rim+int/aqueous}$ ranged from 0.07 ± 0.02 to 0.50 ± 0.08 with an average of 0.38 ± 0.04 (three of four experiments had an total matrix partition coefficient higher than 0.41) (The uncertainties of these partition coefficients reflect the propagated standard deviation of the mean (1σ) of the indium concentrations. All future uncertainties of partition coefficients and efficiencies of removal will be presented this way.). However, the low $D_{In}^{rim+int/aqueous}$ of JH-B8 was an outlier among experiments with a water/rock = 1. All analyses of the strongly altered rim in JH-B8 had indium concentrations below detection, whereas the interior has regions with indium in concentrations above the detection limit. In order to evaluate the potential for an analytical problem, additional analyses were performed and yielded concentrations below the detection limit. Therefore, JH-B8 is the only experiment where there are no analyses in the rim with concentrations about the

detection limit. Additionally, JH-B8 is the only experiment where $D_{In}^{rim/aqueous}$ is less than $D_{In}^{int/aqueous}$ (Figure 7). This could be explained by the experimental charge rupturing during the experimental run. This would allow for indium to partition from the aqueous solution into the altered basalt (both interior and rim regions). However, once the charge failed (i.e. ruptured), water used to pressurize the vessel could have flooded the charge, which would lead to elevated water-rock interactions (i.e. water/rock >> 1). At that point, indium may have partitioned from the altered matrix back into the aqueous solution. There is no way to test this hypothesis. It is simply a scenario that may explain why JH-B8 exhibits these unexpected patterns.

Excluding experiment JH-B8, experiments with a water/rock = 1 had $D_{In}^{rim+int/aqueous}$ ranging from 0.42 ± 0.11 to 0.51 ± 0.10 with an average of 0.48 ± 0.06. On the other hand, experiments with a water/rock = 2 had $D_{In}^{rim+int/aqueous}$ that ranged from 0.11 ± 0.01 to 0.28 ± 0.10 with an average of 0.17 ± 0.03 (Figure 8). These partition coefficients indicate that indium is sequestered more readily in the altered basalt when the water/rock is low, which could inhibit the formation of a potential ore-forming fluid.

Efficiencies of removal can then be calculated in order to evaluate how much indium would partition into the hydrothermal solution in natural systems. Efficiencies of removal were subsequently calculated using the same data and can be expressed by the following equation:

$$\varepsilon = \frac{m_{In}^{aqueous\ final}}{m_{In}^{total}} \quad (3)$$

where the efficiency of removal is equal to the mass of indium in the final aqueous solution divided by the mass of indium in the entire system. We can then derive an

equation that relates the efficiency of removal to the water/rock and partition coefficient of indium between the altered basalt and the aqueous solution:

$$\varepsilon = \frac{1}{1+\frac{D}{W/R}} \quad (4)$$

where D, in this case, is $D_{In}^{rim+int+xl/aqueous}$ ($D_{In}^{rim+int+xl/aqueous} = D_{In}^{rim+int/aqueous} * V\%_{rim+int} + D_{In}^{xl/aqueous} * V\%_{xl}$). The efficiency of removal will change as the ratio of D to water/rock changes. As D to water/rock gets higher, the efficiency of removal will decrease and vice versa.

In order to calculate efficiencies of removal for these experiments, we must consider that the altered matrix makes up 65 ± 4% of the altered basalt and indium is primarily partitioning into the alteration products of the matrix. With this in mind, efficiencies of removal for experiments with water/rock = 1 ranged from 74 ± 4% to 78 ± 5% and had an average efficiency of removal of 76 ± 5% (81 ± 3% if including JH-B8). Experiments with a water/rock = 2 ranged from 90 ± 4 % to 96 ± 1% and had an average efficiency of removal of 94 ± 2% (Figure 9). These results indicate that by simply doubling the water/rock from 1 to 2, ~20% (16% if including JH-B8) more indium can be removed from the altered basalt into aqueous solution, thereby making a more potent ore-forming fluid.

Table 3. Partition coefficients for indium between the interior, rim, or total matrix and the aqueous solution, as well as the areas of the interior and rim in each experiment. Uncertainties reflect the propagated standard deviation of the mean (1σ) from the analyzed indium concentrations.

	$D_{In}^{int/aqueous}$	V% Interior	$D_{In}^{rim/aqueous}$	V% Rim	$D_{In}^{rim+int/aqueous}$
JH-B1	0.25 ± 0.09	34.7%	0.65 ± 0.14	65.3%	0.51 ± 0.10
JH-B2	0.06 ± 0.01	14.0%	0.12 ± 0.02	86.0%	0.11 ± 0.01
JH-B4	0.15 ± 0.04	34.8%	0.35 ± 0.16	65.2%	0.28 ± 0.10
JH-B6	0.13 ± 0.04	28.8%	0.18 ± 0.07	71.2%	0.17 ± 0.05
JH-B7	0.39 ± 0.08	31.2%	0.44 ± 0.16	68.8%	0.42 ± 0.11
JH-B8	0.13 ± 0.04	39.4%	0.04 ± 0.00	60.6%	0.07 ± 0.02
JH-B9	0.05 ± 0.01	2.3%	0.13 ± 0.04	97.7%	0.12 ± 0.04
JH-B10	0.48 ± 0.06	37.2%	0.51 ± 0.13	62.8%	0.50 ± 0.08

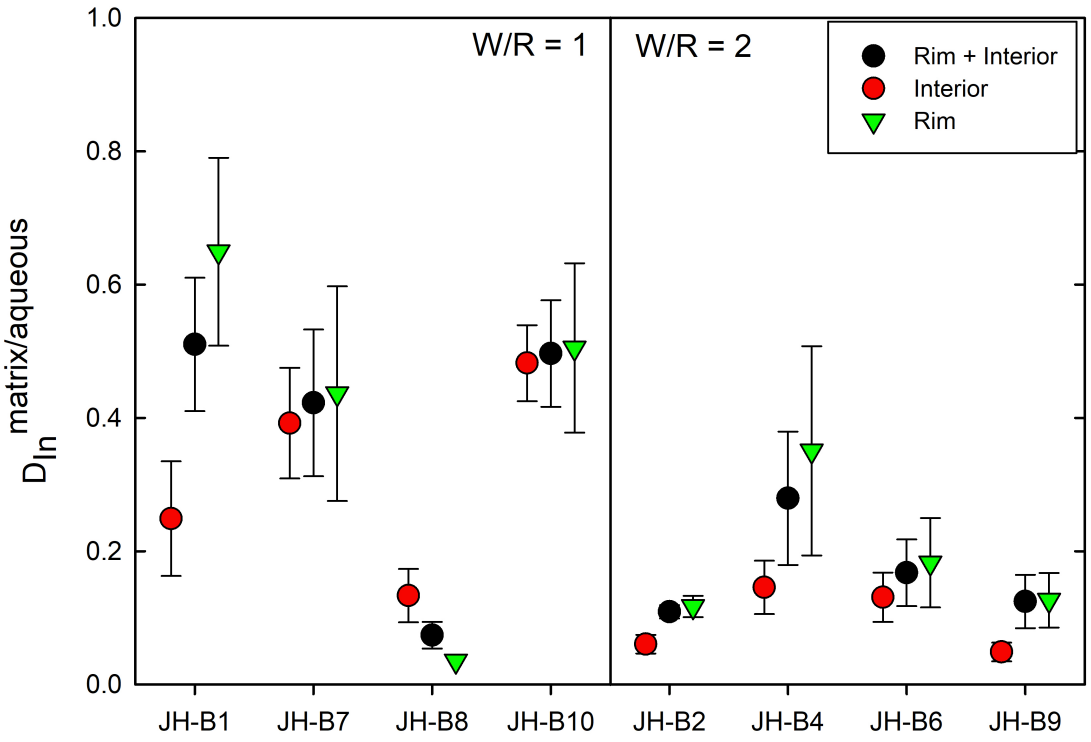

Figure 7. Partition coefficients for indium between the altered matrix and aqueous solution in the interior, rim, and the total matrix versus water/rock.

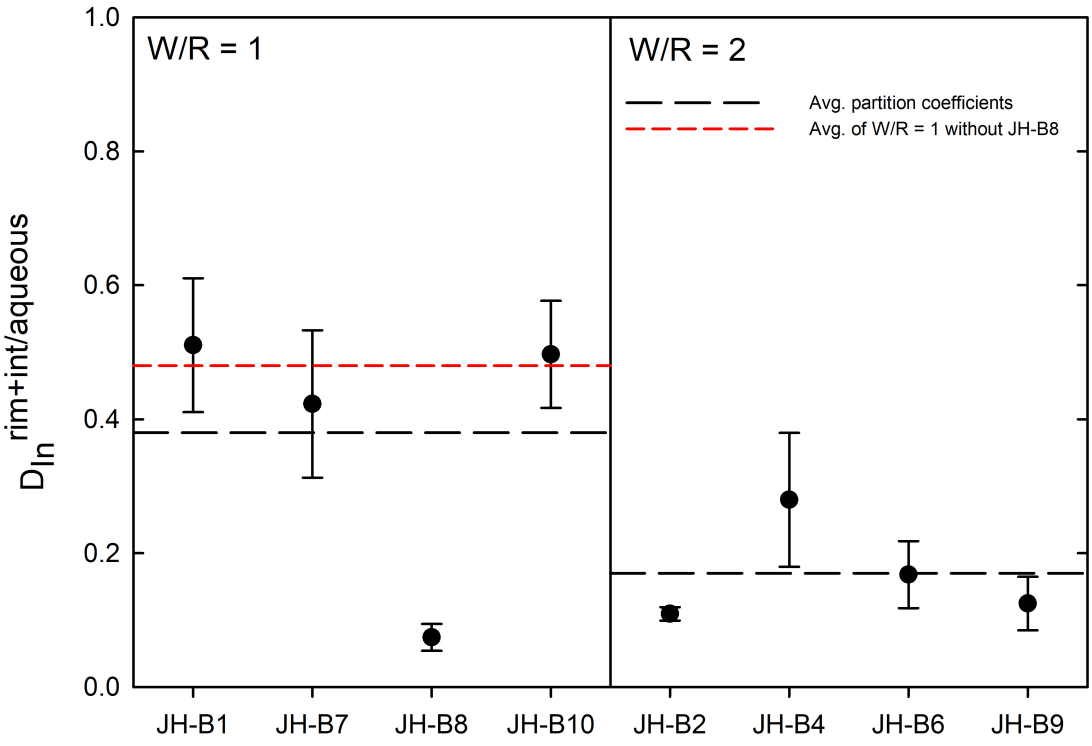

Figure 8. Matrix/aqueous solution partition coefficients as a function of water/rock. Average partition coefficients for experiments with water/rock = 1 and water/rock = 2 shown by dashed lines.

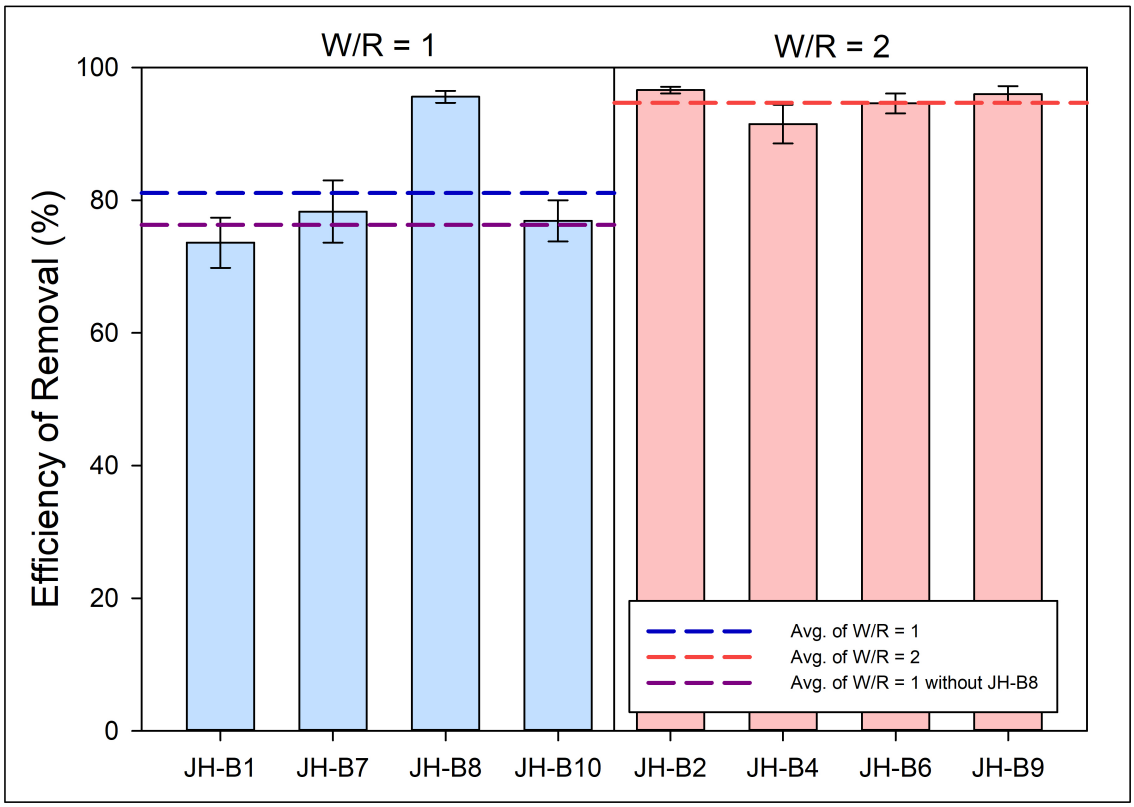

Figure 9. Plot of efficiencies of removal for experiments with water/rock = 1 and water/rock = 2. Experiments with a water/rock = 2 have a higher efficiency of removal of indium into the aqueous solution, thereby creating a more potent ore-forming fluid.

I performed t-tests by using two different methods to assess the significance of the total matrix partition coefficients. (1) First, a t-test was performed in order to assess whether or not the total matrix partition coefficients fell into two distinct populations. Without JH-B8, the t-test yielded a t-parameter of 6.50 and a corresponding critical $\alpha(2) < 0.01$, which signifies the probability that water/rock affects the total matrix partition coefficient of indium between hydrothermally altered basaltic matrix and aqueous solution is above 99%. When JH-B8 was included, the resulting t-parameter was 1.88 and a corresponding critical $\alpha(2)$ of more than 0.10, which signifies the probability that water/rock affects the total matrix partition coefficient of indium between hydrothermally

altered basaltic matrix and aqueous solution is less than 90%. However, these t-tests do not take into account the standard deviations found within each experiment. (2) In order to account for this fact, partition coefficients were determined for every indium analysis both in the interior and the rim. Thus for a given analysis, the measured indium concentration was considered to represent the concentration of the entire altered basalt. Without JH-B8, the t-test yielded a t-parameter of 2.68 and a corresponding critical $\alpha(2) < 0.01$. When JH-B8 was included, the t-parameter was 2.46 and a corresponding critical $\alpha(2)$ between 0.025 and 0.01.

The rims of the altered basalts represent the most severely altered regions in these experiments. In a natural hydrothermal ore-bearing system, the rim would represent the altered source rock in which the ore deposit derives most of its metals. The less altered interior regions of these experiments could serve as source rocks in a natural setting. However, the majority of the material in an ore deposit will likely be derived from the most altered region (i.e. rim). Consequently, it is important to assess the efficiencies of removal by only considering the rim data. In all experiments (except JH-B8, which has not been included in this exercise), the rim had higher and more variable average indium concentrations when compared to the interior. This results in a lower estimated efficiency of removal for both sets of experiments with larger standard deviations. The original calculations (include rim and interior indium data) resulted in an average efficiency of removal of 76 ± 5% for experiments with a water/rock = 1 and 95 ± 2% for experiments with a water/rock = 2. However, when only considering the data within the rim, the experiments with a water/rock = 1 have an average efficiency of removal of 74 ± 6%, whereas experiments with a water/rock = 2 have an average of 94 ± 3% (Table 4; Figure

10). Despite the slight decrease in efficiency of removal produced by this new calculation, the difference between the average efficiency of removal between the two groups becomes larger. Thus the efficiencies of removal calculated by both methods suggest that by simply raising the water/rock from 1 to 2, about 18-20% more indium will be removed from the source rock into the aqueous solution.

I also calculated partition coefficients using another method, Method 2, which utilizes data of the individual regions of the altered matrix (Regions 1 to 3). The methodology for this alternative method can be found in Appendices F and G, along with the results and a discussion.

Table 4. Efficiencies of removal calculated using only the indium data from the rim.

W/R = 1		**W/R = 2**	
JH-B1	69 ± 5 %	JH-B2	96 ± 1%
JH-B7	78 ± 6%	JH-B4	90 ± 4%
JH-B10	77 ± 5%	JH-B6	94 ± 2%
		JH-B9	96 ± 1%
Average	**74 ± 6%**	**Average**	**94 ± 3%**

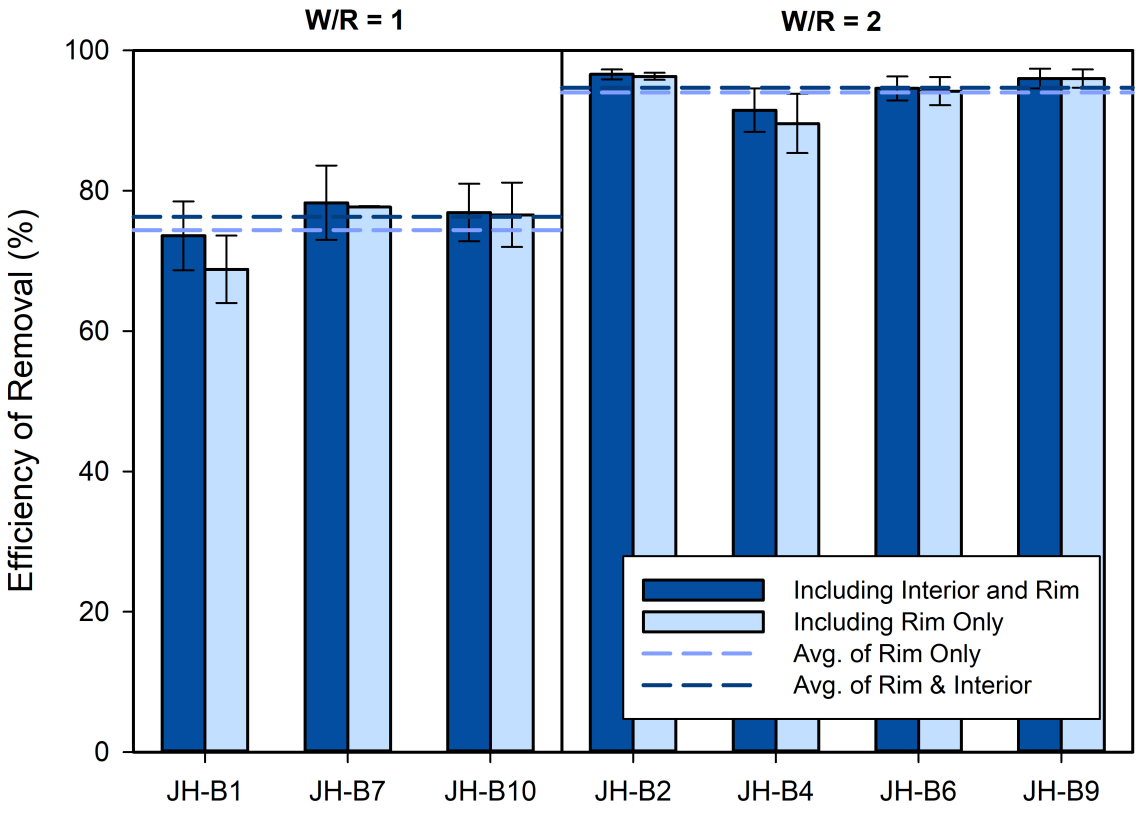

Figure 10. Efficiencies of removal calculated using indium data from (1) the interior and the rim of the altered basalt and (2) the rim only. Average efficiencies of removal for experiments with water/rock equal to 1 and 2 are shown by the dashed lines.

Water/Rock Effect

Out of all the variables evaluated, water/rock has the largest effect on the $D_{In}^{rim+int/aqueous}$. Time and NaCl wt. % equivalent seem to have little effect on the partition coefficient. $D_{In}^{rim+int/aqueous}$ decreases with increasing water/rock (Figure 8). In some ways this is a surprising result, given that an experiment with a water/rock = 2 has twice as much indium by mass as the same experiment with a water/rock = 1. This suggests that the pattern of decreasing $D_{In}^{rim+int/aqueous}$ with increasing water/rock is not due to the system being "flooded" by indium, meaning that high water/rock experiments

do not contain more indium in the system than the altered basalt can possibly sequester, thus artificially lowering $D_{In}^{rim+int/aqueous}$ by adding more indium to the solution. One might assume the inverse trend has to do with the degree of alteration. Because higher degrees of hydrothermal alteration occur at higher water/rock, one might suspect indium is sequestered in lesser amounts in basalts that experienced a relatively low degree of alteration. However, this cannot be the case because the strongly altered rim tends to sequester more indium than the weakly altered interior of the basalt.

Temperature, pressure, and pH all play important roles in the partitioning of metals in hydrothermal systems. However, temperature and pressure were kept constant throughout these experiments. Consequently, pH is likely the reason why indium partitioning varies between experiments with varying water/rock. A likely hypothesis is that during the hydrothermal alteration, hydrolytic reactions are consuming H^+, which results in an increase in pH. This is very similar to the silicate hydrolysis reactions discussed in the introduction of this document, but with a distinction in the process of generating and maintaining the H^+. The H^+ generated in seawater-basalt hydrothermal alteration are produced by hydrolysis reactions. In the case of these experiments, the HCl-bearing aqueous solution had a starting pH of 0-1 at 25°C, meaning a significant H^+ ion component already existed. This excess H^+ can then be consumed in hydrolytic reactions, which would raise the pH of the aqueous solution. For example: $2Mg_2SiO_4 + 2SiO_2 + 2H^+ \rightarrow Mg_3Si_4O_{10}(OH)_2 + Mg^{2+}$. In this reaction, forsterite, SiO_2, and H^+ ions react to form talc and Mg^{2+}. Evidence for a similar reaction occurring in these experiments includes the alteration of olivine to talc and the mobilization of Mg from pre-existing phases (i.e. olivine and augite) to form Mg-rich minerals like talc and

smectite. Water/rock becomes important because experiments with a water/rock = 2 have twice as much moles of H^+ (relative to the amount of rock to react with) as experiments with a water/rock = 1. Therefore, aqueous solutions used in experiments with a water/rock = 2 can maintain their low pH more effectively because a lower proportion of H^+ is consumed, which in turn promotes increased indium mobilization into the aqueous solution.

Effect of Chloride Availability

As previously stated, the addition of ligands in an aqueous solution can increase the solubility of a given mineral, thus removing metals of economic interest from that mineral into the aqueous solution. The primary ligands for indium in acidic conditions are most likely to be Cl^-, F^-, and HS^- (Wood and Samson, 2006). In these experiments, Cl^- is the primary ligand due to the 0.1-1 M HCl solution and, in some cases, added NaCl and KCl to the starting aqueous solution. The concentration of Cl^- in the starting aqueous solutions are (a) 0.4 wt% for the 0.1 M HCl solution, (b) 3.5 wt% for the 1 M HCl solution, and (c) 7.0 wt% for 1 M HCl + 0.5 M NaCl + 0.5 M KCl solution. There is not a statistical difference between the partition coefficients determined for experiments using a 1 M HCl solution and that using a 1 M HCl + 0.5 M NaCl and KCl solution.

3.4 Conclusions

Partition coefficients for indium between altered basalt and aqueous solution were determined experimentally. All experiments had $D_{In}^{rim+int/aqueous} < 1$, indicating that

indium preferentially partitions into the aqueous solution relative to the altered matrix (65 ± 4% of the basalt). Of the variables tested, water/rock had the largest affect on $D_{In}^{rim+int/aqueous}$ and efficiency of removal. Experiments with a water/rock = 1 had an average $D_{In}^{rim+int/aqueous}$ of 0.48 ± 0.06, whereas experiments with a water/rock = 2 had an average $D_{In}^{rim+int/aqueous}$ of 0.17 ± 0.03. Experiments with water/rock of 1 and 2 had average efficiencies of removal of 76 ± 5% and 95 ± 2%, respectively. By using these data, models can be developed for different basalts with varying degrees of matrix/glass in order to assess potential indium-bearing ore deposits.

4. High Initial pH, Sulfur-bearing Seawater Experiments

This set high initial pH, sulfur-bearing seawater experiments was designed to examine the geochemical behavior of indium under hydrothermal conditions similar to those of volcanogenic massive sulfide (VMS) deposit formation. These deposits form when seawater flows through fractures in oceanic basalts and is heated by underlying magma chamber(s). The seawater hydrothermally reacts with the surrounding rock, resulting in hydrothermal alteration and the mobilization of metals into aqueous solution. The hot ore fluid is then buoyantly transported upwards through the hydrothermal system until it comes into contact with cold seawater, which triggers precipitation of sulfides (Figure 11). The primary difference between these experiments and the experiments previously described in Chapter 3 is the presence of seawater, which strongly influences the resulting mineralogy and geochemistry because it not only contains appreciable amounts of Mg^{2+}, Na^{+}, Cl^{-}, and SO_4^{2-}, but also exerts some control on the acidity of the system. Unlike the previous HCl-bearing experiments where the initial aqueous solution pH was ~0-1, the aqueous solution used in these experiments has a starting pH of ~8 (pH of seawater). The acidity is then produced by hydrolysis reactions. The water/rock is important in that it influences the ability of the aqueous solution to generate and maintain the acidic conditions (see Section 2.2 for further discussion).

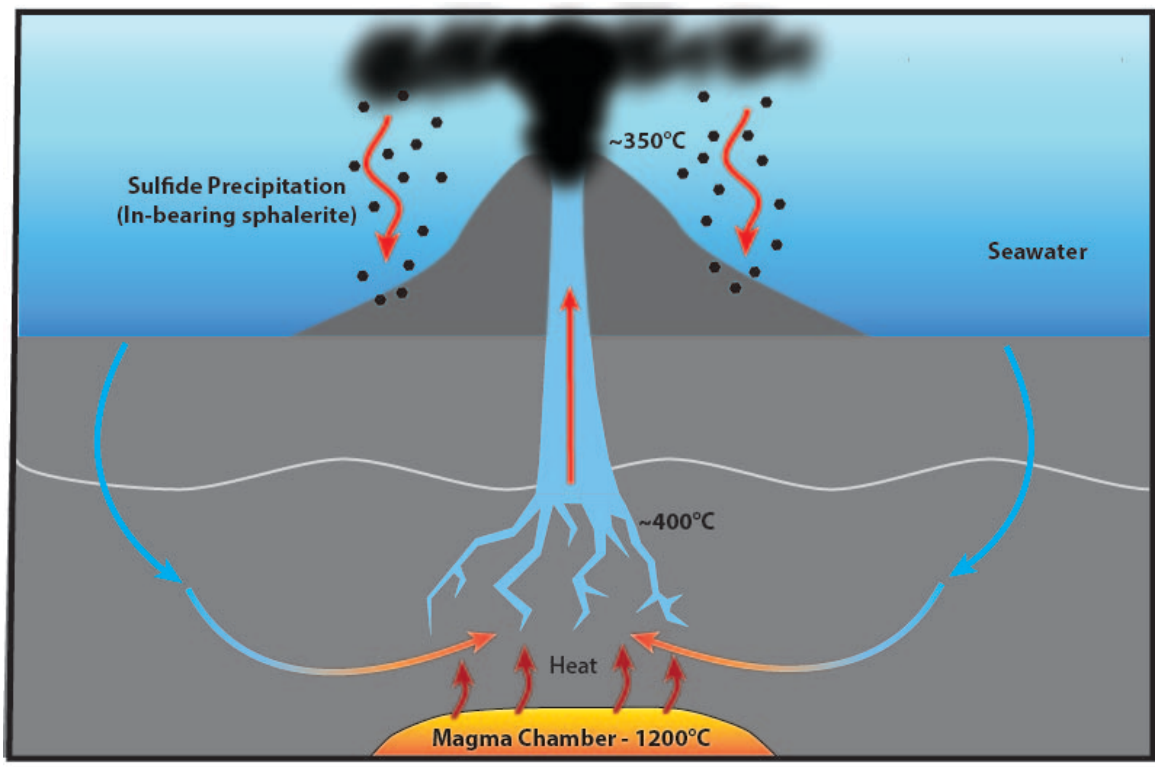

Figure 11. Schematic (not to scale) depicting the formation of a volcanogenic massive sulfide deposit. First, seawater infiltrates the basalt overlying a magma chamber, thus heating the seawater. Once heated, the seawater hydrothermally alters the surrounding basalt. Metals, including indium, can then partition from the altered basalt into the hot ore fluid, which is then transported upwards through the hydrothermal system. Once the ore fluid comes into contact with cold seawater, sulfides, such as indium-bearing sphalerite can precipitate.

4.1 Methods

Experimental Design

Experimental charges consisted of a sub-angular piece of basaltic glass from the Juan de Fuca mid-ocean ridge, seawater collected from Ocean City, MD, and indium (III) trichloride-bearing ($InCl_3$) distilled water sealed within a 2 cm long and 5 mm wide (outer diameter) Au capsule with 0.127 mm thick walls. Two starting aqueous solutions were necessary because indium-bearing sulfides precipitated when $InCl_3$ crystals were dissolved in seawater. In order to create the $InCl_3$-bearing aqueous solution, indium metal was first dissolved in 12.1 M HCl and heated until dried, which resulted in the

precipitation of $InCl_3$ crystals. The crystals were then dissolved in distilled water to form a 9641 ± 98 ppm indium-bearing aqueous solution, as determined by ICP-MS. The proportion of seawater to $InCl_3$-bearing aqueous solution (by mass) is 9:1 in all experiments, thus the indium concentration in the mixed aqueous solution is ~964 ppm indium. The seawater was filtered using a 0.45 μm filter to remove particulate organic matter. The water/rock ranged from 1 to 10.

Once sealed, experimental charges were placed in an oven at ~150°C in order to ensure the charge was properly sealed prior to being placed in the furnace. Experimental charges were then loaded into a René 41 cold seal pressure vessel, which was subsequently placed in a near-horizontal furnace (inclined at 8°). All experiments were run at 500°C and 50 MPa. Run time ranged from four to eight weeks (Table 6, Appendix J). Upon completion, experiments were quenched and had a distinct dark-green color, which is characteristic of greenschist facies alteration.

Table 5. Independent variables for seawater experiments.

	JH-S1	JH-S2	JH-S3	JH-S5	JH-S8
W/R	1	2	3	3	10
Run Duration (weeks)	4	4	4	8	6

Analytical Methods

After quench, the altered basalt run products were removed from the capsule, mounted in epoxy, and subsequently polished for EPMA use. Upon opening up the experimental charge, the distinct odor of H_2S was present in all successful experiments with run times of 4 and 6 weeks. However, this odor disappeared in the 8-week experiment. All run products were first analyzed by using EDS in order to aid in the

determination of alteration phases. Additionally, indium concentrations and major element composition were determined with WDS (See Appendix I for more information), using a 10 μm beam.

4.2 Mineralogy

The fragments of basaltic glass were highly altered upon termination of each experiment and consisted mostly of relatively homogeneous, fine-grained material. Other phases/mixtures were present in the run products but could not be identified with the EPMA because they were too small to analyze. Pervasive plagioclase veins (oligoclase/andesine, $An_{30 \pm 1}$) (See Appendix K for major element compositions) dissect the altered glass (Figure 12). Additionally, radial plagioclase crystals are found inside vesicles, where strong dissolution occurred; they also occur external to the basalt fragment. Other secondary phases found outside the altered basalt include: an abundance of a fibrous phase that contained Fe + Mg + Si ± Al, a Ti-rich Fe-oxide, and trace amounts of pyrite and anhydrite. Mottl and Holland (1978) identified a similar occurrence in their experiments and observed a smectite coating on the walls of their capsules at 200-400°C and talc at 500°C. The location of these phases could be important as they likely indicate that these phases precipitated upon quench. Previous experiments, such as those performed by Mottl and Holland (1978) and Mottl et al. (1979), used powdered basalt as their starting run material, which makes it hard to identify whether or not certain phases precipitated upon quench.

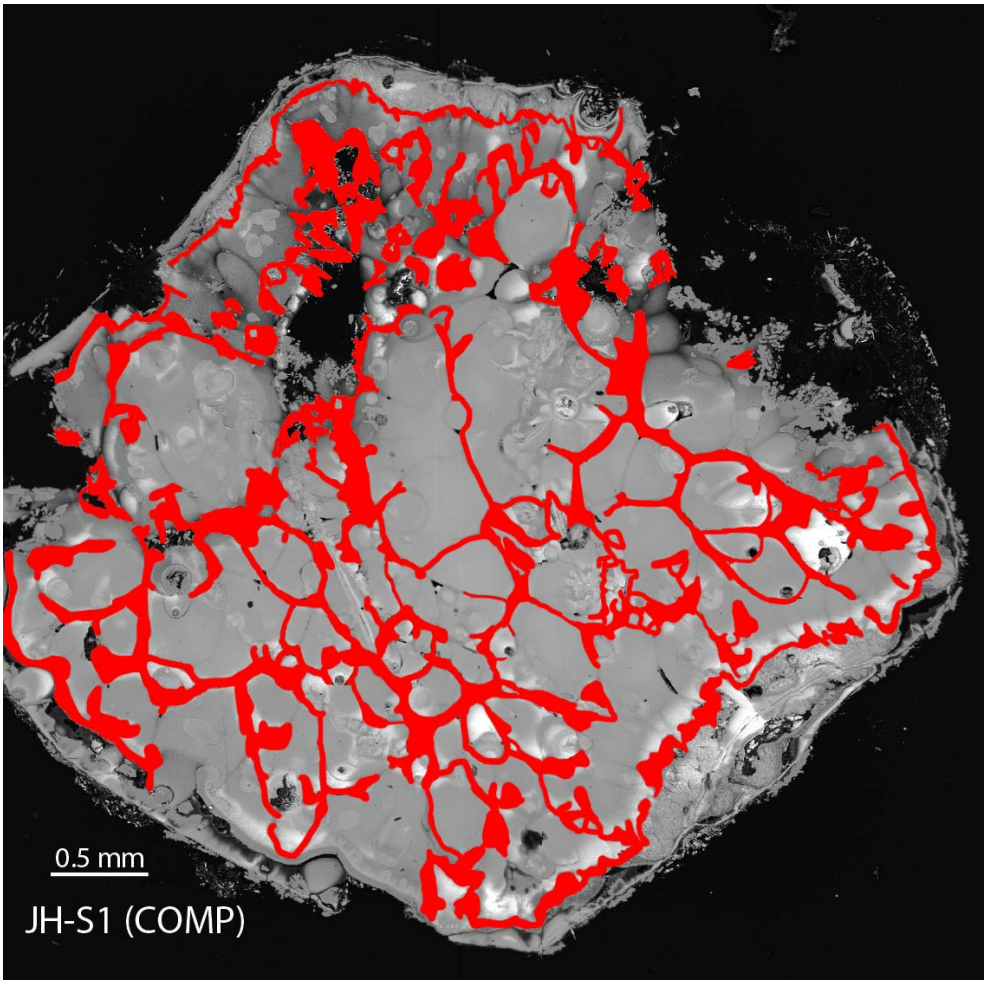

Figure 12. A mosaic of BSE images from JH-S1 with regions interpreted to be plagioclase veins and crystals colored in red.

Plagioclase is the only phase described above that is not believed to have formed on quench. In order to produce plagioclase on quench, large concentrations of SiO_2 are required to be in the aqueous solution, which is unrealistic. Von Damm et al. (1991) used thermodynamic data to calculate quartz solubility in hydrothermal seawater from 150-1000 bar and 200-450°C. At 450°C (50°C lower than the temperature used in these experiments) and 500 bars, quartz solubility is ~1200 ppm SiO_2. The quartz solubility at 500 bars and 500°C can be estimated from the trends in this study and is likely close to

1000 ppm SiO_2, a concentration not enough to account for the abundance of secondary plagioclase present in the run products. Furthermore, monomineralic albite veins in metabasaltic rocks are associated with greenschist facies retrogression (Miller and Cartwright, 2006).

4.3 Geochemistry

Altered Glass Geochemistry

The altered basaltic glass consists primarily of a mixture of fine-grained material. The major element composition of the altered glass can be found in Appendix K. In order to estimate the mineralogy that constitutes the altered glass, ACF diagrams were generated for the altered glass in the interior and rim of the basalt grain (Figure 13 and 14). Most analyses plot inside the epidote-chlorite-actinolite/tremolite field, which suggests that the altered glass may consist of a mixture of epidote + chlorite + actinolite/tremolite or an isochemically equivalent assemblage. All of these phases we would expect to be associated with greenschist facies hydrothermal alteration. Additionally, these diagrams suggest that most of the altered glass is actinolite-tremolite, which agrees with Mottl (1983), who argued that at water/rock < 10, altered basalt would be epidote + actinolite-rich. Furthermore, there appears to be no apparent geochemical difference between the interior and rim other than the fact that the rim has more homogeneous compositions across the range of water/rock.

In the interior region of the altered basaltic glass, it would appear that as water/rock increases, the amount of actinolite-tremolite decreases, which would be in agreement with the model proposed by Mottl (1983). However, upon further inspection,

what is driving this trend is not the increase or decrease of the F or C components, but rather the increase of the A component (i.e. moles Al_2O_3 - K_2O - Na_2O), which decreases the contributions of the F and C components to the overall ternary system. This increase in the A component is not due to an increase in Al_2O_3 but is due to the decrease in Na_2O. Experiments with a water/rock ≤ 2 have 0.38 ± 0.03 moles of Na_2O (based on 8 O p.f.u.), whereas experiments with a water/rock > 2 have 0.14 ± 0.01 moles of Na_2O. Instead of decreasing amounts of actinolite-tremolite, this trend may indicate that less plagioclase is forming as water/rock increases, which agrees with the model of Mottl (1983) (Figure 15).

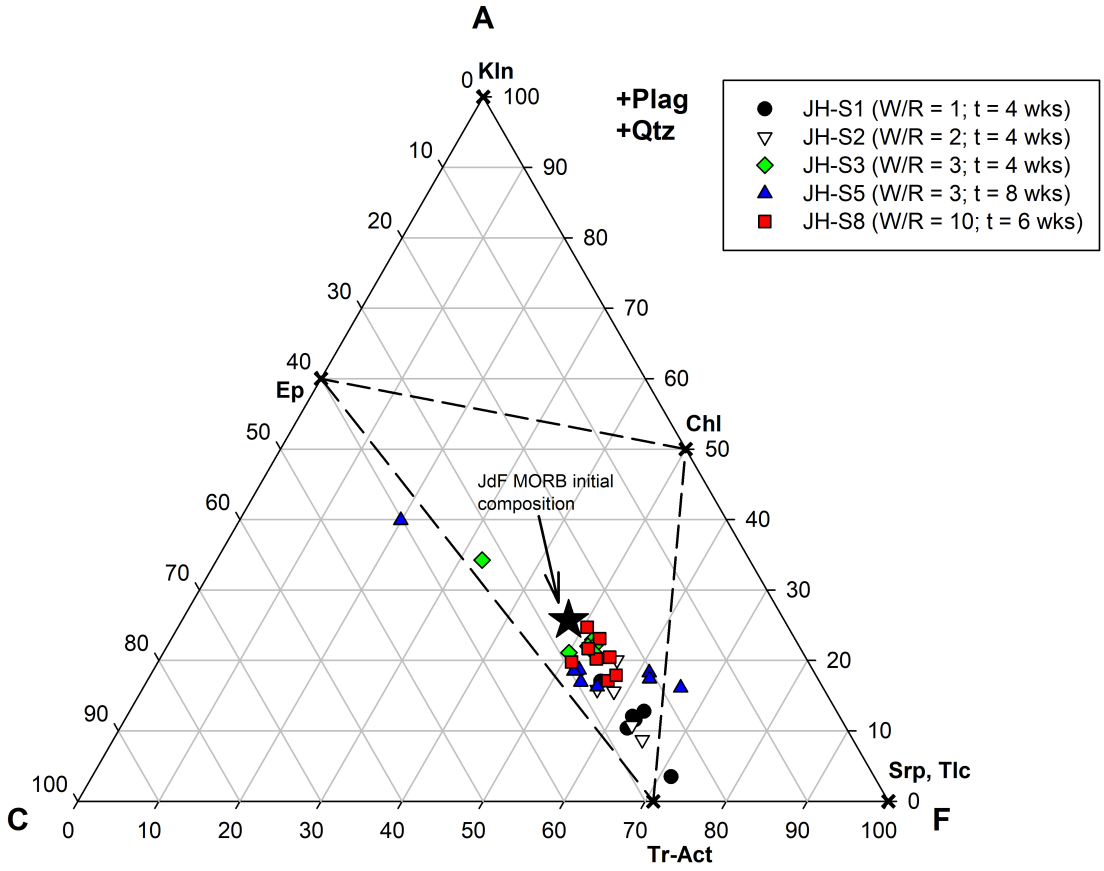

Figure 13. ACF diagram for the interior fine-grained altered basaltic glass. The two points plotting to the upper left of the initial Juan de Fuca MORB composition both have anomalously high Al_2O_3 (~17 to 19 wt%) and low MgO (1.4 to 2.4 wt%). Initial Juan de Fuca (JdF) MORB composition from Arévalo and McDonough (2008) (Table K-1).

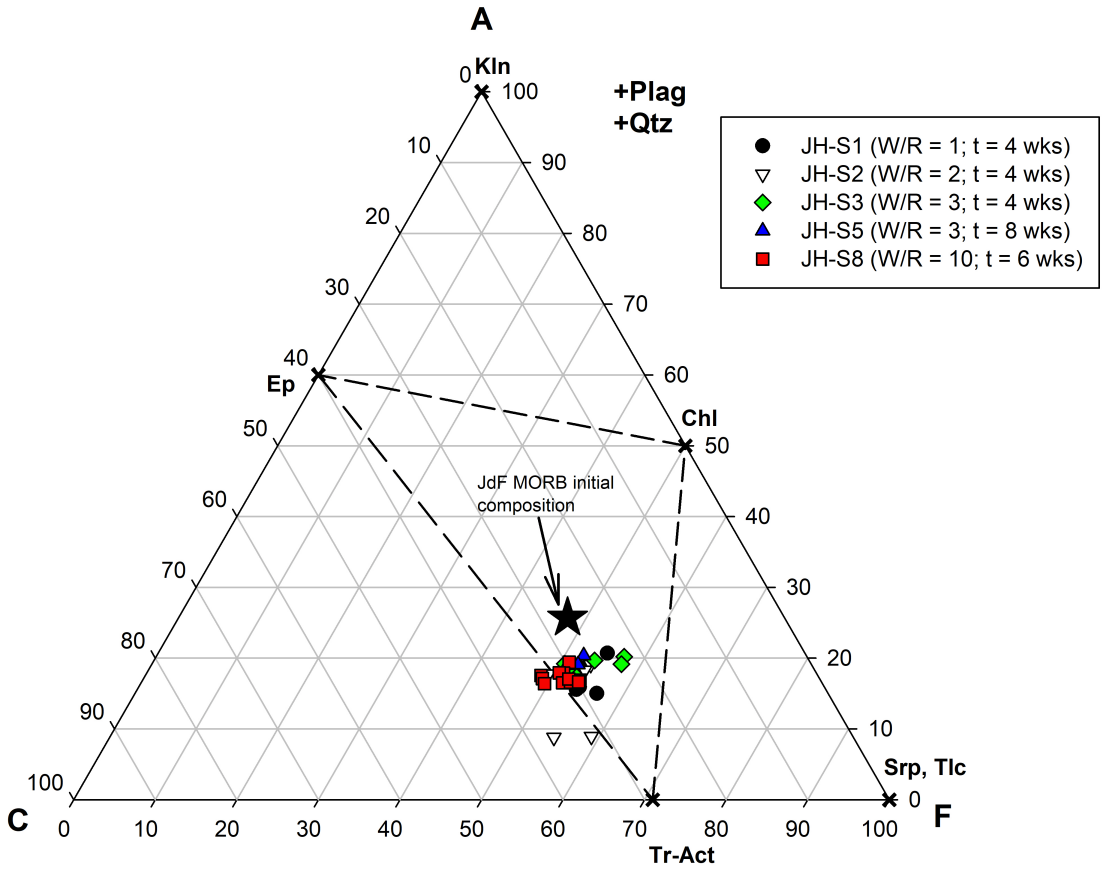

Figure 14. ACF diagram for the rim fine-grained altered basaltic glass. Initial Juan de Fuca (JdF) MORB composition from Arévalo and McDonough (2008).

Plagioclase Geochemistry

Plagioclase veins/crystals were Na-rich and had an An# of 30 ± 1 (Appendix K). A more albitic plagioclase composition is not surprising because of the cation exchanges between the seawater and the basalt. Na_2O increases in the basalt due to the input from the seawater and CaO decreases in the basalt due the Ca^{2+} exchange for Mg^{2+} in the seawater. However, plagioclase analyses yielded variable amounts of FeO and MgO ranging from 0.3-7.8 wt% and below detection (bd)-3.9 wt%, respectively. These analyses suggest that either the EPMA beam analyzed underlying altered glass or the plagioclase in the veins may be mixed with other fine-grained material. These data were

subsequently filtered in order to ensure that only analyses that provided plagioclase compositions were considered in our data analysis. Analyses that were removed satisfied the three following criteria: (1) total cations were greater than or less than 5.00 ± 0.05; (2) Al + Si cations were less than or equal to 3.70; (3) Fe cations were greater than 0.15.

Bulk Geochemistry

In order to evaluate the exchange of cations between the seawater and the altered basaltic glass, an overall bulk altered basalt chemistry was estimated for each experiment. To do this, the area proportions of plagioclase and altered basaltic glass were estimated (Table 8) and were then multiplied by the average concentration of each oxide within that region. These were then added together to obtain an overall, bulk chemistry.. This calculation assumes the densities of the materials are similar. In the case of the altered basaltic glass, the composition was normalized so that the oxides totaled 100 wt%. This bulk composition was then compared to the initial Juan de Fuca MORB composition (Arévalo and McDonough, 2008). Oxides that increased (by wt%) in the majority of the experiments include: Na_2O, MgO, K_2O, SO_3, and TiO_2. Oxides that decreased include: FeO, Al_2O_3, and SiO_2.

Previous work on seawater-basalt interactions show there is an increase of Na_2O and MgO and a decrease in CaO in the altered basalt. This is due to the exchange of Mg^{2+} and Na^{+} in seawater for Ca^{2+} in the basalt (Hajash, 1975; Mottl, 1983; Mottl and Holland, 1978; Nakamura et al., 2007; Seyfried and Bischoff, 1977; Seyfried and Mottl, 1982). Although we see this trend for MgO and Na_2O in some of the experiments, no experiments display CaO depletion. However, this could be due to the pervasive

plagioclase (An_{30}) veins and the fact that Mottl and Holland (1978) noticed that Ca^{2+} concentrations in the aqueous solution decreased from >3000 ppm to <1000 ppm as temperatures rose from 300 to 500°C. When we consider these two factors together, it is possible that no discernable CaO depletions will be observed using this method unless at higher water/rock.

Increases in K_2O and SO_3 are also expected and due to their partitioning from the seawater solution into the altered basalt. The fact that TiO_2 increased may be due to the altered basalt losing other oxides relative to TiO_2, because it is considered an immobile oxide. However, Ti-rich Fe-oxide was found outside the altered basalt, which has been interpreted to have precipitated upon quench. Therefore, TiO_2 is likely being mobilized in small quantities into the aqueous solution, but the fact that the concentration seems to be increasing may indicate that the basalt is losing other oxides relative to TiO_2. Results of previous work also predict that Fe will partition into solution as base metals typically mobilize from the altered rock into aqueous solution. In addition, Al_2O_3, which is relatively immobile, decreased in the altered basalt. Lastly, SiO_2 decreased in the altered basalt, which is not surprising as previous work indicates it will likely partition into the aqueous solution based on an approximate quartz solubility of about 1000 ppm.

The minerals interpreted to have precipitated upon quench indicate that Ca^{2+}, Al^{3+}, Mg^{2+}, Fe^{2+}, Ti^{4+} and Si^{4+} are partitioning from the altered volcanic glass into aqueous solution. Thus far, all experiments have little to no free aqueous solution in the experimental charge when opened after quench. This is likely due to adsorption of water on the many fine-grained precipitates and reaction products, as well as the incorporation of water into hydrous minerals.

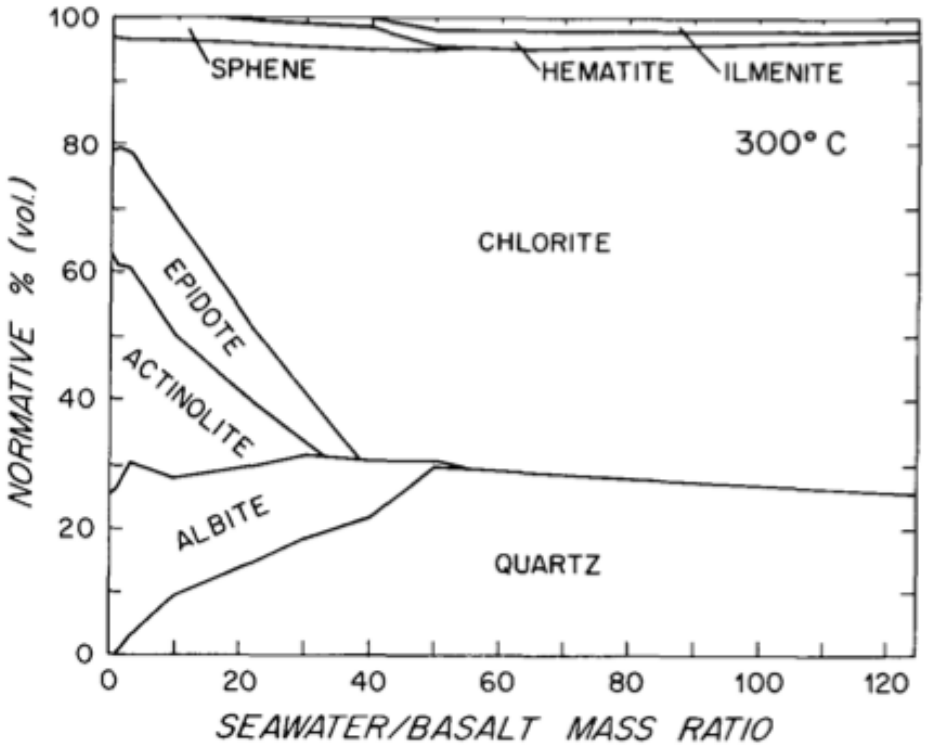

Figure 15. Model of mineralogy versus water/rock during the hydrothermal alteration of basalt by seawater (figure from Mottl, 1983).

Indium

The altered basaltic glass and the plagioclase veins/crystals were analyzed for indium (See Appendix J for analyses) and had a detection limit of 17 ppm. Indium in the altered basaltic glass was highest in the rim when compared to the interior. This trend likely results from the fact that there is a higher degree of water-rock interaction towards the rim of the glass, which is significant because the aqueous solution is the source of indium in these experiments. Indium concentrations in both the altered glass and the plagioclase typically increased with increasing water/rock. Table 7 lists the averages and standard deviations of indium concentrations found in each region of each of the experiments.

In the case of JH-S8, a region in the rim of the altered basalt was noticeably lighter in BSE images than the remainder of the rim, indicating the presence of elements with higher atomic numbers (Figure 16). Four WDS analyses of the light region result in an average indium concentration of ~2.4 ± 0.2 wt%. Other than this difference in indium concentrations, major element data between this "light" region and the rest of the rim were similar in JH-S8. Therefore, the indium concentrations in this light region has not been included in our calculations, as we have no reason to believe it follows any reproducible behavior. It is possible, however, that it is caused by small mineralogical differences that we are unable to detect.

The trend of increasing indium concentration with increasing water/rock is surprising because the amount of indium in the entire system increases with water/rock. Consequently, there is more indium available to partition into the altered basaltic glass. Lastly, there are other altered phases/mixtures of phases that were not considered for the geochemical modeling of indium because they are too small to identify and in low abundance.

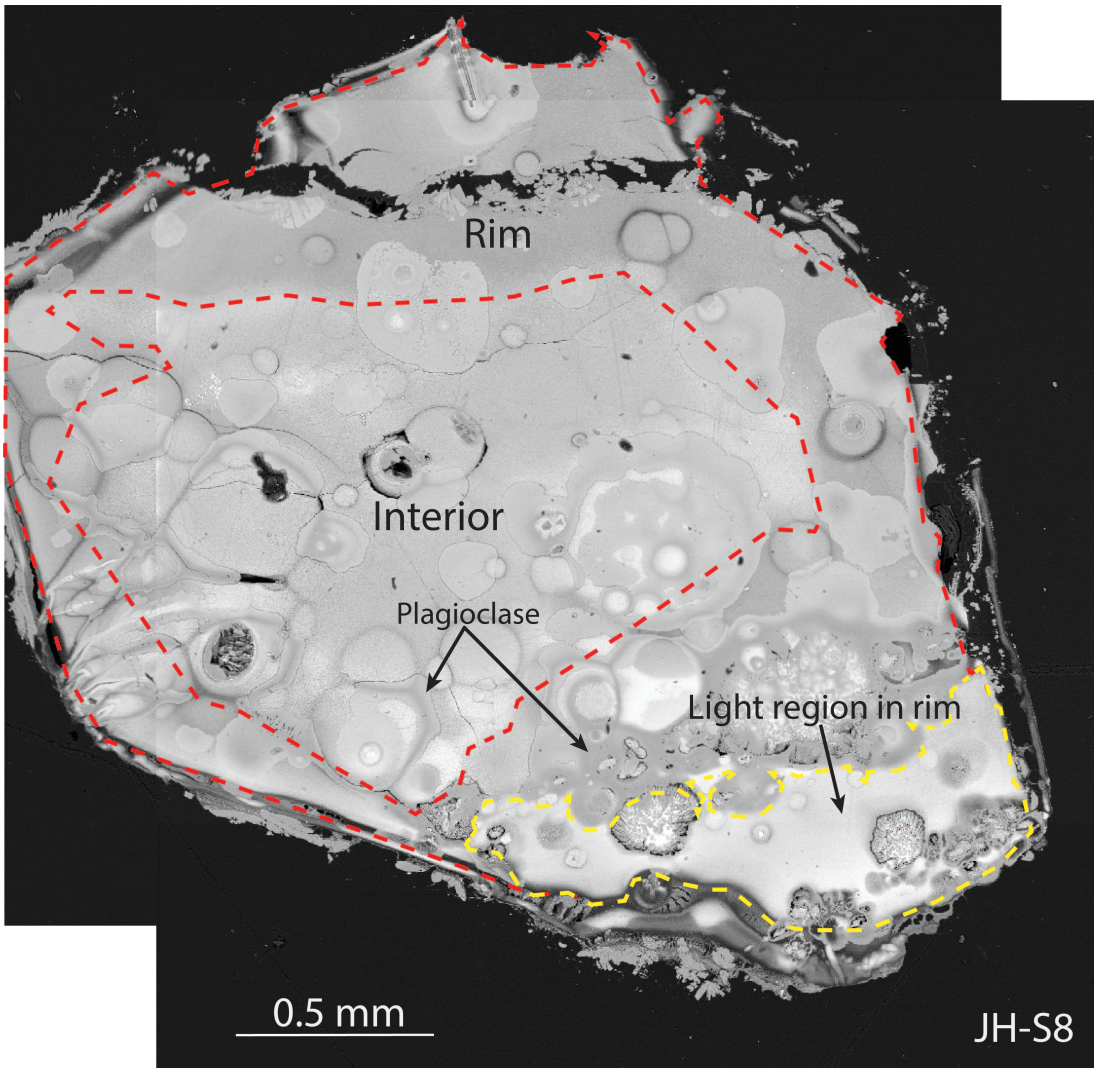

Figure 16. A mosaic of BSE images from experiment JH-S8. Note the light region that has >2 wt% indium.

Table 6. Average indium concentrations (ppm) in various regions of the altered basalt. Plagioclase data is from both the plagioclase veins and crystals. Note the high standard deviation of the rim region of JH-S5, which is caused by a low number of analyses (n = 3) and one analysis having very high indium concentrations (3561 ppm). For analyses below the detection limit, I chose the midpoint between 0 ppm and 17 ppm (8.5 ppm) to represent these analyses. From this point on, 8.5 ppm will be used for any indium concentration below the detection limit.

Region	JH-S1 *(W/R = 1)*	JH-S2 *(W/R = 2)*	JH-S3 *(W/R = 3)*	JH-S5 *(W/R = 3)*	JH-S8 *(W/R = 10)*
Interior	241 ± 41	233 ± 31	519 ± 44	614 ± 88	1806 ± 211
Rim	451 ± 29	534 ± 201	792 ± 30	1877 ± 846	4062 ± 311
Plagioclase	43 ± 7	36 ± 22	173 ± 18	204 ± 5	658 ± 231

4.4 Discussion

Partition Coefficients and Efficiency of Removal

Although the rim in this set of experiments tended to have higher indium concentrations than the interior, it was often challenging to distinguish the two in BSE images. As a result, partition coefficients were determined for the altered basaltic glass and plagioclase. $D_{In}^{ag+plag/aqueous}$ ($D_{In}^{ag+plag/aqueous} = Area\%_{plag} * D_{In}^{plag/aqueous} + Area\%_{ag} * D_{In}^{ag/aqueous}$) were then determined using the area percentages of the altered glass (not differentiating between the interior and the rim) and plagioclase. In the case of these experiments, area must be used because it is impossible to estimate the volume of the plagioclase veins (See Appendix L for methods). However, as water/rock increased, polishing the samples became more challenging. Often, pieces of the altered glass were plucked from the sample. It therefore became impossible to estimate the relative area proportions of the plagioclase and altered glass in experiments JH-S3, JH-S5, and JH-S8. Consequently, the modal abundance of plagioclase in experiments JH-S1 and JH-S2 were very similar (~26-27%) and were therefore used for modeling purposes for the other three experiments (Table 8). The only case where the rim and interior were easily distinguishable was in experiment JH-S8 and the modal areas of these regions were used in the $D_{In}^{ag+plag/aqueous}$ calculation.

All partition coefficients ($D_{In}^{plag/aqueous}$, $D_{In}^{ag/aqueous}$, and $D_{In}^{ag+plag/aqueous}$) can be found in Table 8. Overall, these partition coefficients increase with increasing water/rock (Figure 17 and 18). Note that in these figures, experiment JH-S5 was plotted both with and without an analysis that yielded an anomalously high indium concentration (3561 ppm) that was three times as high as the second highest concentration. By adding

an additional data point without this high value, I present an alternative and perhaps a more representative composition for this experiment in case this analysis was indeed anomalous. When this analysis is removed, the $D_{In}^{ag+plag/aqueous}$ of JH-S3 and JH-S5 are very similar. $D_{In}^{ag+plag/aqueous}$ values range from 0.29 ± 0.08 to 3.32 ± 0.20 as water/rock increases from 1 to 2, the $D_{In}^{ag+plag/aqueous}$ remains about the same but as water/rock increases from 2 to 10, the $D_{In}^{ag+plag/aqueous}$ increases. However, this trend of increasing $D_{In}^{ag+plag/aqueous}$ with increasing water/rock may be simply due to adding more indium by mass into the system by increasing water/rock. By doing so, the concentration of indium in the aqueous solution will be the same initially. Although, there is more indium by mass in the system, the concentration of indium in the aqueous solution will be less sensitive to change as indium partitions into the altered basaltic glass. In other words, the concentration of indium in the aqueous solution will decrease at a slower rate when higher water/rock are present.

Table 7. Partition coefficients calculated for each region in the altered basalt. $\mathbf{D_{In}^{ag+plag/aqueous}}$ is calculated by multiplying $\mathbf{D_{In}^{ag/aqueous}}$ and $\mathbf{D_{In}^{plag/aqueous}}$ by their area abundance and summing them together. *The area percentages in JH-S3, JH-S5 and JH-S8 are estimated based on the average of JH-S1 and JH-S2.

	JH-S1 *(W/R = 1)*	**JH-S2** *(W/R = 2)*	**JH-S3** *(W/R = 3)*	**JH-S5** *(W/R = 3)*	**JH-S8** *(W/R = 10)*
$\mathbf{D_{In}^{ag/aqueous}}$	0.42 ± 0.05	0.39 ± 0.11	0.77 ± 0.06	1.16 ± 0.31	4.21 ± 0.25
$\mathbf{Area_{ag}\%}$	73.8%	72.7%	73.3%*	73.3%*	73.3%*
$\mathbf{D_{In}^{plag/aqueous}}$	0.05 ± 0.01	0.04 ± 0.02	0.20 ± 0.02	0.26 ± 0.13	0.88 ± 0.31
$\mathbf{Area_{plag.}\%}$	26.2%	27.3%	26.7%*	26.7%*	26.7%*
$\mathbf{D_{In}^{ag+plag/aqueous}}$	0.32 ± 0.04	0.29 ± 0.08	0.62 ± 0.04	0.92 ± 0.23	3.32 ± 0.20
Efficiency of Removal	75 ± 2%	87 ± 3%	83 ± 1%	77 ± 4%	75 ± 1%

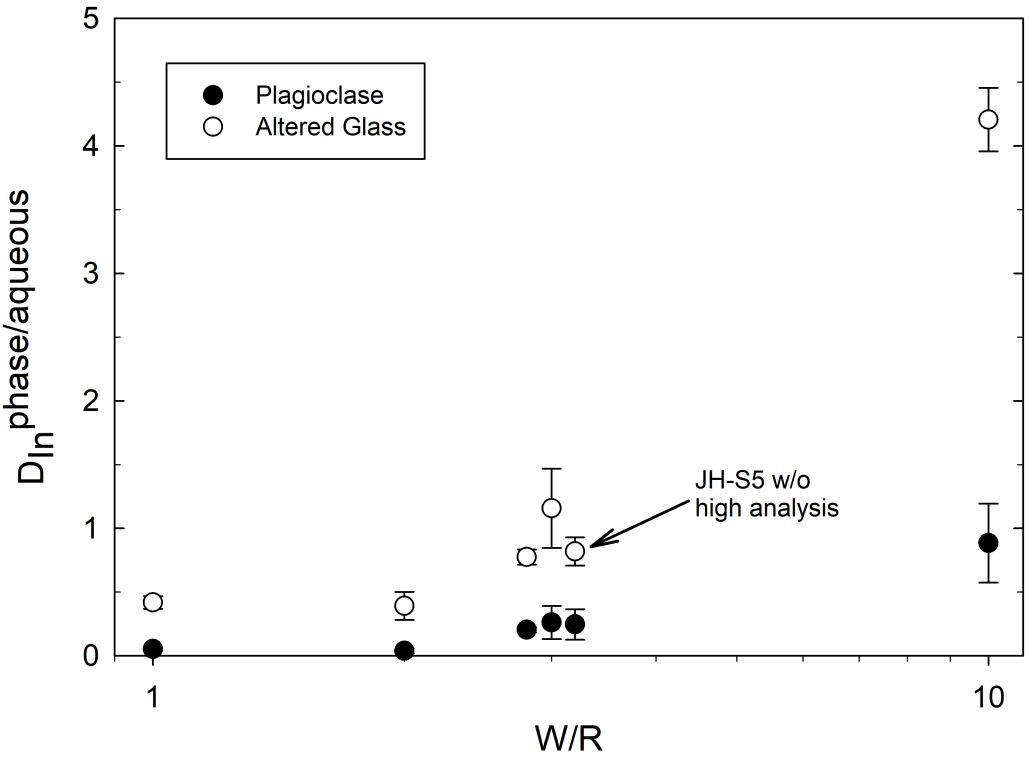

Figure 17. Partition coefficients for the altered glass or plagioclase and the aqueous solution. Experiments JH-S3 and JH-S5 both have water/rock = 3 but are plotted side by side in order to distinguish them. JH-S5 was also calculated without an analysis with an anomalously high indium concentration that is four times larger than the average of the other analyses.

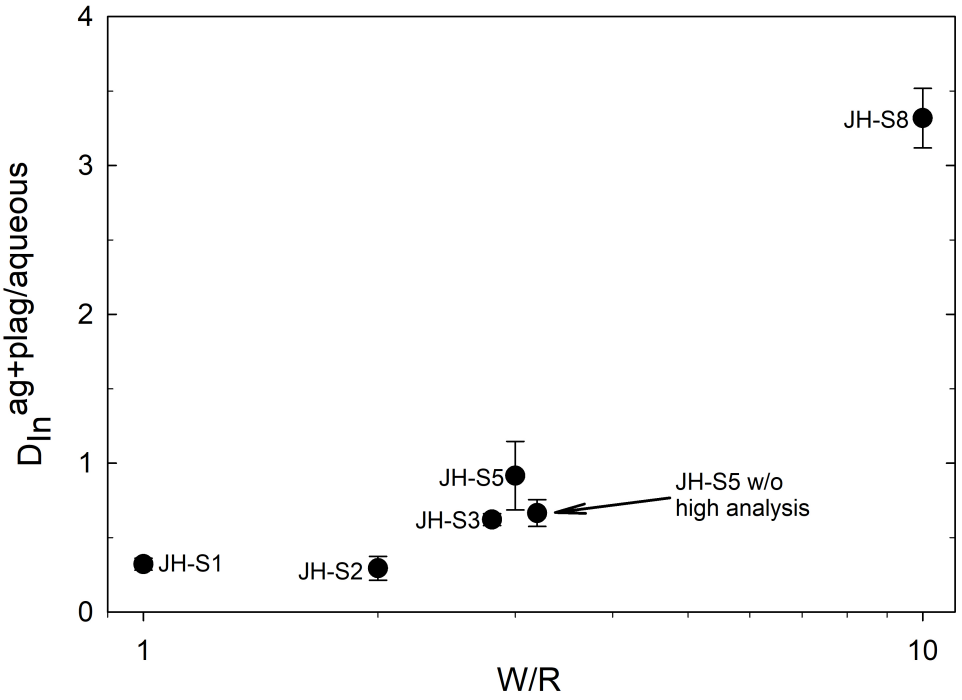

Figure 18. $\mathbf{D_{In}^{ag+plag/aqueous}}$ for each experiment plotted versus water/rock. Experiments JH-S3 and JH-S5 both have water/rock = 3 but are plotted side by side in order to distinguish them. Note that JH-S5 is once again calculated with and without the high indium analysis.

Partition coefficients do not fully describe the geochemical behavior of indium in these experiments. For example, if two experiments had a $D_{In}^{ag+plag/aqueous}$ = 1 but one had a water/rock = 1 and the other had a water/rock = 10 (i.e. same concentration of indium in the aqueous solution and altered basalt), the resulting efficiencies of removal would be 50.0 % and 90.9%, respectively. Therefore, the efficiency of which indium can be removed from an altered basalt into the aqueous solution must be evaluated in order to fully understand how indium behaves in these experiments. Efficiencies of removal were calculated for each experiment (Table 8, Figure 19). Efficiencies of removal show a trend of increasing as water/rock increases from 1 (75 ± 2 %) to 2 (87 ± 3%) and then decreasing as water/rock increases from 2 to 10 (75 ± 1%). This is an intriguing trend

because as water/rock increases, the concentration of indium in the altered basaltic glass increases and the bulk partition coefficient generally increases. Equation 4 (Section 3.3) shows that as the partition coefficient increases, the efficiency of removal decreases. Conversely, as water/rock increases, the efficiency of removal increases. The efficiency of removal trend displayed in these experiments can generally be described as a cancelation of these two effects. The question becomes what effect does water/rock play in the partitioning of indium and is it related to changes in acidity and/or mineralogy?

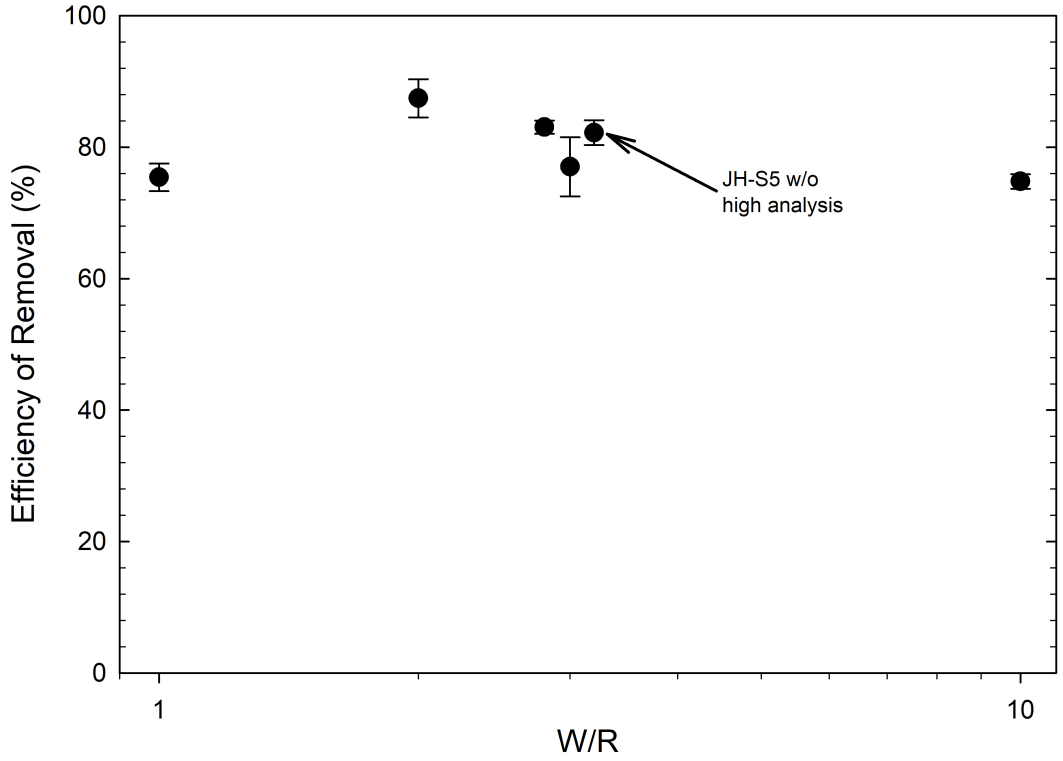

Figure 19. Efficiencies of removal for the high pH, sulfur-bearing seawater experiments. Experiments JH-S3 and JH-S5 both have water/rock = 3 but are plotted side by side in order to distinguish them. Note that JH-S5 is once again calculated with and without the high indium analysis.

Water/Rock Effect

As in the low pH experiments that utilized an HCl-bearing aqueous solution, the alteration assemblage depends on the composition of the aqueous solution used in these seawater experiments. However, in the case of these initial high pH, sulfur-bearing seawater experiments, the acidity of the aqueous solution is generated by hydrolysis reactions that result from the hydrothermal alteration of basalt by seawater. This induces a decrease in pH (at 25°C) from ~8 (pH value of seawater) to 3-4 at 500°C (Mottl et al., 1979). The ability of seawater to maintain these acidic conditions is reliant on the water/rock. At a water/rock ~50, acidic conditions can be produced and maintained indefinitely (Bischoff and Dickson, 1975; Mottl and Seyfried, 1980; Mottl, 1983; Seyfried and Bischoff, 1977; Seyfried and Mottl, 1982), although at very high water/rock there will be a point at which buffer capacity is reached and pH changes very little. Each of the experiments performed in this study have water/rock well under the required value to maintain maximum acidic conditions. Consequently, each of these experiments likely experienced an increase in pH during the experiment. This cannot be said with certainty because pH was not directly measured. However, Bischoff and Dickerson (1975) measured the change in pH over time at 200°C and noticed that after a period of around 40 days (~6 weeks), the pH increased by more than 0.5 above the minimum pH, which was generated initially. This likely implies that the pH of the aqueous solutions in this study also increased during the experiment. Nevertheless, it is important to note that the values of Bischoff and Dickerson (1975) are not directly relatable to these experiments as their experiments likely had a different pH due to the temperature difference. Mottl et al.

(1979) and Hajash (1975) found that the pH of the aqueous solution at quench by this process decreased from 300°C to 500°C.

Despite the water/rock being at rock-dominated values, it likely still played an important role in the generation and maintenance of acidic conditions. Because hydrolysis reactions produce the acidity in the aqueous solution, an increase in the amount of aqueous solution relative to the rock (i.e. increase water/rock) from 1 to 10 will allow hydrolysis reactions to occur approximately ten times more often on a molar basis. Consequently, increasing water/rock should result in more acidic conditions. These acidic conditions are an important mechanism for indium partitioning in hydrothermal environments.

Another way water/rock influences the partitioning of indium from aqueous solution into the altered basalt is its effect on alteration mineralogy. The aqueous solution (i.e. seawater) used in these experiments contains significant quantities of various cations and anions (i.e. Mg^{2+}, Na^{+}, K^{+}, SO_4^{2-}, etc.), which will exchange for cations in the basalt, namely Ca^{2+}. As water/rock increases, the moles of cations in the seawater increase relative to the moles of exchangeable cations in the rock. The model of Mottl (1983) (Figure 15) suggests that as water/rock increases, the abundance of chlorite and quartz increases and epidote and actinolite decreases. At water/rock < 10, the altered basalt is expected to be epidote + actinolite-rich, whereas at water/rock > 10, the altered basalt would be chlorite + quartz-rich. This change in mineralogy may greatly influence the partitioning of indium because secondary ferromagnesian phases may sequester indium at various efficiencies.

Unfortunately, the experiments in this study use water/rock from 1 to 10 and do reach the high water/rock required to drastically change the alteration mineralogy according to Mottl's (1983) model. Despite this, there is a small decrease of Na_2O in the interior as W/R increases (described above in the Results section), which may suggest plagioclase becomes less abundant at higher water/rock. However, I do not notice any significant differences in the major element geochemistry of the altered rim that would indicate there is any significant difference in mineralogies across the five experiments. Consequently, it is not possible to conclude that changing mineralogy plays a significant role in the sequestration of indium in these experiments. It is possible that a wider range of water/rock and longer run times would result in varying alteration assemblages (i.e. varying abundances of ferromagnesian phases) and would have show a clearer effect on the sequestration of indium.

4.5 Conclusions

Partition coefficients for indium were determined experimentally by altering basaltic glass with an aqueous solution that consisted of ~90% seawater and ~10% $InCl_3$-bearing distilled water. Generally, $D_{In}^{ag+plag/aqueous}$ increased with increasing water/rock and ranged from 0.29 ± 0.08 to 3.32 ± 0.20. Efficiencies of removal range from 75 ± 1% to 87 ± 3%. However, these efficiencies initially increase as water/rock increases from 1 to 2 and then decrease as water/rock increases from 2 to 10. This trend can be explained using Equation 4, and recognizing the rate of increase of $D_{In}^{ag+plag/aqueous}$ must be higher than the rate of increase of water/rock as it increases from 2 to 10. I am, however, unable to fully identify the cause of this change. The efficiency of removal might continue to

increase due to the effect water/rock has on the acidity of the aqueous solution. The cause of this change could also be due to changes in alteration mineralogies, yet geochemical analyses would suggest that there is no distinct difference. Additional experiments that have longer run times may elucidate this problem as the basalt will have longer time to alter.

5. Implications

5.1 Application to Mineral Exploration

This work can be directly applied to the development of exploration vectors for the discovery of indium-bearing hydrothermal ore deposits. This study found that water/rock had the largest effect on the partition coefficient of indium between an aqueous fluid and altered matrix. Using these data, models can be generated in order to estimate the efficiency of removal of indium. For example, Figure 20 was constructed with data from the low initial pH, HCl-bearing experiments. The model poses two scenarios for which water/rock is the only independent variable. Our data suggest that by doubling the water/rock from 1 to 2, 29% more indium is removed from the basalt into the aqueous fluid, such that more indium is available in a potential ore-forming fluid.

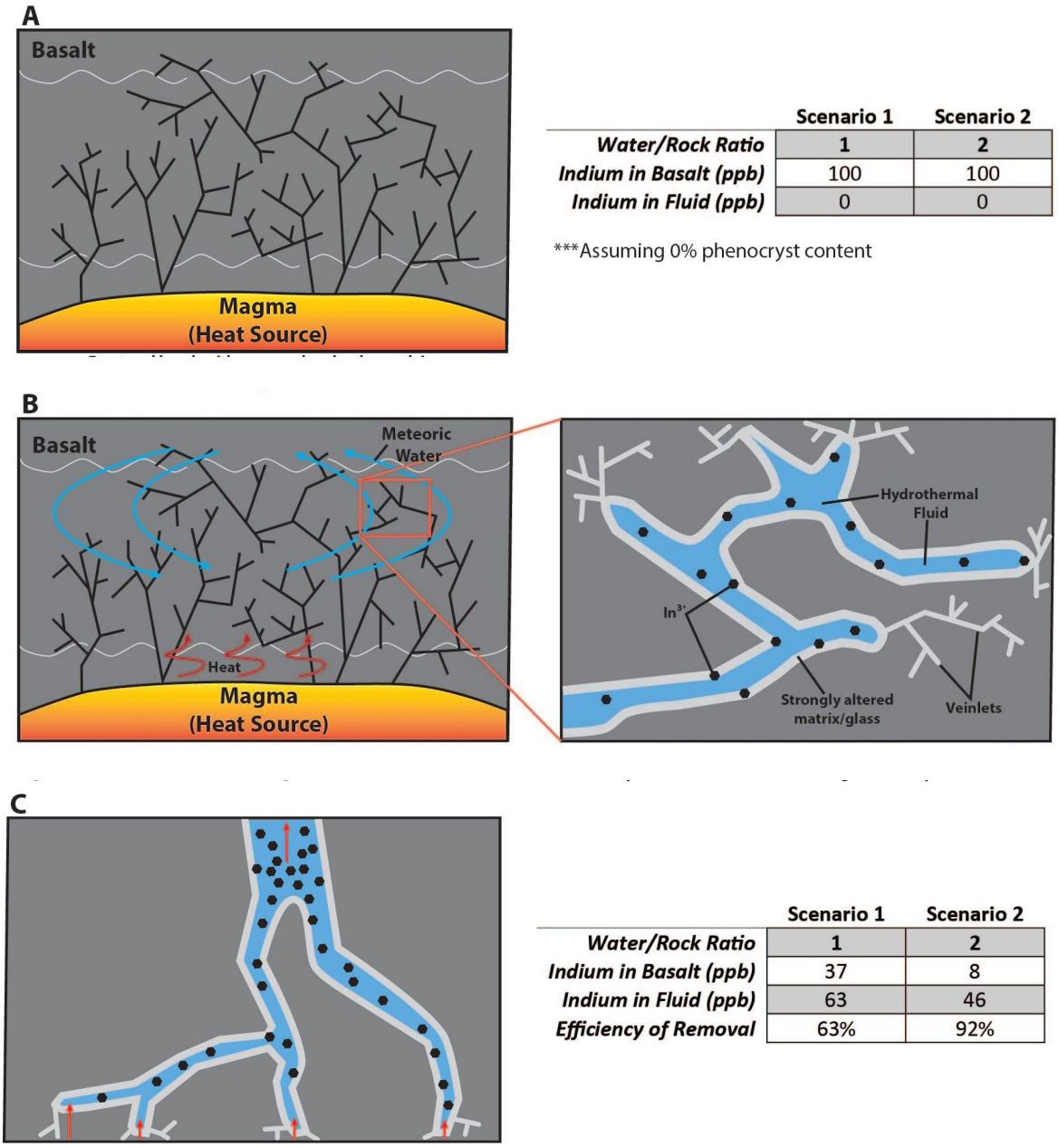

	Scenario 1	Scenario 2
Water/Rock Ratio	1	2
Indium in Basalt (ppb)	100	100
Indium in Fluid (ppb)	0	0

***Assuming 0% phenocryst content

	Scenario 1	Scenario 2
Water/Rock Ratio	1	2
Indium in Basalt (ppb)	37	8
Indium in Fluid (ppb)	63	46
Efficiency of Removal	63%	92%

Figure 20. Efficiency of removal model: (A) Fractured basalt is underlain by magma chamber. The basalt has 100 ppb indium. Scenario 1 has a water/rock = 1, whereas Scenario 2 has a water/rock = 2. (B) Circulating meteoric water is heated by the magma chamber, which hydrothermally alters the basalt. As this occurs, indium is preferentially removed from the altered matrix/glass into the aqueous fluid. (C) By doing so, this solution can be transported and potentially form an ore deposit. By the end of this model, the efficiency of removal for a system with a water/rock = 2 is 29% higher than a system with a water/rock = 1.

In mineral exploration, these results can be used to help estimate the quality of the deposit of interest. To do so, the effective water/rock must be determined through the use of stable isotope data. Most studies use O and H isotopes in order to make their water/rock determinations, although other studies focus on the use of other stable isotopes (i.e. Li, B, and C), (Fernández-Nieto et al., 2003; Simon et al., 2017). Taylor (1978) derived a set of mass balance equations that relate water/rock to stable isotope data:

$$\frac{W}{R} = \left(\frac{\delta^{f}_{rock} - \delta^{i}_{rock}}{\delta^{i}_{water} - (\delta^{f}_{rock} - \Delta_{r-w})}\right) \quad (5)$$

where W/R is the ratio of an element in water to that same element in rock (i.e. atom %) and $\Delta_{r-w} = \delta^{f}_{rock} + \delta^{f}_{water}$. For example, if O isotopes were used, W/R would define the ratio of oxygen in water to the ratio of oxygen in rock (i.e. water/rock by atom %). Therefore, a water/rock (by mass) = 1 will result in about a water/rock (atom %) = 2 because there is ~89 wt% O in water and 45-50 wt% O in a typical granitic rock (Taylor, 1978). $\Delta_{r\text{-}w}$ should ideally be calculated by taking into account the amount of oxygen each mineral in the altered rock contributes to the overall whole-rock oxygen isotope signature. Miller et al. (2001) provides an equation to determine $\Delta_{r\text{-}w}$:

$$\Delta_{r-w} = \Sigma P_i \, (A_i 10^6 T^{-2} + B_i) \quad (6)$$

where P_i is the proportion of oxygen atoms that mineral *i* contributes to the final altered rock and A_i and B_i are fractionation coefficients from mineral *i*-water. However, calculating $\Delta_{r\text{-}w}$ in this manner is often not feasible and studies often assume mineral(s) (i.e. feldspar, chlorite, etc.) are in isotopic equilibrium with the rest of the rock. This enables the use of mineral-water geothermometers, which may then be used to calculate $\Delta_{mineral\text{-}water}$ at any temperature (Taylor, 1978). Initial $\delta^{18}O_f$ can be determined using fluid

inclusion data (Ohmoto and Rye, 1974), whereas initial $\delta^{18}O_r$ can be estimated from either evaluating adjacent unaltered rocks or by using average values from similar rock types. Lastly, Equation 5 only applies to closed systems, although Taylor (1978) also has calculations for open system behavior.

5.2 $\delta^{18}O$ as a Tool for Exploration Potential

Numerous previous studies have focused on utilizing $\delta^{18}O$ signatures of hydrothermally altered rocks as potential exploration vectors (Green and Taheri, 1992; Hoy, 1983). Rearranging Equation 5 to solve for δ^{f}_{rock} reveals that the $\delta^{18}O$ signature of a hydrothermally altered rock is influenced by multiple variables, such as, water/rock, fluid composition, rock composition (rhyolites and basalts can have different $\delta^{18}O$), temperature, and mineralogy:

$$\frac{\frac{W}{R}(\delta^{i}_{water} + \Delta_{r-w}) + \delta^{i}_{rock}}{1 + \frac{W}{R}} = \delta^{f}_{rock} \quad (7)$$

where $\Delta_{r\text{-}w}$ accounts for the effects of both temperature and mineralogy (Equation 6). When pure seawater ($\delta^{18}O$ ~0‰) hydrothermally alters rock with a given initial $\delta^{18}O_r$ and forms a given alteration assemblage, variations in temperature and water/rock will control the regional isotopic signature of the altered rock. This can result in distinct $\delta^{18}O$ haloes where concentric $\delta^{18}O$ contours form around the ore deposit of interest (Green and Taheri, 1992; Green et al., 1983). Hoy (1993) correlated $\delta^{18}O$ signatures of the whole rock with the tonnage of multiple deposits in the Noranda District, Quebec. As previously discussed, these isotopic signatures could have been produced by any number of potential

variables. Nonetheless, previous work and work done in this thesis has shown that temperature and water/rock can affect the partitioning of metals in hydrothermal environments. Therefore, temperature and/or water/rock are reasonable hypotheses for the primary variables causing variations in $\delta^{18}O$ for hydrothermal ore deposits within a given district, where δ^{i}_{rock} and δ^{i}_{water} may be assumed to be constant. If that is indeed the case, temperature and/or water/rock should correlate well with tonnage. In order to test this hypothesis, temperatures, water/rock, and tonnages of known hydrothermal deposits were collected from the literature (Table 9). For this exercise, I only considered water/rock that were determined using oxygen isotopes either by itself or in conjunction with other stable isotopes.

There are a few challenges associated with compiling these data and calculating water/rock. First, isotopic compositions and temperatures are often reported as a wide range of values. Second, the tonnages of a deposit should be reported as production plus reserves, although some sources only report production. Reserves are estimates that are subject to change over time as economic conditions and knowledge of the deposit grows. Third, these calculations often yield a range of potential water/rock, which in some cases are not well constrained. For example, Figure 21 displays data of a hypothetical deposit formed from a rock with an initial $\delta^{18}O_r$ of +8‰ and an initial $\delta^{18}O_w$ of 0‰. Hypothetical temperatures of alteration range from 200-275°C and result in a 100% chlorite assemblage (i.e. $\Delta_{r\text{-}w} = \Delta_{chlorite\text{-}water}$) with final $\delta^{18}O_r$ of +4‰ (Scenario 1) or +2‰ (Scenario 2). By assuming two different δ^{f}_{rock}, the calculated water/rock (atom %) becomes significantly different. Scenario 1 results in water/rock (atomic %) of 1.1 to 2.3, whereas Scenario 2 results in a range of 4 to ∞. Consequently, it is sometimes only

possible to report a minimum water/rock value. Considering all of these uncertainties and challenges together, it is only possible to qualify, not quantify, a relationship between temperature–tonnage and water/rock–tonnage.

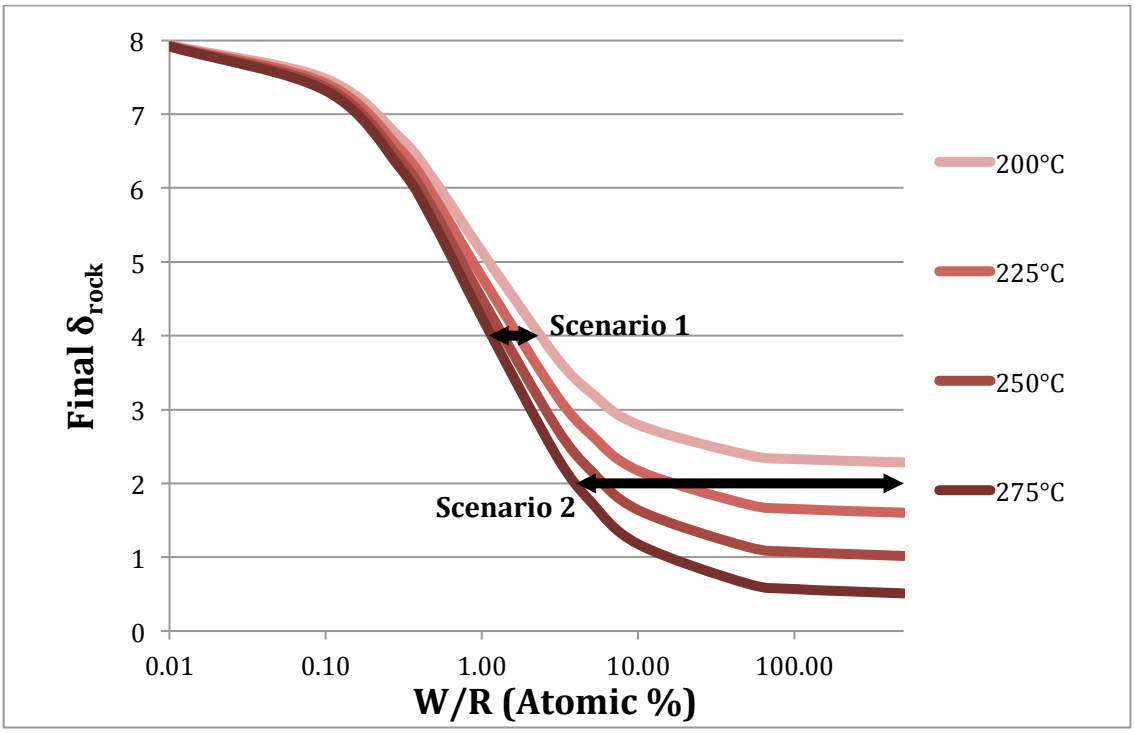

Figure 21. Calculated scenarios for $\boldsymbol{\delta^{f}_{rock}}$ a function of water/rock. Note the variation in the spread of water/rock for different values of the final $\boldsymbol{\delta^{f}_{rock}}$. In Scenario 1, there is a small range of possible water/rock, whereas in Scenario 2, the water/rock could reach to infinity. Consequently, Scenario 2 would only produce a minimum water/rock.

Table 8. Hydrothermal deposits, water/rock, temperatures of formation and estimated tonnages.

Deposit	Type	Location	T (°C)	Water/Rock	Tonnage (Mt)	References
Kidd Creek	VMS	Ontario, CAN	>300	>2.7	38	Huston & Taylor, 1999; Huston et al., 1995
Horne, Noranda	VMS	Quebec, CAN	250-350	≥2	67.6	Hoy, 1993; MacLean & Hoy, 1991
Amulet, Noranda	VMS	Quebec, CAN	250-350	>1	4.5	Beaty and Taylor, 1982; Hoy, 1993
Corbet, Noranda	VMS	Quebec, CAN	250-300	**0.5 to 2.3**	2.7	Barrett et al., 1993; Hoy, 1993
Kosaka & Fukazowa	VMS	Japan	200-400	>0.5	17.8	Green et al., 1983; Werner et al., 2017
Thalanga	VMS	Australia	150-250	**0.1 to 0.2**	5.8	Miller et al., 2001
LaRonde Penna	VMS	Quebec, CAN	~150	0.5 to 26.7	78.5	Beaudoin et al., 2014
Apliki	VMS	Cyprus	>220-300	>1 to 5	1.5†	Heaton and Sheppard, 1976
Kokkinopezoula	VMS	Cyprus	>220-300	>1 to 5	5†	Heaton and Sheppard, 1976
Limni	VMS	Cyprus	>220-300	>1 to 5	4.2†	Heaton and Sheppard, 1976
Mathiati North	VMS	Cyprus	>220-300	>1 to 5	2.5†	Heaton and Sheppard, 1976
Mavrovouni	VMS	Cyprus	>220-300	>1 to 5	15†	Heaton and Sheppard, 1976
Mousoulos-Kalavasos	VMS	Cyprus	>220-300	>1 to 5	6.9†	Heaton and Sheppard, 1976
Skouriotissa	VMS	Cyprus	>220-300	>1 to 5	5.4†	Heaton and Sheppard, 1976
Hishikari	Epithermal	Japan	170-250	0.1 to 3.0	5.2	Faure et al., 2002

Gies (Geis)	Epithermal	Montana, USA	225-300	<0.1	<0.1†	Zhang and Spry, 1994
Mule Canyon	Epithermal	Nevada, USA	>200	~1	8.2	John et al., 2003
Tonopah	Epithermal	Nevada, USA	250-300	>1	2.5	Taylor, 1973; Saunders, 1984
Comstock Lode	Epithermal	Nevada, USA	250-300	0.2 to 2.5	18	Taylor, 1973; Berger et al., 2003
Goldfield	Epithermal	Nevada, USA	125-200	0.2 to 1.5	11.2	Taylor, 1973; Rockwell, 2000
Meikle	Carlin	Nevada, USA	~220	~1	8.5†	Emsbo et al., 2003
Sierra Menera	Gossan	Spain	100-150	>10	78	Fernández-Nieto et al., 2003

All water/rock are calculated by mass

*Bolded water/rock were calculated in this study.

† Tonnages were obtained by using the USGS Mineral Resource Data System (MRDS) at https://mrdata.usgs.gov/mrds/.

Notes: Comstock Lode tonnage reported as minimum tonnage produced (Berger et al., 2003). Water/rock of Comstock Lode and Goldfield were estimated based on water/rock plots made by Taylor, 1973. Water/rock experienced at Cyprus mines within the Troodos complex are the same because Heaton and Sheppard used various sample locations around the complex to determine a single water/rock.

In addition to water/rock reported in other studies, minimum water/rock were calculated herein for two deposits, the Corbet and Thalanga deposits. In order to perform this calculation, isotope and temperature data were collected from various sources in order to calculate $\Delta_{r\text{-}w}$ values. Often studies only reported final whole-rock isotopic composition and not modal mineralogy. This presents a problem when calculating $\Delta_{r\text{-}w}$ because it is ideally calculated by using Equation 6, which accounts for the fraction of oxygen a given mineral contributes to the assemblage. Two different methods were employed for calculating $\Delta_{r\text{-}w}$ for the two deposits (discussed below). Once $\Delta_{r\text{-}w}$ was calculated, water/rock (atom %) vs. δ^{f}_{rock} plots were created to display the range of data for each deposit including δ^{i}_{water}, temperature, and mineralogy. All values used in calculations are found in Table 10. Minimum water/rock or ranges of possible water/rock were subsequently determined by plotting the average reported δ^{f}_{rock} of the deposit. These values are calculated in order to display how water/rock calculations work and to generate an approximate water/rock for these deposits. The specific methodology used to calculate water/rock for each deposit follows:

Table 9. Data used for calculating the water/rock of the Corbet and Thalanga deposits.

Location	Initial $\delta^{18}O_r$	Final $\delta^{18}O_r$	Initial $\delta^{18}O_w$	T (°C)
Corbet	6‰	2.0‰	-2.0‰	250-300
Thalanga (a)	8‰	10.7‰	2.5‰	150-200
Thalanga (b)	8‰	9.3‰	2.5‰	200-250

(1) For the Corbet deposit, mineralogical and isotopic data was taken from Barrett et al. (1993) and Hoy (1993). Ore metals in the Corbet deposit are likely sourced from two volcanic rocks, the Flavrian Andesite and the Northwest Rhyolite, but is hosted within

the more altered Flavrian Andesite. Alteration mineralogies range from chlorite-rich zones near the orebody to chlorite + sericite + quartz + albite above the ore body (Barrett et al., 1993). When determining the mineralogy used to calculate water/rock, the chlorite-rich zone was chosen as Barrett et al. mention this likely represents the highest degree of alteration given that the formation of chlorite and sericite is an indication of the alteration of feldspar and the mobilization of Al. Because chlorite-rich regions are almost entirely chlorite ± quartz ± sericite, the water/rock calculation assumes two end member cases: (a) 100% chlorite and (b) 50% chlorite + 50% sericite. Therefore, for case (a), $\Delta_{r\text{-}w}$ was calculated by using $\Delta_{chlorite\text{-}water} = 1.56\ (10^6/T^2) - 4.70$ (Wenner and Taylor, 1971) at temperatures of 250°C and 300°C. In the case of (b), $\Delta_{r\text{-}w}$ was calculated by using Equation 6 and the values in Table 11 at temperatures of 250°C and 300°C. Initial $\delta^{18}O_r$ was set to +6‰ as andesites at Noranda typically range from +5-6‰ (Beaty and Taylor, 1982). Initial $\delta^{18}O_f$ values are estimated to range from -4 to 0‰. After converting the water/rock (atom %) to water/rock using a value of 46 wt% O for andesites (calculated using data from Wilkinson, 1986) and assuming a final $\delta^{18}O_r$ of +2‰, this methodology provides a water/rock (by mass) = 0.5 to 2.3 (Figure 22).

Table 10. Mineral fractionation factors (i.e. $\Delta_{mineral\text{-}water)}$ used in determining $\Delta_{r\text{-}w}$.

Mineral	A	B	Reference
Quartz	3.38	-2.9	Clayton et al., 1972
Sericite	2.38	-3.4	O'Neil and Taylor, 1969
Feldspar	2.91	-3.41	O'Neil and Taylor, 1967
Chlorite	1.56	-4.7	Wenner and Taylor, 1971

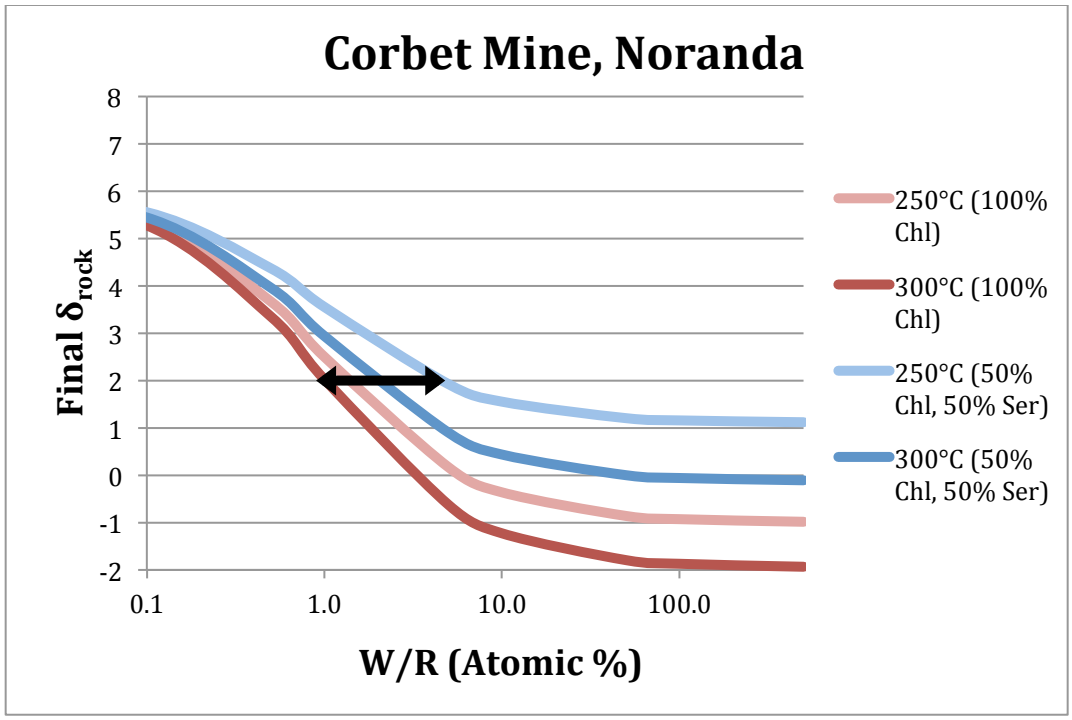

Figure 22. Water/rock (atom %) vs. δ^{f}_{rock} plot for the Corbet deposit assuming an initial $\delta^{18}O_w$ = -2‰. Calculated water/rock range is shown by the black arrows at final δ_r = +2‰.

(2) The Thalanga deposit is located within the Cambro-Ordovician Mount Windsor Volcanics, which is a belt of felsic to intermediate volcanics and marine sediments (Miller et al., 2001). Miller et al. (2001) reported the modal mineralogy and whole-rock isotopic data. Generally, the alteration mineralogy of the deposit fell into can be simplified in the following manner for the sake of this illustration: (Assemblage 1) 33% quartz + 33% sericite + 33% chlorite; (Assemblage 2) 50% quartz + 50% sericite; (Assemblage 3) 50% quartz + 50% feldspar. Using Equation 6 and values listed in Table 11, $\Delta_{r\text{-}w}$ were calculated for temperatures ranging from 150-250°C (Miller et al., 2001). However, Miller et al. (2001) assumes an initial fluid $\delta^{18}O$ composition of 0‰ (seawater), which may have resulted in an underestimation of the temperatures they inferred from their model. Instead, they believe the initial fluid compositions range from

+2 to +3‰. For the purpose of this calculation, an initial $\delta^{18}O_f$ composition of +2.5‰ was chosen. The initial $\delta^{18}O_r$ at Thalanga was chosen to be +8‰ as rhyolites range from about +6-10‰ (Taylor, 1968). Consequently, using a value of +8‰ for $\delta^{18}O_r$ might simplify the deposit too much. However, the measured $\delta^{18}O$ of the altered rocks fit into two populations: (a) final $\delta^{18}O$ values of 10.7 ± 1.4‰ and were altered at temperatures from 150-200°C; (b) final $\delta^{18}O$ values of 9.3 ± 0.7‰ and were altered at 200-250°C (Miller et al., 2001). To account for the two populations, separate water/rock were calculated using the mean final $\delta^{18}O_r$ for each group, resulting in (a) water/rock ranging from 0.1 to 0.2; (b) water/rock (by mass) ranging from less than 0.1 to 0.2 (Figure 23). Therefore, the Thalanga deposit was likely hydrothermally altered at water/rock (by mass) ranging from less than 0.1 to 0.2. If Miller et al. (2001) underestimated the temperatures, then the resulting water/rock would not differ greatly. The water/rock ranges of (a) and (b) might increase slightly but would likely be >0.5. Furthermore, if the $\delta^{18}O_r$ is set to +6‰, the maximum water/rock is still >0.5.

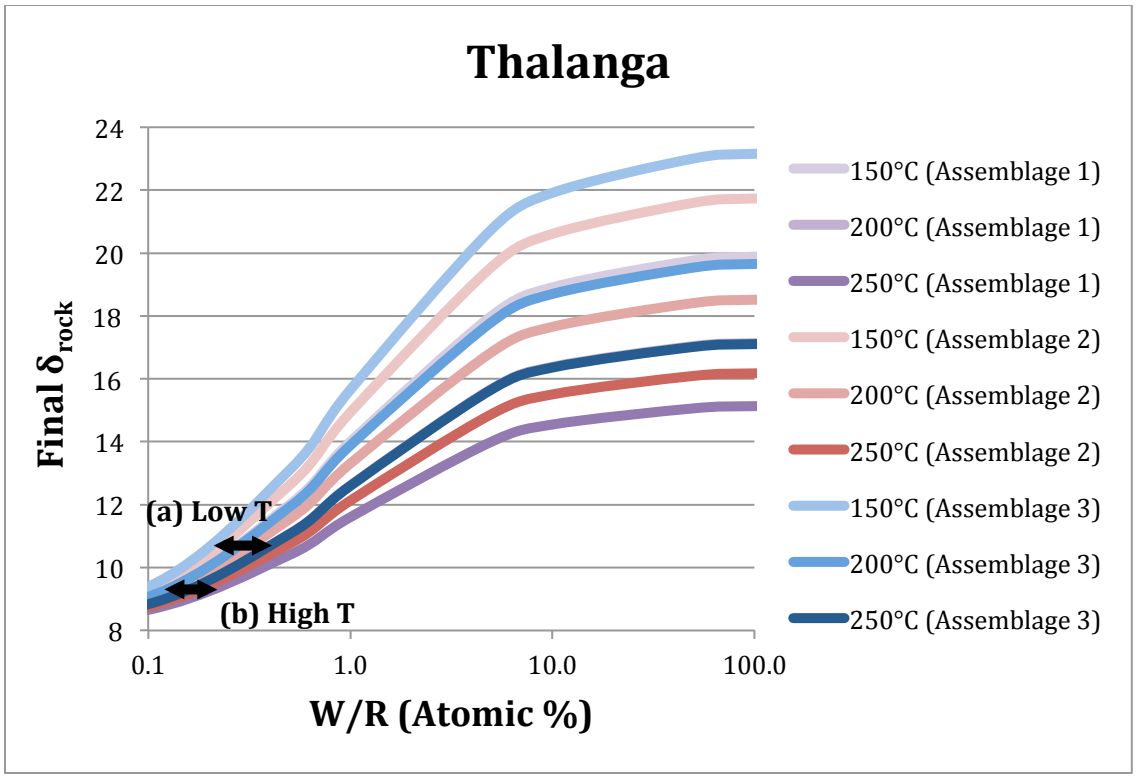

Figure 23. Plot of water/rock (atom %) vs. δ^{f}_{rock} for the Thalanga deposit. Calculated water/rock ranges are shown by black arrows at a final $\delta^{18}O_r$ = (a) +10.7‰ (low temperature assemblages = 150-200°C) and (b) +9.3‰ (high temperature assemblages = 200-250°C).

Relationships between tonnage and minimum water/rock /temperature are plotted in Figure 24 and 25. Interestingly, there appears to be a small correlation of water/rock and tonnage for VMS and epithermal deposits, whereas temperature does not correlate with either. This could suggest that a high water/rock may be essential for creating large, high tonnage hydrothermal ore deposits. Although both water/rock and temperature are important variables when considering mobilizing metals, the transport of metals is limited by the amount of hydrothermal aqueous fluid in the system. For example, a source rock that experienced hydrothermal alteration at high water/rock will be more strongly altered and have a higher efficiency of removal for various metals, thus contributing more metals

to the hydrothermal system. Quite simply, the more hydrothermal fluid there is, the more material can be transported.

In summary, $\delta^{18}O$ anomalies have been suggested as potential exploration vectors for hydrothermal deposits. These anomalies are associated with water-rock interaction that results in $\delta^{18}O$ haloes around the deposit of interest. Although many variables contribute to the $\delta^{18}O$ composition of a rock, temperature and water/rock are likely the two most important factors. Hoy (1993) noticed that these $\delta^{18}O$ anomalies correlate well with tonnage in the Noranda district, Quebec. However, no work was completed to explain whether or not temperature and/or water/rock correlated to tonnage as a proxy for $\delta^{18}O$. Water/rock, temperature, and isotope data from various papers was collected as a part of this study in order to examine this. The results show that water/rock may correlate with tonnage, whereas temperature does not, thus signifying that high water/rock may be an essential characteristic of high tonnage hydrothermal deposits. Therefore, using water/rock as an exploration vector may be useful for indium-bearing deposits and hydrothermal deposits in general.

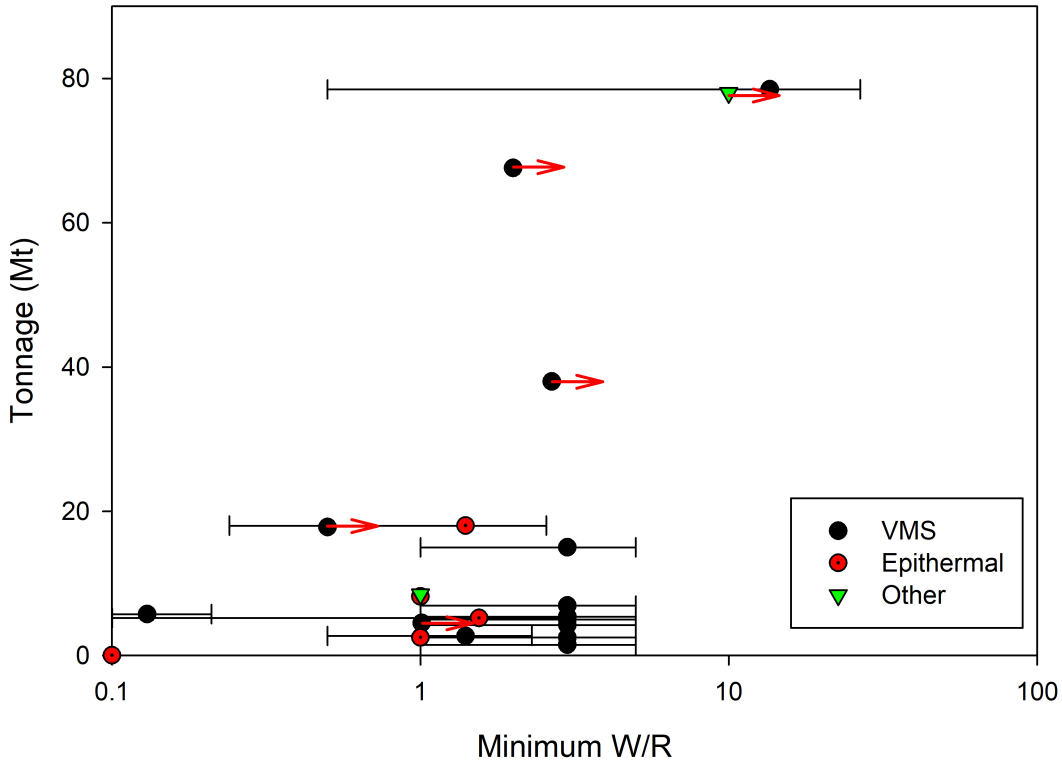

Figure 24. Plot of water/rock vs. tonnage of various hydrothermal ore deposit types found in Table 9. Data points without uncertainty indicate they are an approximation. Arrows indicate that data points are minimum values.

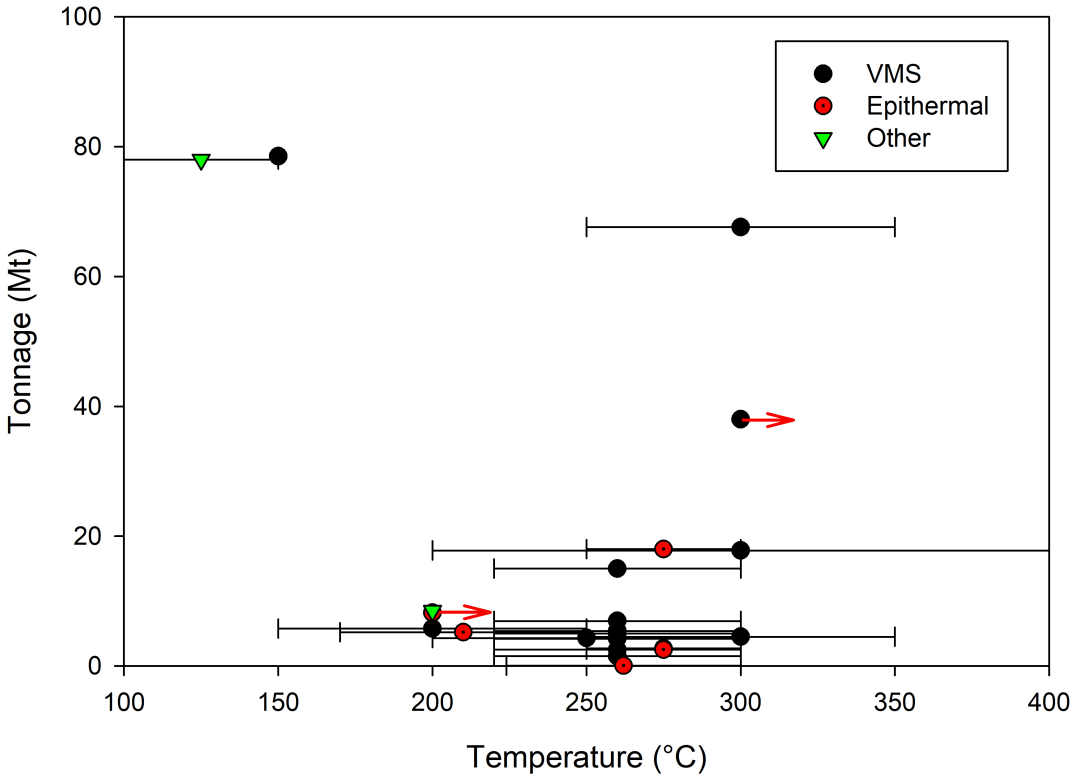

Figure 25. Plot of temperature vs. tonnage of various hydrothermal ore deposit types found in Table 9. Data points without uncertainty indicate they are an approximation. Arrows indicate that data points are minimum values.

6. Appendices

Appendix A. Methods for Creating Starting HCl-bearing Aqueous Solutions

Starting solutions were created by first diluting 12.1 M HCl with distilled water to make a 0.1 or 1 M HCl-bearing aqueous solution. Afterwards, indium metal was dissolved in 12.1 M HCl in a 100 mL beaker. Once the indium was fully dissolved, the beaker was then placed on a hot plate. The added heat induced slow evaporation of the HCl, which resulted in the formation of $InCl_3$ crystals on the bottom of the beaker. $InCl_3$ is highly deliquescent and, consequently, needs to be added to the 0.1/1 M HCl solutions before it has the opportunity to incorporate any water vapor. To do so, the HCl solution was poured into the $InCl_3$-bearing beaker and swirled around to dissolve the crystals. About 20 mL of the 1 M HCl solution was poured into separate glassware, and 0.734 g KCl and 0.563 g NaCl was added to make a 1 M HCl + 0.5 M KCl + 0.5 M NaCl aqueous solution.

Appendix B. Experimental Conditions for Low Initial pH, HCl-bearing Experiments

Table 11. Experimental conditions for all low initial pH, HCl-bearing experiments. Indium concentrations are of the starting aqueous solution. The initial and final masses (m_i and m_f) are the masses of the experimental charge before they were placed in the furnace and after they were taken out of the furnace. Δ mass is the change of the mass of the experimental charge. In the case of JH-B4, the final mass was approximated because the mass was rapidly decreasing while weighing due to a rupture in the experimental charge.

Sample	time (wk)	W/R	In (ppm)	Rock (mg)	Solution (mg)	M HCl	M NaCl, M KCl	NaCl wt.% eq	m_i (mg)	m_f (mg)	Δ mass
JH-B1	2	0.93	368	54.93	50.82	1	0	3.59	1387.93	1384.16	-3.77
JH-B2	2	1.98	368	50.53	100.09	1	0	3.59	1208.91	1267.73	58.82
JH-B4	2	1.95	368	52.48	102.08	1	0	3.59	840.79	756	-84.79
JH-B6	2	1.92	345	55.62	106.86	1	0.5, 0.5	10.52	873.11	822.13	-50.98
JH-B7	2	0.99	345	64.11	63.43	1	0.5, 0.5	10.52	815.65	816.16	0.51
JH-B8	4	1.03	368	79.01	81.63	1	0	3.59	884.16	889.44	5.28
JH-B9	4	1.95	368	55.42	108.19	1	0	3.59	1005.16	997.89	-7.27
JH-B10	4	1.07	345	61.62	65.95	1	0.5, 0.5	10.52	791.34	791.65	0.31
JH-B11	4	1.00	503	69.91	69.97	0.1	0	0.36	884.34	927.81	43.47
JH-B12	4	0.99	503	54.83	54.29	0.1	0	0.36	806.28	807.47	1.19
JH-B13	4	1.95	503	59.21	115.4	0.1	0	0.36	917.07	1041.23	124.16
JH-B14	4	3.02	368	37.02	111.63	1	0	3.59	972.9	852.81	-120.09
JH-B15	4	3.01	345	41.97	126.46	1	0.5, 0.5	10.52	1365.36	1358.81	-6.55
JH-B16	4	3.05	503	29.52	90.01	0.1	0	0.36	893.38	879.31	-14.07
JH-B17	8	1.03	368	46.23	47.49	1	0	3.59	1300.67	1301.45	0.78
JH-B18	8	1.98	368	41.28	81.76	1	0	3.59	725.25	740.92	14.75

Appendix C. Method for Calculating Modes

ImageJ is a free image analysis/manipulation program available from the National Institute of Health. Backscatter electron images (raw TIFF images) were read directly into ImageJ and modal analyses (area of minerals) were then performed. BSE images were collected at a magnification of 500x on the starting basalt and select run product regions (Figure 26). The procedure that follows was employed to determine modal abundances based on image gray-scale intensities. In ImageJ, open the BSE image of interest (File → Open). Convert the image to an 8-bit image (Image →Type → 8-bit). The threshold function (Image → Adjust → Threshold) can then be used threshold the phase(s) of interest. Five textural or chemical domains have been identified in all of the BSE images: dark domains, light domains, white grains, phenocrysts, and other (includes ambiguous regions, such as vugs, small vesicles, and alteration products that is too ambiguous to tell where it belongs).

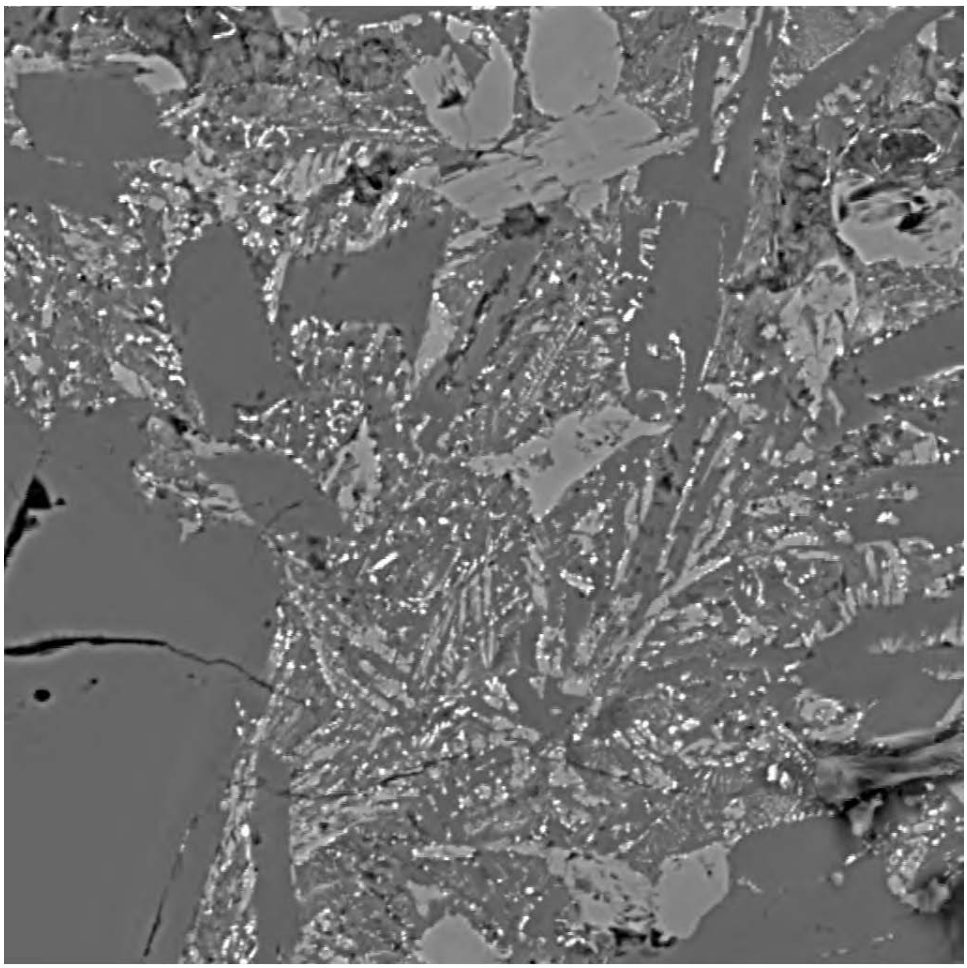

Figure 26. BSE image of experiment JH-B4 Region E (500x) that is uploaded into ImageJ prior to performing the threshold function.

Determination of the Mode of Other Features

Using the threshold function, move the sliders so that the 'other features' are highlighted. On the BSE images, these are generally the darkest features. Once the features have been highlighted, manually record the numeric values for the position of the sliders. Measure the area (Analyze → Measure) of the 'other features' and record the area percentage of the highlighted features. The percentage of 'other features' is used to normalize all other domains since this value will not be used as a component of the mode

for reasons stated above. As a result of not using the areas of the 'other regions', the final mode then assumes that these 'other regions' have the same modal proportions as the rest of the basalt. However, since these regions only consist of ~0-6% of the basalt, the overall effect is small (***Note it is easiest to record the threshold values used for each textural domain, which makes it easier to determine where to start calculating the modes for the next domain and minimize the potential for double counting or skipping regions).

Determination of the Mode of Dark Regions

The dark regions include plagioclase phenocrysts in addition to matrix glass (i.e. region 1). In order to determine the mode of matrix glass, the phenocrysts (microphenocrysts) of plagioclase need to be manually erased. The easiest way to do this is to reopen the original BSE image (Image → Adjust → Threshold → Apply) and manually erase the plagioclase phenocrysts from the dark regions using the pencil tool (Figure 27). Once the plagioclase phenocrysts are erased, measure the area of the dark regions. Save the new image, using 'save as,' for future reference. Quit the program, re-open ImageJ and re-open the original TIFF image.



Figure 27. BSE image of experiment JH-B4 Region E after filtering with ImageJ. Black represents Region 1 (i.e. the dark regions), whereas white represents all other regions.

Determination of the Mode of Light Regions

The light regions include light-colored matrix (i.e. region 2), and pyroxene and olivine phenocrysts. Do not include the bright white grains if possible. You must use the same method as the determination of the dark domain to remove the pyroxene and olivine phenocrysts from the modal concentration. However, some phenocrysts are ambiguous as to whether or not they are matrix or microphenocrysts. If they have straight, well-formed grain boundaries or had a grain size much larger than the surrounding matrix, they were

considered phenocrysts (Figure 28). Typically, light regions tended to be small enough to easily distinguish the light regions from the phenocrysts, but sometimes this determination can be ambiguous. Threshold and measure the area to calculate the mode (record threshold values, and the mode).



Figure 28. BSE image of experiment JH-B4 Region E after filtering with ImageJ. Black represents Region 2 (i.e. light regions), whereas white represents all other regions.

Determination of the Mode of White Grains

Lastly, calculate the mode of the white grains (i.e. region 3; simply the upper threshold number of the light region, to the MAX value of 255). However, because they comprise such a low total of the bulk matrix, the large uncertainty associated with this measurement will not have a large affect on your total bulk composition calculation. To calculate the percentage phenocrysts subtract the sum of the modes of the three domains (dark, light, white grains) from 100. To determine the final modes of the three regions within the matrix (i.e. excluding vesicles and phenocrysts for example), normalize the modes using the following equation, which will calculate the final modes for region 1:

$$\text{modes}_{\text{x-normalized}} = \text{mode}_{\text{x}} * (100(100 - \text{total of modes}_{\text{x,y,z}}))$$

Where x is region 1, y is region 2, and z is region 3.

Appendix D. Long Valley Moat Basalt Composition

Table 12. Composition of the starting basalt matrix and phenocrysts. SD is the standard deviation of the mean (1σ) of the concentrations in a given experiment.

	Na_2O	FeO	CaO	TiO_2	Al_2O_3	MgO	MnO	K_2O	Cr_2O_3	NiO	P_2O_5	SiO_2	Total
Starting Matrix													
	3.15	11.32	7.19	2.47	13.80	4.34		2.35	0.03		0.77	51.78	97.21
	2.50	12.85	6.95	3.17	14.37	3.16		1.53	bd		1.04	50.57	96.15
	4.08	8.82	7.64	2.32	14.89	2.40		2.68	bd		0.65	55.21	98.70
	4.11	9.20	5.42	2.23	16.02	2.53		2.77	bd		0.62	54.02	96.92
	3.92	11.77	5.48	2.33	14.68	2.67		2.65	bd		0.64	53.08	97.22
	4.30	13.37	3.49	1.41	13.34	8.76		1.58	bd		0.35	51.87	98.46
	4.30	10.74	4.31	2.53	16.47	1.37		2.01	bd		0.56	52.38	94.67
	3.89	6.47	8.84	2.18	16.66	2.28		2.31	0.06		0.41	53.48	96.60
	3.89	8.31	9.39	2.07	14.52	5.01		1.91	bd		0.45	53.68	99.23
	4.95	8.23	4.39	1.91	16.59	1.37		2.99	bd		0.53	56.01	96.98
	3.82	8.00	6.83	1.87	16.48	3.23		2.20	bd		0.73	52.74	95.92
	3.54	11.67	5.53	2.63	13.53	2.99		3.11	bd		0.45	53.63	97.11
	3.98	8.39	4.90	2.65	17.97	1.37		3.23	bd		0.61	52.92	96.01
	4.60	9.11	6.93	2.18	15.88	2.57		2.00	bd		0.37	54.34	97.99
	3.97	10.84	5.90	2.41	14.37	2.85		2.70	bd		0.45	54.31	97.79
	3.86	8.46	8.37	2.14	13.29	4.52		2.38	bd		0.46	54.05	97.53
	4.59	9.77	6.30	2.45	15.04	2.56		2.45	bd		0.46	54.39	97.99
	4.05	10.10	5.44	2.35	15.21	2.04		3.12	bd		0.51	55.22	98.06
	4.52	9.41	7.39	2.27	14.43	3.89	0.15	2.17			0.72	54.80	99.77
	5.46	8.38	5.00	1.98	16.40	1.85	0.13	2.84			0.92	56.29	99.29
	5.31	10.81	4.31	2.95	16.00	1.14	0.09	3.04			0.81	54.81	99.30
	4.33	11.22	5.11	2.65	13.71	2.41	0.17	2.98			0.60	53.65	96.87
	5.08	8.74	4.91	2.00	15.54	2.24	0.16	2.94			0.67	57.65	99.96
	3.51	11.88	9.68	2.67	12.00	4.97	0.26	1.78			0.40	51.83	98.99
	4.41	10.40	6.86	2.67	13.16	3.86	0.20	3.13			0.52	53.97	99.21
	4.14	10.85	3.84	2.63	13.57	2.36	0.18	4.17			0.48	53.09	95.34
	4.82	9.30	6.93	2.62	14.44	2.38	0.17	2.95			0.52	55.06	99.23
	3.51	9.06	9.31	2.39	11.98	5.17	0.18	2.48			0.57	51.51	96.19
	5.62	9.58	2.95	2.74	15.55	0.58	0.16	3.27			0.47	57.04	98.01
	5.96	9.11	5.03	2.59	17.47	0.88	0.09	2.22			0.44	55.22	99.03
	5.77	6.27	3.58	1.94	16.15	1.21	0.13	4.00			0.69	58.72	98.49
	4.90	15.54	2.65	2.18	13.19	2.90	0.30	3.07			0.59	53.50	98.86
	5.27	10.79	3.73	2.51	15.37	1.25	0.11	2.91			0.53	54.67	97.16

	Na_2O	FeO	CaO	TiO_2	Al_2O_3	MgO	MnO	K_2O	Cr_2O_3	NiO	P_2O_5	SiO_2	Total
	4.86	8.02	5.15	2.12	15.98	1.37	0.09	3.01			0.66	56.30	97.57
	5.24	5.86	4.63	1.60	16.65	1.51	0.07	3.67			0.58	58.18	98.01
	4.49	7.39	8.15	1.93	14.76	3.94	0.11	2.11			0.46	55.18	98.53
	4.32	9.40	7.39	2.21	13.88	4.00	0.17	2.35			0.50	53.71	97.97
	3.25	10.12	7.05	2.92	12.55	4.57	0.18	3.34			0.54	53.06	97.61
AVG	**4.37**	**9.73**	**5.97**	**2.34**	**14.89**	**2.85**	**0.16**	**2.70**	**0.01**		**0.57**	**54.26**	**97.79**
SD	**0.12**	**0.31**	**0.29**	**0.06**	**0.23**	**0.25**	**0.01**	**0.10**	**0.00**		**0.02**	**0.29**	**0.20**
Plagioclase													
	3.19	0.44	14.14	bd	31.42	0.18		0.20	bd		bd	50.19	99.78
	3.41	0.45	13.69	0.10	31.78	0.09		0.20	bd		bd	52.84	102.55
	3.70	0.47	12.73	0.06	30.08	0.14		0.21	bd		bd	52.40	99.80
	2.90	0.54	14.54	0.06	31.90	0.09		0.19	bd		bd	50.29	100.51
	3.58	0.48	13.36	0.07	30.89	0.15		0.21	bd		bd	51.96	100.70
	3.28	0.55	14.18	bd	31.59	0.15		0.22	bd		bd	51.33	101.31
	4.09	0.36	12.43	0.04	29.92	0.16		0.26	bd		bd	53.08	100.33
AVG	**3.45**	**0.47**	**13.58**	**0.05**	**31.08**	**0.14**		**0.21**	**bd**		**bd**	**51.73**	**100.71**
SD	**0.15**	**0.02**	**0.30**	**0.01**	**0.31**	**0.01**		**0.01**	**bd**		**bd**	**0.44**	**0.37**
Olivine													
		17.39	0.25		0.04	42.61	0.35			0.11		38.72	99.46
		16.79	0.23		bd	42.64	0.19			0.15		38.39	98.41
		16.86	0.23		0.07	43.33	0.20			0.12		39.76	100.59
		17.99	0.21		0.04	41.34	0.26			0.11		38.58	98.53
		17.99	0.20		0.03	42.11	0.26			0.07		39.27	99.93
		19.80	0.21		bd	40.88	0.29			0.10		39.08	100.35
		15.62	0.20		0.04	43.79	0.21			0.18		39.39	99.43
		14.89	0.18		bd	43.63	0.20			0.10		39.75	98.76
AVG		**17.17**	**0.21**		**0.03**	**42.54**	**0.25**			**0.12**		**39.12**	**99.43**
SD		**0.54**	**0.01**		**0.01**	**0.37**	**0.02**			**0.01**		**0.18**	**0.29**
Pyroxene													
	0.31	8.21	19.95	1.18	2.18	16.09	0.18	bd	0.11		0.09	51.55	99.86
	0.35	7.92	19.79	1.31	3.44	15.20	0.15	bd	0.36		0.09	50.88	99.49

	Na_2O	FeO	CaO	TiO_2	Al_2O_3	MgO	MnO	K_2O	Cr_2O_3	NiO	P_2O_5	SiO_2	Total
	0.39	7.78	21.01	1.35	3.30	15.10	0.17	0.02	0.28		0.07	51.68	101.15
	0.36	7.58	20.64	1.22	3.38	15.22	0.20	bd	0.33		0.05	50.82	99.80
	0.45	7.30	20.40	0.80	1.93	15.90	0.17	0.03	0.21		0.05	51.98	99.32
	0.35	7.94	20.55	0.93	2.53	15.69	0.23	0.03	0.28		0.09	51.37	99.99
	0.22	14.39	11.24	0.63	1.81	26.46	0.27	0.03	0.22		0.06	45.19	100.53
	0.33	7.34	20.61	0.84	1.74	15.97	0.21	0.01	0.25		bd	51.91	99.23
	0.39	8.32	20.77	1.42	3.51	15.10	0.23	0.02	0.25		0.10	50.28	100.41
AVG	**0.35**	**8.53**	**19.44**	**1.08**	**2.65**	**16.75**	**0.20**	**0.02**	**0.25**		**0.07**	**50.63**	**99.97**
SD	**0.02**	**0.74**	**1.03**	**0.09**	**0.25**	**1.22**	**0.01**	**0.00**	**0.02**		**0.01**	**0.70**	**0.21**

Appendix E. Major and Trace Element Data

Table 13. Major element data for the altered matrices found in the interior and the rim of the experimental run products. SD is the standard deviation of the mean (1σ) of the concentrations in a given experiment.

	Na_2O	FeO	CaO	TiO_2	Al_2O_3	MgO	Cr_2O_3	K_2O	SiO_2	Cl	MnO	P_2O_5	Total
JH-B1													
Interior 1	3.13	11.53	7.90	2.75	13.48	2.94	bd	0.94	52.50			0.73	95.89
Interior 2	2.71	10.64	6.17	2.30	14.09	2.20	bd	0.98	55.29			0.88	95.26
Interior 3	2.64	14.05	6.26	3.36	12.00	2.06	bd	0.66	54.71			0.74	96.49
Interior 4	2.87	8.00	7.62	1.86	14.28	3.65	0.04	1.24	54.73			0.95	95.25
Interior 5	3.35	8.43	9.88	1.91	15.92	4.46	bd	0.91	52.75			0.48	98.10
Interior 6	0.94	8.26	17.77	1.62	5.90	13.40	0.29	0.24	49.31			0.26	98.00
Interior 7	3.72	11.35	4.68	2.22	16.14	4.66	bd	1.85	46.54			0.84	92.01
AVG	**2.77**	**10.32**	**8.61**	**2.29**	**13.12**	**4.77**	**0.05**	**0.98**	**52.26**			**0.70**	**95.86**
SD	**0.34**	**0.84**	**1.65**	**0.22**	**1.32**	**1.49**	**0.04**	**0.19**	**1.22**			**0.09**	**0.78**
Rim 1	0.27	7.46	0.49	0.29	6.79	17.89	bd	1.48	39.98			bd	74.65
Rim 2	0.14	8.75	1.20	0.55	8.42	15.12	bd	1.60	32.05			bd	67.84
Rim 3	0.33	4.52	0.33	0.13	4.94	20.86	bd	0.29	44.66			bd	76.09
AVG	**0.25**	**6.91**	**0.67**	**0.32**	**6.71**	**17.96**	**bd**	**1.12**	**38.90**			**bd**	**72.86**
SD	**0.05**	**1.25**	**0.27**	**0.12**	**1.01**	**1.66**	**bd**	**0.42**	**3.68**			**bd**	**2.54**
JH-B2													
Interior 1	1.75	11.41	12.63	2.63	10.82	6.43	bd	0.26	51.21			0.33	97.48
Interior 2	2.35	10.94	6.63	2.54	12.51	3.00	bd	0.71	56.21			0.61	95.49
Interior 3	1.23	17.14	5.32	2.69	10.82	8.55	0.04	2.07	46.41			0.42	94.71
Interior 4	2.34	11.29	7.49	2.21	17.63	2.92	0.05	0.80	51.74			0.94	97.41
Interior 5	3.15	10.98	6.05	3.02	15.69	1.49	bd	0.82	55.94			0.69	97.84
AVG	**2.17**	**12.35**	**7.62**	**2.62**	**13.49**	**4.48**	**0.02**	**0.93**	**52.30**			**0.60**	**96.59**
SD	**0.32**	**1.20**	**1.30**	**0.13**	**1.36**	**1.30**	**0.01**	**0.30**	**1.80**			**0.11**	**0.62**
Rim 1	2.50	1.79	8.11	3.76	18.48	3.40	bd	0.50	39.71			1.17	79.44
Rim 2	2.88	0.87	7.69	1.56	21.05	1.81	bd	0.38	45.64			0.21	82.09
Rim 3	2.08	2.04	8.08	3.33	18.55	4.71	0.06	0.52	37.05			1.89	78.30
Rim 4	2.89	1.50	9.59	3.42	22.27	2.32	0.04	0.44	42.87			1.20	86.54
Rim 5	0.42	4.38	4.42	3.93	17.70	5.89	bd	0.92	38.88			0.68	77.22
AVG	**2.15**	**2.12**	**7.58**	**3.20**	**19.61**	**3.63**	**0.02**	**0.55**	**40.83**			**1.03**	**80.72**
SD	**0.46**	**0.60**	**0.85**	**0.42**	**0.87**	**0.75**	**0.01**	**0.09**	**1.53**			**0.28**	**1.67**

	Na_2O	FeO	CaO	TiO_2	Al_2O_3	MgO	Cr_2O_3	K_2O	SiO_2	Cl	MnO	P_2O_5	Total
JH-B4													
Interior 1	3.82	12.12	5.44	3.54	15.22	0.95	bd	1.07	55.59	0.23		0.58	98.50
Interior 2	3.98	9.39	6.76	2.43	15.08	1.75	0.04	1.15	57.85	0.17		0.51	99.07
Interior 3	3.74	10.10	7.08	2.66	14.96	1.68	bd	0.84	56.39	0.18		0.44	98.01
Interior 4	3.54	7.32	7.07	1.89	12.20	3.69	bd	3.12	57.45	0.10		0.87	97.23
Interior 5	4.39	8.81	3.70	2.31	13.80	1.13	bd	3.13	59.68	0.10		0.55	97.59
Interior 6	3.52	10.10	7.05	2.77	15.57	2.86	bd	0.57	55.01	0.15		0.29	97.88
Interior 7	4.31	7.64	3.69	2.12	15.05	1.50	bd	4.21	59.75	0.06		0.54	98.88
Interior 8	3.88	9.09	4.11	1.73	14.07	4.11	bd	2.25	56.43	0.39		0.43	96.43
Interior 9	5.43	9.66	4.48	2.66	15.88	1.47	0.03	2.39	57.12	0.05		0.32	99.49
Interior 10	4.88	10.00	3.55	2.85	15.20	1.17	bd	3.20	56.52	0.08		0.64	98.07
AVG	**4.15**	**9.42**	**5.29**	**2.50**	**14.70**	**2.03**	**0.01**	**2.19**	**57.18**	**0.15**		**0.52**	**98.11**
SD	**0.19**	**0.43**	**0.49**	**0.17**	**0.34**	**0.35**	**0.00**	**0.39**	**0.50**	**0.03**		**0.05**	**0.29**
Rim 1	2.66	6.98	1.97	1.81	7.57	16.39	bd	0.63	19.65	0.05		bd	57.72
Rim 2	2.69	4.82	4.94	1.95	13.86	7.92	bd	1.34	44.13	0.35		0.26	82.19
Rim 3	0.61	4.08	0.63	2.50	3.28	22.03	0.12	0.24	39.92	0.25		0.12	73.74
Rim 4	0.40	4.71	6.30	3.48	4.01	8.39	0.03	0.98	21.16	0.92		3.52	53.70
Rim 5	0.06	2.92	0.37	0.03	0.13	22.83	0.04	bd	40.40	0.32		0.12	67.15
Rim 6	0.22	7.03	13.19	0.85	2.78	12.38	0.32	0.14	50.96	0.10		0.06	88.02
Rim 7	2.85	1.65	8.69	2.70	19.15	2.10	bd	0.69	51.54	0.27		0.91	90.50
Rim 8	1.16	8.04	0.74	0.44	9.46	11.31	0.08	0.66	37.29	0.14		bd	69.31
Rim 9	0.31	8.27	1.74	0.44	7.16	19.91	0.07	0.54	46.41	0.83		bd	85.50
Rim 10	0.32	6.67	1.34	2.18	4.70	21.34	0.05	0.30	47.89	1.08		bd	85.64
AVG	**1.13**	**5.52**	**3.99**	**1.64**	**7.21**	**14.46**	**0.07**	**0.55**	**39.93**	**0.43**		**0.50**	**75.35**
SD	**0.36**	**0.70**	**1.35**	**0.36**	**1.81**	**2.25**	**0.03**	**0.13**	**3.57**	**0.12**		**0.35**	**4.13**
JH-B6													
Interior 1	2.69	7.31	7.13	2.18	10.83	4.35	bd	3.43	59.13	0.11		0.42	97.56
Interior 2	4.67	6.96	7.05	1.69	17.40	2.02	bd	2.81	56.26	0.08		0.27	99.21
Interior 3	1.88	12.23	8.70	3.49	10.35	4.95	0.09	4.21	52.05	0.12		0.74	98.77
Interior 4	3.05	8.63	7.24	2.24	11.08	3.92	bd	4.03	58.43	0.34		0.53	99.43

	Na_2O	FeO	CaO	TiO_2	Al_2O_3	MgO	Cr_2O_3	K_2O	SiO_2	Cl	MnO	P_2O_5	Total
Interior 5	5.39	8.19	6.53	2.36	14.78	2.35	bd	2.65	57.07	0.02		0.15	99.50
Interior 6	4.26	8.24	8.79	2.35	14.11	3.67	0.06	2.89	54.30	0.06		0.29	99.00
Interior 7	5.23	11.99	3.75	3.15	15.62	1.07	0.06	3.45	54.60	0.04		0.23	99.19
Interior 8	3.95	9.85	6.50	2.61	13.26	2.82	bd	4.50	56.10	0.07		0.46	100.11
Interior 9	3.62	7.87	9.17	2.20	12.71	4.89	bd	2.95	56.53	0.15		0.49	100.55
Interior 10	0.36	8.43	20.50	1.07	2.34	**16.27**	0.12	0.03	53.35	bd		0.14	102.62
AVG	**3.51**	**8.97**	**8.54**	**2.33**	**12.25**	**4.63**	**0.03**	**3.09**	**55.78**	**0.10**		**0.37**	**99.59**
SD	**0.50**	**0.58**	**1.42**	**0.21**	**1.31**	**1.35**	**0.02**	**0.40**	**0.70**	**0.03**		**0.06**	**0.42**
Rim 1	1.58	6.05	1.25	2.72	10.54	12.86	0.04	2.42	41.72	0.20		0.07	79.41
Rim 2	1.83	9.40	0.74	2.43	7.97	19.79	0.21	1.96	36.88	0.15		0.05	81.37
Rim 3	3.71	2.05	1.88	2.57	16.26	4.07	0.04	6.10	58.28	0.15		0.32	95.40
Rim 4	1.34	6.67	0.61	1.34	5.21	19.40	0.09	0.88	37.21	0.22		bd	72.91
Rim 5	1.05	9.78	1.55	1.95	7.91	15.71	bd	2.47	36.18	0.27		0.23	77.06
Rim 6	1.59	8.82	0.98	2.30	7.49	18.28	0.47	1.74	35.77	0.32		bd	77.69
Rim 7	2.36	5.68	2.05	2.79	12.32	12.35	0.06	4.05	48.64	0.22		0.51	90.98
Rim 8	3.79	3.02	1.69	2.87	13.22	4.29	0.03	6.04	48.76	0.13		0.53	84.32
Rim 9	1.41	6.53	1.73	4.02	10.39	13.89	0.06	2.14	45.92	0.32		0.17	86.51
Rim 10	0.54	4.26	1.62	4.32	12.44	4.16	0.03	6.75	39.79	0.16		0.34	74.37
AVG	**1.92**	**6.23**	**1.41**	**2.73**	**10.37**	**12.48**	**0.10**	**3.45**	**42.92**	**0.21**		**0.22**	**82.00**
SD	**0.34**	**0.83**	**0.16**	**0.28**	**1.04**	**1.98**	**0.04**	**0.67**	**2.33**	**0.02**		**0.06**	**2.30**
JH-B7													
Interior 1	4.35	9.20	1.95	2.44	14.89	0.66	bd	6.76	58.54	0.33		0.67	99.72
Interior 2	2.18	7.79	13.32	1.85	8.86	9.30	0.18	2.75	54.38	0.05		0.35	101.00
Interior 3	3.75	8.86	5.02	2.05	13.04	2.81	0.06	5.17	57.48	0.20		0.51	98.92
Interior 4	5.70	9.31	3.92	2.79	16.73	0.68	0.03	3.56	56.16	0.07		0.38	99.31
Interior 5	4.55	10.18	1.94	3.13	15.10	0.71	bd	5.91	56.80	0.07		0.39	98.77
Interior 6	3.06	7.66	2.35	1.21	10.78	1.48	0.03	4.69	61.04	1.70		0.58	94.19
Interior 7	4.46	7.46	3.49	3.17	13.88	1.83	bd	4.30	59.84	0.13		0.81	99.34
Interior 8	6.41	6.33	3.28	1.90	18.20	0.30	bd	3.19	59.64	0.05		0.25	99.53
Interior 9	3.31	11.35	8.02	2.72	11.46	4.77	bd	3.19	53.24	0.15		0.53	98.73
Interior 10	3.11	9.23	5.45	2.73	12.64	2.78	0.04	5.79	53.31	0.28		0.67	95.98

	Na_2O	FeO	CaO	TiO_2	Al_2O_3	MgO	Cr_2O_3	K_2O	SiO_2	Cl	MnO	P_2O_5	Total
AVG	**4.09**	**8.74**	**4.87**	**2.40**	**13.56**	**2.53**	**0.03**	**4.53**	**57.04**	**0.30**		**0.51**	**98.55**
SD	**0.41**	**0.46**	**1.11**	**0.20**	**0.89**	**0.87**	**0.02**	**0.43**	**0.88**	**0.16**		**0.05**	**0.63**
Rim 1	2.97	1.99	4.76	0.78	16.69	0.58	bd	2.12	47.90	0.24		0.04	78.02
Rim 2	2.05	6.18	0.95	1.18	9.81	3.78	0.04	6.38	37.47	0.46		0.04	68.25
Rim 3	0.78	6.58	1.67	1.57	11.58	15.44	0.03	4.44	43.09	0.44		0.31	85.84
Rim 4	1.31	5.97	1.40	3.48	7.90	19.45	0.23	2.35	35.10	0.44		0.26	77.80
Rim 5	2.48	1.64	2.74	2.66	14.16	2.69	0.03	7.78	54.41	0.32		1.50	90.35
Rim 6	0.47	4.34	0.94	5.68	6.28	17.08	0.07	2.24	30.83	0.61		0.21	68.63
Rim 8	5.96	0.95	5.23	0.60	6.35	2.63	bd	2.00	18.07	0.18		0.06	40.77
Rim 9	1.46	1.38	0.58	2.44	11.07	1.53	0.03	8.59	43.63	0.45		bd	71.05
AVG	**2.19**	**3.63**	**2.28**	**2.30**	**10.48**	**7.90**	**0.06**	**4.49**	**38.81**	**0.39**		**0.30**	**72.59**
SD	**0.61**	**0.85**	**0.64**	**0.60**	**1.31**	**2.81**	**0.03**	**0.97**	**3.96**	**0.05**		**0.18**	**5.34**
JH-B8													
Interior 1	3.49	8.09	2.63	2.66	14.89	3.45	bd	6.19	55.56	0.22	0.09	0.71	97.95
Interior 2	4.31	6.58	2.96	2.30	14.67	2.51	0.05	4.25	58.64	0.33	0.09	0.75	97.37
Interior 3	3.92	12.97	4.81	3.00	14.23	2.99	bd	3.37	53.19	0.22	0.15	0.84	99.64
Interior 4	5.57	6.51	4.85	3.47	16.72	1.19	bd	2.32	57.18	0.16	0.09	1.01	99.05
Interior 5	0.18	18.75	0.82	1.94	11.70	12.83	bd	6.04	40.33	0.50	0.15	0.41	93.56
Interior 6	2.01	12.58	10.77	2.47	11.84	8.09	bd	1.93	48.04	0.29	0.20	0.49	98.67
Interior 7	4.05	10.99	2.89	2.81	13.51	3.04	bd	3.49	55.99	0.25	0.09	0.59	97.65
Interior 8	4.67	6.13	2.58	2.70	16.06	0.87	bd	6.01	61.09	0.11	0.12	0.76	101.06
Interior 9	3.86	8.57	4.18	2.60	14.57	1.97	bd	5.67	56.04	0.19	0.10	0.86	98.58
Interior 10	3.23	8.41	13.08	2.06	12.25	7.76	bd	1.10	52.30	0.09	0.18	0.39	100.82
AVG	**3.53**	**9.96**	**4.96**	**2.60**	**14.04**	**4.47**	**0.01**	**4.04**	**53.84**	**0.24**	**0.13**	**0.68**	**98.44**
SD	**0.47**	**1.25**	**1.23**	**0.14**	**0.54**	**1.22**	**0.01**	**0.60**	**1.88**	**0.04**	**0.01**	**0.06**	**0.67**
Rim 1	1.67	14.01	10.64	2.37	10.94	8.84	0.05	2.14	47.05	0.32	0.25	0.38	98.59
Rim 2	0.61	14.55	2.01	3.66	8.60	12.30	bd	1.76	36.68	1.44	0.18	0.10	81.56
Rim 3	0.55	12.07	1.22	0.49	8.48	14.64	0.08	2.26	37.42	1.27	0.14	0.06	78.41
Rim 4	0.33	11.68	0.94	0.52	9.04	15.25	0.06	2.16	38.95	0.89	0.06	bd	79.69
Rim 5	0.55	12.45	1.62	0.61	8.53	15.28	0.06	0.92	36.44	0.80	0.05	0.05	77.18

	Na_2O	FeO	CaO	TiO_2	Al_2O_3	MgO	Cr_2O_3	K_2O	SiO_2	Cl	MnO	P_2O_5	Total
Rim 6	4.18	5.84	4.83	2.43	18.27	4.36	bd	1.83	48.82	0.52	0.05	0.33	91.35
Rim 7	2.27	7.40	4.08	1.40	13.11	7.96	0.05	1.46	40.82	0.64	0.09	1.09	80.21
Rim 8	1.75	8.45	4.36	1.87	10.32	8.46	bd	2.20	32.57	0.74	0.06	2.05	72.67
Rim 9	1.67	12.04	1.42	2.32	7.65	13.66	0.04	2.62	34.77	2.06	0.22	bd	78.00
Rim 10	0.58	8.60	1.45	1.56	6.96	7.72	bd	3.16	22.02	0.85	0.14	0.63	53.48
AVG	**1.42**	**10.71**	**3.26**	**1.72**	**10.19**	**10.85**	**0.04**	**2.05**	**37.55**	**0.95**	**0.12**	**0.47**	**79.11**
SD	**0.37**	**0.93**	**0.94**	**0.32**	**1.06**	**1.22**	**0.01**	**0.19**	**2.37**	**0.16**	**0.02**	**0.22**	**3.71**
JH-B9													
Interior 1	0.50	13.51	13.20	2.77	7.63	11.37	bd	1.66	47.41	0.27	0.14	0.36	98.79
Interior 2	3.01	9.66	4.01	2.77	13.35	1.48	bd	2.32	62.40	0.10	0.08	0.57	99.74
Interior 3	3.00	6.07	8.25	2.19	18.19	2.44	bd	0.75	56.31	0.13	0.05	0.53	97.89
Interior 4	4.04	12.10	7.46	2.65	13.09	4.46	bd	1.78	54.21	0.07	0.15	0.35	100.35
Interior 5	3.12	7.95	6.42	2.87	14.98	1.22	bd	1.08	60.62	0.18	0.08	1.20	99.67
Interior 6	5.21	10.64	4.49	2.81	17.30	0.83	bd	1.86	56.26	0.09	0.09	0.72	100.29
Interior 7	4.00	7.29	4.04	1.99	15.41	2.53	bd	2.77	59.72	0.13	bd	0.72	98.59
Interior 8	2.32	8.79	6.08	3.16	13.77	2.65	bd	1.62	59.52	0.26	0.10	0.69	98.90
Interior 9	4.52	4.44	6.46	1.28	17.48	1.38	bd	1.31	60.69	0.19	0.05	0.53	98.29
Interior 10	0.34	19.24	4.70	2.90	10.91	9.82	0.03	4.42	43.49	0.51	0.13	0.40	96.78
AVG	**3.01**	**9.97**	**6.51**	**2.54**	**14.21**	**3.82**	**0.00**	**1.96**	**56.06**	**0.19**	**0.09**	**0.61**	**98.93**
SD	**0.51**	**1.34**	**0.87**	**0.18**	**1.02**	**1.18**	**0.00**	**0.33**	**1.96**	**0.04**	**0.01**	**0.08**	**0.35**
Rim 1	2.16	7.55	6.56	2.14	17.33	5.15	bd	1.77	40.15	0.33	0.03	0.88	83.97
Rim 2	0.32	13.51	1.22	1.59	10.08	11.18	0.04	3.79	34.03	0.39	0.05	0.47	76.59
Rim 3	1.88	7.83	5.71	2.22	16.08	4.80	bd	1.75	36.95	0.27	0.05	0.39	77.87
Rim 4	3.26	3.85	9.35	2.51	20.70	1.57	bd	0.53	41.22	0.20	0.07	0.74	83.95
Rim 5	0.92	10.67	3.04	6.05	9.58	8.09	bd	1.05	29.97	0.55	0.08	0.38	70.26
Rim 6	1.19	10.19	7.80	3.54	17.26	3.19	bd	1.54	42.49	0.51	0.09	1.51	89.21
Rim 7	2.28	6.65	7.30	1.25	17.33	6.63	0.03	1.50	42.98	0.64	0.03	0.82	87.30
Rim 8	2.89	3.19	9.85	1.60	21.51	1.46	bd	0.60	41.80	0.30	0.03	0.91	84.06
Rim 9	2.67	5.05	8.15	1.44	19.47	3.61	bd	1.02	40.61	0.32	0.07	0.63	82.96
Rim 10	3.05	8.49	7.29	3.09	17.62	4.74	0.04	1.57	42.07	0.24	0.03	1.02	89.20
AVG	**2.06**	**7.70**	**6.63**	**2.54**	**16.70**	**5.04**	**0.02**	**1.51**	**39.23**	**0.37**	**0.05**	**0.77**	**82.54**

	Na_2O	FeO	CaO	TiO_2	Al_2O_3	MgO	Cr_2O_3	K_2O	SiO_2	Cl	MnO	P_2O_5	Total
SD	**0.31**	**1.02**	**0.85**	**0.45**	**1.26**	**0.94**	**0.01**	**0.29**	**1.35**	**0.05**	**0.01**	**0.11**	**1.90**
JH-B10													
Interior 1	2.93	6.94	2.93	1.82	14.28	1.48	bd	7.93	59.68	0.50	0.04	1.76	100.18
Interior 2	3.40	7.16	2.98	1.82	15.04	1.13	bd	7.53	59.85	0.22	0.08	0.87	100.03
Interior 3	1.42	9.74	6.93	1.95	11.70	8.81	bd	5.60	48.68	0.39	0.07	2.54	97.74
Interior 4	2.87	10.19	8.59	2.32	11.63	6.63	bd	3.85	52.81	0.14	0.11	0.71	99.85
Interior 5	4.37	11.94	2.50	3.10	13.97	2.24	bd	4.63	55.38	0.27	0.03	0.92	99.29
Interior 6	4.50	6.41	2.28	1.92	15.97	0.33	bd	6.72	59.83	0.12	0.04	0.87	98.99
Interior 7	4.65	7.29	2.31	2.18	16.18	0.46	bd	6.48	58.98	0.16	0.06	0.80	99.52
Interior 8	4.33	4.60	1.90	1.48	16.51	0.51	bd	7.62	61.50	0.15	0.04	0.75	99.35
Interior 9	1.36	11.24	3.44	1.32	12.47	10.14	bd	7.03	47.19	1.20	0.07	0.75	95.95
Interior 10	4.52	7.09	1.90	2.22	16.09	1.37	bd	6.73	59.36	0.23	0.04	0.62	100.11
AVG	**3.12**	**7.51**	**3.25**	**1.83**	**13.08**	**3.01**	**bd**	**5.83**	**51.20**	**0.31**	**0.05**	**0.96**	**90.09**
SD	**0.40**	**0.75**	**0.72**	**0.16**	**0.60**	**1.18**	**bd**	**0.42**	**1.61**	**0.10**	**0.01**	**0.19**	**0.42**
Rim 2	3.59	11.35	2.69	2.11	15.14	4.41	bd	4.93	48.23	0.45	0.05	0.52	93.37
Rim 3	0.63	5.19	0.98	0.59	5.97	12.68	0.19	2.78	29.10	1.17	0.03	0.16	59.20
Rim 4	4.69	7.74	2.28	2.53	6.97	10.14	bd	4.69	35.13	5.86	0.11	0.06	78.90
Rim 5	1.68	2.77	2.71	3.94	8.53	5.67	0.05	3.85	31.46	1.42	bd	1.11	62.89
Rim 6	0.78	4.71	1.50	0.76	5.22	11.85	0.03	2.17	27.46	1.25	bd	0.46	55.93
Rim 7	0.68	4.63	0.93	1.92	6.21	14.84	bd	1.76	33.16	1.14	bd	0.04	65.07
Rim 8	1.92	5.35	2.54	2.76	9.78	8.63	0.09	2.60	37.74	1.60	0.05	0.34	73.03
Rim 9	2.83	5.48	2.61	0.33	4.43	13.95	0.03	2.28	38.14	5.17	0.13	bd	74.22
Rim 10	0.71	9.41	2.27	1.24	6.51	13.44	0.21	2.20	31.33	2.99	0.13	0.16	69.93
AVG	**1.95**	**6.29**	**2.06**	**1.80**	**7.64**	**10.62**	**0.07**	**3.03**	**34.64**	**2.34**	**0.05**	**0.32**	**70.28**
SD	**0.49**	**0.90**	**0.24**	**0.39**	**1.08**	**1.24**	**0.03**	**0.39**	**2.08**	**0.64**	**0.02**	**0.12**	**3.80**

Table 14. Major element data for talc and smectite alteration products found in experiment JH-B16.

	Na_2O	FeO	CaO	K_2O	Al_2O_3	MgO	TiO_2	Cl	SiO_2	MnO	P_2O_5	Total
Talc-1	0.04	5.33	0.07	bd	0.47	26.02	0.04	0.00	60.11	bd		92.10
Talc-2	0.07	5.18	0.01	bd	1.50	12.98	bd	0.37	33.71	bd		53.80
Talc-3	0.04	5.88	0.05	bd	0.27	25.72	bd	0.01	60.17	bd		92.15
Talc-4	0.11	5.68	0.01	bd	1.14	22.99	bd	0.08	52.35	0.03		82.40
Smectite-1	0.20	5.79	1.42	1.36	5.95	7.79	1.06	0.54	22.39	0.06	0.27	46.71
Smectite-2	0.13	7.52	6.93	2.07	5.82	9.52	1.73	0.43	26.15	0.13	3.71	64.05
Smectite-3	0.15	6.70	1.78	2.32	5.23	9.15	1.07	0.34	19.81	0.09	0.37	46.95

Table 15. Indium analyses of the interior and rim of the run products. SD is the standard deviation of the mean (1σ) of the concentrations in a given experiment. Indium concentrations listed as bd indicate the analysis was below the detection limit (25 ppm) and so the concentration was set at one half the detection limit (12.5 ppm).

	Interior			*Rim*	
Analysis #	**In (ppm)**	**1σ (abs)**	**Analysis #**	**In (ppm)**	**1σ (abs)**
JH-B1-1	bd		JH-B1-1	177	20
JH-B1-2	142	21	JH-B1-2	160	19
JH-B1-3	86	15	JH-B1-3	113	17
JH-B1-4	31	29	JH-B1-4	185	17
JH-B1-5	66	19	JH-B1-5	128	17
			JH-B1-6	74	24
			JH-B1-7	47	18
			JH-B1-8	222	20
			JH-B1-9	461	19
			JH-B1-10	196	18
AVG	**68**		**AVG**	**176**	
SD	**23**		**SD**	**36**	
JH-B2-1	bd		JH-B2-1	30	21
JH-B2-2	bd		JH-B2-2	30	24
JH-B2-3	34	34	JH-B2-3	28	10
JH-B2-4	59	29	JH-B2-4	45	15
JH-B2-5	bd		JH-B2-5	74	21
JH-B2-6	36	>36	JH-B2-6	66	15
JH-B2-7	bd		JH-B2-7	36	37
JH-B2-8	bd		JH-B2-8	bd	
JH-B2-9	bd		JH-B2-9	47	16
JH-B2-10	bd		JH-B2-10	49	14
AVG	**22**		**AVG**	**42**	
SD	**5**		**SD**	**6**	
JH-B4-1	bd		JH-B4-1	46	12
JH-B4-2	33	158	JH-B4-2	122	18
JH-B4-3	bd		JH-B4-3	85	19
JH-B4-4	67	14	JH-B4-4	bd	
JH-B4-5	74	21	JH-B4-5	bd	
JH-B4-6	bd		JH-B4-6	47	24
JH-B4-7	43	12	JH-B4-7	bd	
JH-B4-8	151	18	JH-B4-8	32	9
JH-B4-9	44	15	JH-B4-9	273	20
JH-B4-10	41	28	JH-B4-10	535	19
AVG	**49**		**AVG**	**118**	
SD	**13**		**SD**	**53**	
		JH-B6			
JH-B6-1	bd		JH-B6-1	60	16
JH-B6-2	bd		JH-B6-2	41	14

	Interior			*Rim*	
Analysis #	**In (ppm)**	**1σ (abs)**	**Analysis #**	**In (ppm)**	**1σ (abs)**
JH-B6-3	103	23	JH-B6-3	bd	
JH-B6-4	56	11	JH-B6-4	bd	
JH-B6-5	96	17	JH-B6-5	228	22
JH-B6-6	bd		JH-B6-6	31	26
JH-B6-7	27	13	JH-B6-7	29	24
JH-B6-8	84	18	JH-B6-8	bd	
JH-B6-9	bd		JH-B6-9	35	23
JH-B6-10	bd		JH-B6-10	136	13
AVG	**43**		**AVG**	**60**	
SD	**12**		**SD**	**22**	
		JH-B7			
JH-B7-1	55	17	JH-B7-1	335	17
JH-B7-2	127	16	JH-B7-2	bd	
JH-B7-3	64	20	JH-B7-3	89	27
JH-B7-4	131	16	JH-B7-4	339	18
JH-B7-5	57	11	JH-B7-5	47	14
JH-B7-6	241	18	JH-B7-6	106	19
JH-B7-7	73	12	JH-B7-7	bd	
JH-B7-8	98	26	JH-B7-8	73	15
JH-B7-9	41	17	JH-B7-9	bd	
JH-B7-10	175	21	JH-B7-10	51	14
AVG	**106**		**AVG**	**118**	
SD	**20**		**SD**	**43**	
		JH-B8			
JH-B8-1	86	15	JH-B8-1	bd	
JH-B8-2	44	11	JH-B8-2	bd	
JH-B8-3	26	14	JH-B8-3	bd	
JH-B8-4	26	12	JH-B8-4	bd	
JH-B8-5	bd		JH-B8-5	bd	
JH-B8-6	bd		JH-B8-6	bd	
JH-B8-7	bd		JH-B8-7	bd	
JH-B8-8	127	19	JH-B8-8	bd	
JH-B8-9	111	14	JH-B8-9	bd	
JH-B8-10	bd		JH-B8-10	bd	
AVG	**47**		**AVG**	**13**	
SD	**14**		**SD**	**0**	
		JH-B9			
JH-B9-1	bd		JH-B9-1	26	17
JH-B9-2	60	23	JH-B9-2	bd	
JH-B9-3	bd		JH-B9-3	bd	
JH-B9-4	bd		JH-B9-4	bd	

	Interior			*Rim*	
Analysis #	**In (ppm)**	**1σ (abs)**	**Analysis #**	**In (ppm)**	**1σ (abs)**
JH-B9-5	bd		JH-B9-5	162	20
JH-B9-6	bd		JH-B9-6	46	15
JH-B9-7	bd		JH-B9-7	74	25
JH-B9-8	bd		JH-B9-8	39	14
JH-B9-9	bd		JH-B9-9	36	21
JH-B9-10	bd		JH-B9-10	26	16
AVG	**17**		**AVG**	**45**	
SD	**5**		**SD**	**14**	
		JH-B10			
JH-B10-1	170	19	JH-B10-1	bd	
JH-B10-2	185	15	JH-B10-2	30	24
JH-B10-3	41	13	JH-B10-3	244	18
JH-B10-4	114	17	JH-B10-4	106	20
JH-B10-5	108	14	JH-B10-5	69	13
JH-B10-6	171	16	JH-B10-6	bd	
JH-B10-7	144	16	JH-B10-7	113	16
JH-B10-8	135	20	JH-B10-8	244	20
JH-B10-9	103	22	JH-B10-9	107	18
JH-B10-10	109	22	JH-B10-10	281	19
AVG	**128**		**AVG**	**134**	
SD	**13**		**SD**	**33**	

Appendix F. Method 2 Methodology, Results, and Discussion

Method 1 will henceforth be used in order to describe the methodology used to analyze the altered basalts in the low initial pH, HCl-bearing aqueous solution experiments. This method is described in detail within the main body of the thesis. Method 2 is an alternative method used to analyze the individual regions in the altered matrix and will be described below.

Methodology

Method 2 involved using a 1 μm beam to analyze each of the three regions in the interior altered basalt. The rim of the basalt was sufficiently altered, such that all of these

regions no longer persisted in each experiment. A total of five analyses were collected for each region within four separate domains, which were spaced across the interior of the altered basalt. The composition of the interior matrix of each experiment was calculated by multiplying the modal proportions (Appendix B) of a given region by the average composition for that region.

Indium

Indium concentrations above the detection limit (25 ppm) were found in all three regions of the altered matrix (Tables F-3 through F-5)**.** Indium concentrations ranged from below the detection limit to 369 ppm (108 ppm average) within Region 1, below detection to 172 ppm (33 ppm average) within Region 2, and below detection to 555 ppm (102 ppm average) within Region 3. A bulk interior indium concentration was calculated for each experiment by taking the sum of average indium concentrations in each region, multiplied by the modal proportion of that region. These indium concentrations are meaningless when comparing across different experiments because the starting concentration of indium within the aqueous solution ranged from 345-503 ppm indium. Furthermore, as water/rock increases, so does the mass of indium within the experimental charge. Instead, it is important to assess the partition coefficients and efficiencies of removal, which are determined by these concentrations.

Partition Coefficients

Method 2 incorporates the data from the three regions within the interior altered matrix. As previously explained, average interior indium concentrations were calculated

by taking the sum of the average indium concentration for each region multiplied by the modal abundance of each region (i.e. $\sum_{n=1}^{3} \%\,\mathrm{region}_n * \mathrm{average}[\mathrm{In}]_n$). However, because this method was used in the weakly altered interior, only $D_{In}^{int/aqueous}$ could be calculated. In order to calculate the final indium concentration in the aqueous solution and thus determine $D_{In}^{int/aqueous}$, rim data obtained using Method 1 was utilized to first calculate the mass of indium in the final solution (i.e. $\mathrm{mass\ In}_{aqueous}^{f} = \mathrm{mass\ In}_{aqueous}^{i} - \mathrm{mass\ In}_{rim} - \mathrm{mass\ In}_{interior}$), which was then used to determine the final concentration of indium in the aqueous solution. Experiments with a water/rock = 1 had $D_{In}^{int/aqueous}$ ranging from 0.24 ± 0.06 to 0.58 ± 0.08 (average of 0.42 ± 0.04), whereas those with a water/rock = 2 had values ranging from 0.14 ± 0.03 to 0.49 ± 0.14 (average of 0.31 ± 0.07). The average $D_{In}^{int/aqueous}$ of experiments with a water/rock = 1 and 2 are much closer than those produced by Method 1. However, this is likely due to the large standard deviation and range associated with the analyses for one experiment, JH-B4, and the low number of experiments analyzed with Method 2.

Assessment of Method 1 vs. Method 2

Both Methods 1 and 2 have advantages and disadvantages associated with their implementation. Method 2 is advantageous because we were able to analyze the individual regions that make up the altered matrix. However, this method also requires much more time and yields lower spatial resolution than Method 1 because it only utilizes five analytical points for each region across the entire altered interior matrix. Consequently, if a point with anomalously high indium concentrations were analyzed, the

average indium concentration would be significantly different due to the low number of analyses. The biggest drawback to Method 1 is that the EPMA was not designed to analyze heterogeneous material. Despite this, McCanta et al. (2017) recently noted that if the grain size of the material (i.e. fine-grained matrix) being measured is small relative to the beam size (ratio = 0.25), an analysis likely samples a representative portion of the material and 6-10 analyses are needed to produce a statistically meaningful result. Because Method 1 utilized a 10 μm beam, grain sizes need to be about 2.5 μm in order for this method to yield representative results of the sample. Figure F-1 shows a BSE image of the altered matrix displaying small grain sizes (<2 μm).

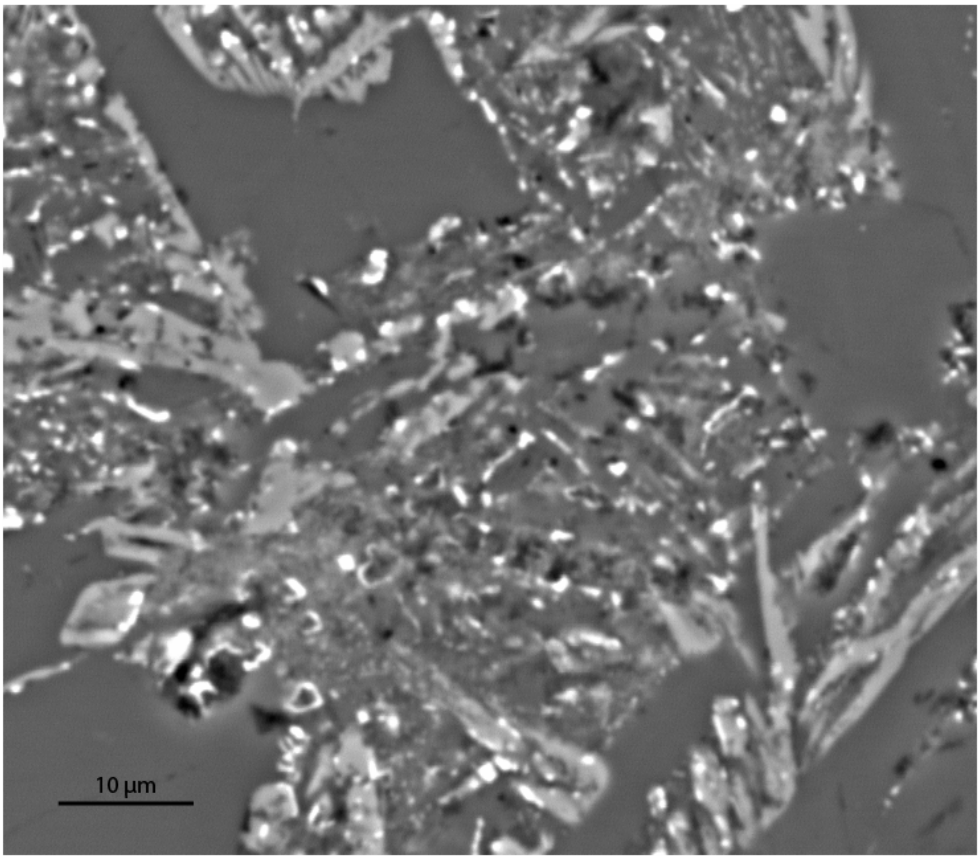

Figure 29. BSE image of the groundmass in JH-B4, depicting the grain size of the altered matrix.

I compared the indium and major element data of five experiments (JH-B1, JH-B2, JH-B4, JH-B7, and JH-B10) between the two methods. With the exception of some oxides in a few of the experiments, most major oxides were similar between the two methods (see Appendix G for data). Currently, seven analyses for JH-B1 and five analyses for JH-B2 have been completed in the interior with Method 1. Therefore, more analyses may be needed in order to obtain a representative composition. Additionally, indium data and partition coefficients were compared between both methods for each experiment (Table F-1). All experiments, except JH-B4 had statistically similar indium concentrations and partition coefficients between the two methods (Figure F-2). Average indium concentrations determined using Methods 1 and 2 are close to 100 ppm apart in experiment JH-B4. However, the large standard deviation of indium concentrations obtained by Method 2 could explain this discrepancy and might indicate that some of the regions measured in Method 2 contained anomalously high indium concentrations.

Table 16. Comparison of indium concentrations and partition coefficients ($D_{In}^{int/aqueous}$) obtained using Method 1 and 2 within the altered interior matrix. Uncertainties reflect the standard deviation (1σ) of the indium concentrations.

		JH-B1	JH-B2	JH-B4	JH-B7	JH-B10
Method	*Indium (ppm)*	68 ± 23	22 ± 5	49 ± 13	106 ± 20	128 ± 14
1	$D_{In}^{int/aqueous}$	0.25 ± 0.09	0.06 ± 0.01	0.15 ± 0.04	0.39 ± 0.08	0.48 ± 0.06
Method	*Indium (ppm)*	54 ± 17	47 ± 10	147 ± 56	101 ± 17	129 ± 22
2	$D_{In}^{int/aqueous}$	0.24 ± 0.06	0.14 ± 0.03	0.49 ± 0.17	0.44 ± 0.07	0.58 ± 0.09

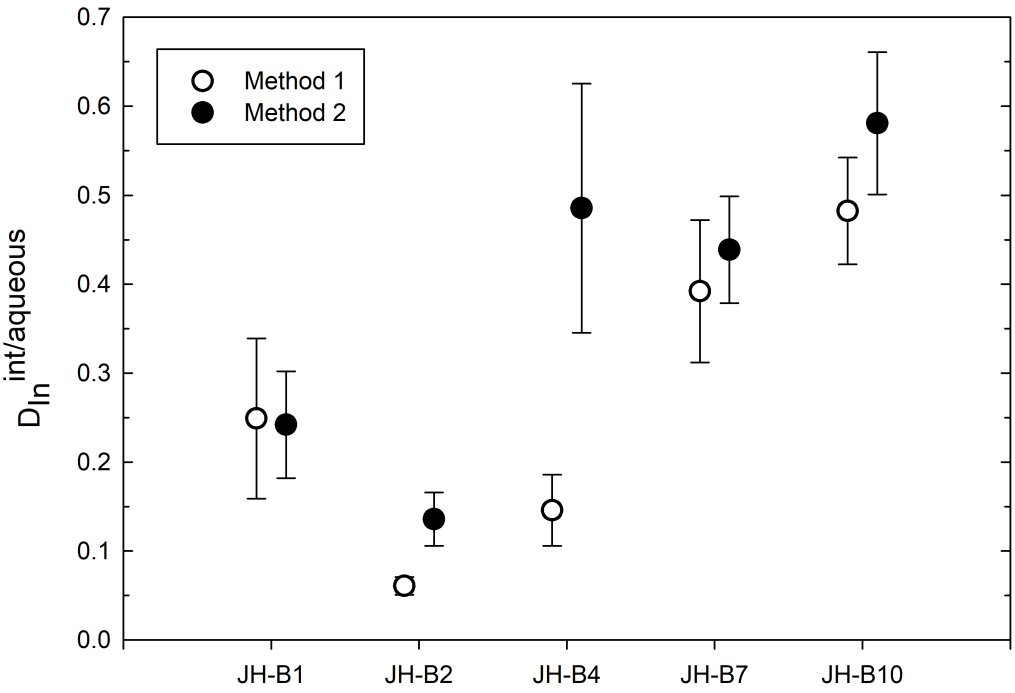

Figure 30. Plot of the partition coefficient of indium between the altered interior matrix and the aqueous fluid calculated using Method 1 and 2.

Table 17. Modal abundance of phenocrysts and matrix regions (Regions 1-3) in the starting basalt and experiments used with Method 2. Region 1 is the dark matrix material, Region 2, is the light matrix material, and Region 3 comprises the small white grains. SD is the standard deviation of the mean (1σ) of the concentrations in a given experiment.

	Region 1	Region 2	Region 3	Phenocrysts
Starting 1	37.4%	15.5%	1.0%	46.1%
Starting 2	30.7%	27.7%	0.1%	41.6%
Starting 3	39.2%	32.0%	2.6%	26.1%
Starting 4	28.0%	31.8%	0.7%	39.4%
Starting 5	33.7%	48.6%	0.6%	17.1%
Starting 6	33.9%	29.3%	0.5%	36.3%
Starting 7	34.8%	24.8%	0.2%	40.1%
AVG	34.0%	30.0%	0.8%	35.3%
SD	1.4%	3.8%	0.3%	3.8%
Region modes	**52.4%**	**46.3%**	**1.3%**	
SD	**3.8%**	**4.2%**	**0.9%**	
B1 Reg A	40.9%	14.9%	1.2%	43.1%
B1 Reg B	44.7%	20.6%	0.5%	34.1%
B1 Reg G	37.4%	17.7%	1.6%	43.3%
B1 Reg H	42.5%	21.1%	1.2%	35.2%
AVG	41.4%	18.6%	1.1%	38.9%
SD	1.5%	1.4%	0.2%	2.5%
Region modes	**67.8%**	**30.4%**	**1.8%**	
SD	**3.1%**	**2.2%**	**0.8%**	
B2 Reg D	38.7%	27.5%	1.0%	32.7%
B2 Reg E	42.0%	21.9%	1.2%	34.9%
B2 Reg F	29.3%	26.4%	1.3%	43.0%
B2 Reg G	36.1%	18.0%	1.7%	44.1%
AVG	36.5%	23.5%	1.3%	38.7%
SD	2.7%	2.2%	0.2%	2.9%
Region modes	**59.6%**	**38.3%**	**2.1%**	
SD	**4.3%**	**3.2%**	**0.7%**	
B4 Reg C	63.8%	14.9%	2.6%	18.7%
B4 Reg E	34.0%	26.9%	1.6%	37.5%
B4 Reg F	37.2%	17.2%	2.9%	42.8%
B4 Reg G	34.9%	14.0%	2.5%	48.6%
AVG	42.4%	18.2%	2.4%	36.9%
SD	7.1%	3.0%	0.3%	6.5%
Region modes	**67.3%**	**28.9%**	**3.8%**	
SD	**9.3%**	**4.5%**	**1.0%**	
B7 Reg A	30.2%	27.6%	1.9%	40.3%
B7 Reg B	40.2%	24.1%	4.1%	31.6%

	Region 1	Region 2	Region 3	Phenocrysts
B7 Reg C	30.4%	26.2%	5.3%	38.0%
B7 Reg D	35.2%	18.6%	3.4%	42.9%
AVG	34.0%	24.1%	3.7%	38.2%
SD	2.4%	2.0%	0.7%	2.4%
Region modes	**55.0%**	**39.5%**	**6.1%**	
SD	**3.8%**	**3.0%**	**1.4%**	
B10 Reg A	44.0%	19.9%	1.0%	35.0%
B10 Reg B	33.3%	25.8%	2.5%	38.4%
B10 Reg C	34.1%	25.3%	1.7%	38.9%
B10 Reg D	33.6%	24.5%	1.9%	40.0%
AVG	36.3%	23.9%	1.8%	38.1%
SD	2.6%	1.3%	0.3%	1.1%
Region modes	**58.5%**	**38.6%**	**2.9%**	
SD	**3.8%**	**2.6%**	**0.9%**	
B16 Reg A	35.4%	32.6%	1.3%	30.7%
B16 Reg B	28.4%	16.0%	0.9%	54.6%
B16 Reg C	31.8%	18.6%	1.2%	48.3%
B16 Reg D	36.6%	21.7%	1.2%	40.5%
AVG	33.1%	22.2%	1.2%	43.5%
SD	1.9%	3.6%	0.1%	5.2%
Region modes	**58.6%**	**39.4%**	**2.1%**	
SD	**4.9%**	**4.4%**	**0.5%**	

Table 18. Major and trace element data for Region 1 in the starting basalt and run products. SD is the standard deviation of the mean (1σ) of the concentrations in a given experiment. Indium concentrations listed as bd indicate the analysis was below the detection limit (25 ppm) and so the concentration was set at one half the detection limit (12.5 ppm).

	Na_2O	FeO	CaO	K_2O	Al_2O_3	MgO	Cr_2O_3	TiO_2	Cl	SiO_2	MnO	P_2O_5	Total	In (ppm)
Starting Basalt														
1	5.47	3.21	3.08	2.96	18.07	0.56	bd	2.06	0.02	61.91	0.07	0.53	97.94	
2	5.68	2.98	4.56	2.44	18.14	0.61	bd	1.11	0.03	59.96	bd	0.32	95.85	
3	2.54	11.22	8.90	2.54	11.87	4.56	0.05	2.72	0.05	51.91	0.19	0.56	97.10	
4	5.26	5.56	2.08	4.31	15.19	0.40	bd	1.87	0.06	59.63	bd	0.67	95.06	
5	4.77	4.41	3.82	3.44	15.50	1.33	bd	1.79	0.01	59.37	0.10	0.64	95.19	
6	2.25	10.82	7.80	3.02	12.56	5.98	bd	2.92	0.03	54.22	0.19	0.53	100.30	
7	5.79	2.50	4.17	2.62	19.26	0.33	0.03	0.73	0.03	60.45	bd	0.40	96.32	
8	5.49	6.58	2.08	3.68	16.43	0.38	bd	1.61	0.07	60.27	0.10	0.68	97.36	
9	5.60	3.37	4.43	2.20	19.50	0.47	0.06	1.30	0.05	62.63	0.07	0.52	100.18	
AVG	**4.76**	**5.63**	**4.55**	**3.02**	**16.28**	**1.62**	**0.01**	**1.79**	**0.04**	**58.93**	**0.08**	**0.54**	**97.26**	
SD	**0.46**	**1.11**	**0.79**	**0.23**	**0.92**	**0.71**	**0.01**	**0.24**	**0.01**	**1.18**	**0.02**	**0.04**	**0.65**	
JH-B1														
1	6.39	1.78	6.01	1.49	22.05	0.50		0.55	0.13	56.28	bd	bd	95.16	112
2	3.07	4.28	5.44	0.76	12.47	0.95		3.08	0.39	65.04	0.04	0.81	96.24	30
3	4.15	6.01	5.57	0.96	14.12	0.69		1.86	0.31	64.52	bd	0.67	98.83	bd
4	6.83	1.33	4.93	1.63	19.76	0.08		0.53	0.15	62.96	bd	0.05	98.21	61
5	7.71	1.12	4.37	2.38	20.53	0.07		0.44	0.29	57.35	bd	bd	94.20	138
AVG	**5.63**	**2.90**	**5.26**	**1.45**	**17.79**	**0.46**		**1.29**	**0.25**	**61.23**	**0.01**	**0.31**	**96.53**	**71**
SD	**0.87**	**0.96**	**0.28**	**0.29**	**1.89**	**0.17**		**0.52**	**0.05**	**1.84**	**0.01**	**0.18**	**0.88**	**24**
JH-B2														
1	3.87	2.61	8.71	0.42	21.64	0.18		0.78	0.27	65.07	0.05	0.04	103.56	48
2	6.38	1.76	5.58	1.19	19.61	0.28		0.81	0.22	65.16	bd	0.06	101.02	58
3	5.83	4.74	9.90	0.79	18.51	3.41		1.11	0.02	56.91	0.09	0.08	101.39	42
4	5.79	5.47	7.55	1.20	17.21	0.59		1.61	0.28	58.51	0.06	1.42	99.62	116
5	4.81	5.76	6.23	1.49	16.89	2.17		1.29	0.32	59.58	bd	0.47	98.95	84
AVG	**5.34**	**4.07**	**7.59**	**1.02**	**18.77**	**1.33**		**1.12**	**0.22**	**61.05**	**0.04**	**0.41**	**100.91**	**70**
SD	**0.45**	**0.80**	**0.79**	**0.19**	**0.86**	**0.63**		**0.16**	**0.05**	**1.72**	**0.02**	**0.26**	**0.80**	**14**
JH-B4														
1	3.21	3.92	3.06	3.17	16.15	9.51		0.42	0.13	56.70	bd	0.19	96.43	bd
2	2.26	11.28	6.84	1.27	15.62	2.25		3.22	0.72	48.35	0.06	0.93	92.63	107
3	3.48	6.88	6.15	2.58	21.04	3.59		2.36	0.59	52.43	0.04	0.22	99.22	155

	Na_2O	FeO	CaO	K_2O	Al_2O_3	MgO	Cr_2O_3	TiO_2	Cl	SiO_2	MnO	P_2O_5	Total	In (ppm)
4	1.32	9.24	5.92	0.54	8.25	7.73		4.23	0.73	56.69	0.12	0.22	94.83	306
5	1.39	17.00	4.95	2.25	13.95	6.27		3.18	0.77	46.82	0.13	0.57	97.11	369
AVG	**2.33**	**9.66**	**5.39**	**1.96**	**15.00**	**5.87**		**2.68**	**0.59**	**52.20**	**0.07**	**0.43**	**96.05**	**190**
SD	**0.45**	**2.21**	**0.66**	**0.47**	**2.06**	**1.33**		**0.64**	**0.12**	**2.05**	**0.02**	**0.14**	**1.11**	**65**
JH-B7														
1	2.36	2.07	1.11	11.76	16.49	0.80		0.73	0.49	61.69	bd	0.42	97.86	77
2	6.87	13.16	3.04	3.11	16.84	0.67		4.36	0.26	55.49	0.15	0.20	104.09	191
3	7.09	2.09	7.51	1.62	21.89	1.12		0.86	0.02	59.59	0.04	0.07	101.89	78
4	6.07	2.61	1.45	5.45	16.94	0.10		1.27	0.04	60.85	0.06	bd	94.86	160
5	4.36	3.34	2.79	8.62	15.57	0.51		1.18	0.41	57.15	0.03	1.70	95.55	155
AVG	**5.35**	**4.66**	**3.18**	**6.11**	**17.55**	**0.64**		**1.68**	**0.25**	**58.95**	**0.06**	**0.48**	**98.85**	**132**
SD	**0.89**	**2.14**	**1.14**	**1.84**	**1.11**	**0.17**		**0.68**	**0.09**	**1.16**	**0.03**	**0.31**	**1.80**	**23**
JH-B10														
1	2.47	12.26	3.62	4.97	10.90	1.90		4.41	0.53	61.47	0.05	0.52	102.98	146
2	3.47	20.70	3.00	2.44	14.06	3.25		4.42	0.59	46.16	0.05	0.63	98.64	127
3	3.14	39.00	4.23	4.47	11.06	1.21		0.78	0.22	44.99	0.11	2.41	111.57	271
4	2.93	13.08	4.68	7.35	14.65	1.93		2.46	0.83	54.51	0.11	0.85	103.17	142
5	0.41	10.19	18.12	0.24	5.13	10.43		2.38	0.37	41.42	0.21	0.36	89.18	151
AVG	**2.48**	**19.05**	**6.73**	**3.89**	**11.16**	**3.74**		**2.89**	**0.51**	**49.71**	**0.10**	**0.95**	**101.11**	**168**
SD	**0.54**	**5.30**	**2.86**	**1.20**	**1.69**	**1.70**		**0.69**	**0.10**	**3.64**	**0.03**	**0.37**	**3.64**	**26**
JH-B13														
1	3.01	8.36	3.76	4.18	12.23	4.86	bd	1.98	0.04	56.67	0.14	0.97	96.19	98
2	5.31	9.06	3.45	3.15	15.07	0.54	bd	2.02	0.05	61.20	0.13	0.64	100.63	176
3	7.05	1.19	5.22	1.69	18.65	0.43	bd	0.60	bd	51.89	bd	bd	86.73	bd
4	5.40	2.66	2.51	5.57	14.38	0.45	bd	1.52	0.03	56.64	0.08	0.94	90.19	83
AVG	**5.19**	**5.32**	**3.74**	**3.65**	**15.08**	**1.57**	**bd**	**1.53**	**0.03**	**56.60**	**0.09**	**0.64**	**93.43**	**95**
SD	**0.83**	**1.99**	**0.56**	**0.82**	**1.33**	**1.10**	**bd**	**0.33**	**0.01**	**1.90**	**0.03**	**0.22**	**3.09**	**34**
JH-B16														
1	4.57	5.67	5.16	3.37	15.46	1.73		1.43	0.01	60.18	0.11	0.34	98.04	98
2	1.02	11.37	15.16	1.50	7.81	11.25		2.57	0.03	45.61	0.23	0.50	97.03	97
3	0.47	10.35	19.10	0.15	5.33	14.30		2.70	0.02	44.76	0.21	0.30	97.68	93

	Na_2O	FeO	CaO	K_2O	Al_2O_3	MgO	Cr_2O_3	TiO_2	Cl	SiO_2	MnO	P_2O_5	Total	In (ppm)
4	5.74	2.79	4.65	2.01	19.10	0.18		1.40	0.02	54.28	0.04	0.07	90.28	bd
5	2.32	8.20	3.10	7.22	15.37	2.50		2.71	0.06	51.51	0.07	1.61	94.65	49
AVG	**2.82**	**7.68**	**9.43**	**2.85**	**12.61**	**5.99**		**2.16**	**0.03**	**51.27**	**0.13**	**0.56**	**95.53**	**70**
SD	**1.02**	**1.56**	**3.22**	**1.21**	**2.59**	**2.84**		**0.31**	**0.01**	**2.85**	**0.04**	**0.27**	**1.44**	**17**

Table 19. Major and trace element data for Region 2 in the starting basalt and run products. SD is the standard deviation of the mean (1σ) of the concentrations in a given experiment. Indium concentrations listed as bd indicate the analysis was below the detection limit (25 ppm) and so the concentration was set at one half the detection limit (12.5 ppm).

	Na2O	FeO	CaO	K2O	Al2O3	MgO	Cr2O3	TiO2	Cl	SiO2	MnO	P2O5	Total	In (ppm)
Starting Basalt														
1	1.49	9.78	12.74	1.69	11.42	7.27	bd	2.75	0.03	53.26	0.19	0.58	101.18	
2	3.71	8.39	9.07	2.02	14.98	2.62	bd	1.84	0.06	56.95	0.10	0.51	100.22	
3	2.61	12.84	8.03	1.73	12.16	5.77	bd	2.31	0.03	54.06	0.25	0.46	100.26	
4	0.67	11.53	16.68	0.78	7.20	8.23	bd	2.77	0.05	46.32	0.25	2.51	96.98	
5	2.70	9.14	10.05	1.50	13.41	5.97	bd	2.54	0.00	53.80	0.18	0.44	99.75	
6	1.21	14.23	13.31	1.00	9.16	9.20	0.04	3.01	0.03	48.77	0.30	0.49	100.76	
7	1.67	12.07	9.48	2.06	12.01	5.66	0.06	2.65	0.02	52.70	0.19	0.55	99.11	
8	1.74	16.26	12.22	1.52	10.51	5.91	bd	3.38	0.02	48.54	0.33	0.51	100.94	
9	2.38	9.67	9.32	2.02	13.19	5.69	bd	2.43	0.03	54.57	0.18	0.59	100.07	
10	1.68	14.56	9.70	1.33	10.75	6.94	0.04	3.03	0.04	49.48	0.27	0.52	98.35	
AVG	**1.99**	**11.85**	**11.06**	**1.56**	**11.48**	**6.33**	**0.01**	**2.67**	**0.03**	**51.85**	**0.23**	**0.72**	**99.76**	
SD	**0.28**	**0.83**	**0.83**	**0.14**	**0.71**	**0.56**	**0.01**	**0.14**	**0.00**	**1.06**	**0.02**	**0.20**	**0.41**	
JH-B1														
1	2.14	10.97	16.21	0.28	8.99	9.83		3.11	0.09	49.06	0.26	0.32	101.24	bd
2	2.59	7.82	11.84	0.70	14.32	3.94		1.85	0.22	51.61	0.13	0.42	95.38	bd
3	1.51	13.00	11.73	0.60	9.32	5.07		2.99	0.30	56.96	0.20	0.43	102.04	bd
4	2.86	12.63	12.21	0.71	11.81	6.42		3.08	0.18	54.34	0.24	0.70	105.13	28
5	1.57	12.68	17.25	0.26	8.72	9.30		2.64	0.07	46.80	0.31	0.19	99.76	bd
AVG	**2.13**	**11.42**	**13.85**	**0.51**	**10.63**	**6.91**		**2.73**	**0.17**	**51.75**	**0.23**	**0.41**	**100.71**	**16**
SD	**0.27**	**0.97**	**1.19**	**0.10**	**1.07**	**1.16**		**0.24**	**0.04**	**1.81**	**0.03**	**0.08**	**1.60**	**3**
JH-B2														
1	1.74	12.65	14.33	0.37	10.37	9.60		2.66	0.28	49.80	0.21	0.24	102.18	bd
2	1.65	10.31	14.90	0.14	9.38	6.68		2.89	0.08	55.55	0.24	0.15	101.95	bd
3	5.61	4.86	8.81	0.88	21.05	2.58		0.65	0.03	59.08	0.05	bd	103.61	bd
4	1.21	12.03	17.76	0.26	7.55	11.11		3.35	0.05	48.84	0.26	0.25	102.66	bd
5	3.45	8.22	11.69	0.42	15.34	3.66		1.75	0.24	53.32	0.15	0.42	98.61	bd
AVG	**2.74**	**9.61**	**13.50**	**0.41**	**12.74**	**6.73**		**2.26**	**0.14**	**53.32**	**0.18**	**0.21**	**101.80**	**bd**
SD	**0.81**	**1.42**	**1.52**	**0.13**	**2.45**	**1.64**		**0.48**	**0.05**	**1.88**	**0.04**	**0.07**	**0.85**	**bd**
JH-B4														
1	6.09	1.94	4.02	2.52	19.88	0.39		0.59	0.49	62.07	0.06	0.24	98.17	bd

	Na_2O	FeO	CaO	K_2O	Al_2O_3	MgO	Cr_2O_3	TiO_2	Cl	SiO_2	MnO	P_2O_5	Total	In (ppm)
2	3.64	4.86	10.03	0.43	18.18	7.32		0.67	0.43	56.34	0.04	0.09	101.93	65
3	5.98	1.25	4.80	2.09	20.56	0.31		0.49	0.21	56.83	0.05	0.21	92.75	33
4	3.69	2.96	7.59	0.74	16.52	2.72		0.99	0.30	60.47	0.04	0.50	96.46	78
5	2.13	3.36	6.02	0.85	12.62	1.65		0.88	0.38	65.71	0.04	1.18	94.73	bd
AVG	**4.31**	**2.87**	**6.49**	**1.33**	**17.55**	**2.48**		**0.72**	**0.36**	**60.29**	**0.05**	**0.45**	**96.81**	**40**
SD	**0.76**	**0.62**	**1.07**	**0.41**	**1.42**	**1.29**		**0.09**	**0.05**	**1.73**	**0.00**	**0.20**	**1.56**	**13**
JH-B7														
1	3.34	10.51	11.24	3.12	11.00	7.70		2.32	1.17	49.74	0.17	0.05	100.10	48
2	1.71	10.96	12.09	3.35	10.36	6.54		2.83	0.08	53.48	0.22	0.43	102.04	81
3	3.76	17.58	9.10	1.65	13.44	4.30		4.65	0.09	50.06	0.19	0.30	105.11	45
4	0.59	11.72	20.21	0.09	4.78	12.20		3.13	0.08	45.21	0.25	0.15	98.40	bd
5	0.80	19.95	12.89	0.71	6.04	5.05		3.31	1.28	35.44	0.32	0.45	85.96	49
AVG	**2.04**	**14.15**	**13.11**	**1.79**	**9.12**	**7.16**		**3.25**	**0.54**	**46.79**	**0.23**	**0.27**	**98.32**	**47**
SD	**0.65**	**1.93**	**1.89**	**0.64**	**1.61**	**1.39**		**0.39**	**0.28**	**3.13**	**0.03**	**0.08**	**3.29**	**11**
JH-B10														
1	0.75	12.00	6.26	7.82	11.19	5.77		2.09	0.25	51.90	0.13	0.66	98.77	43
2	5.16	3.55	2.41	4.51	17.37	1.63		1.05	0.19	62.74	bd	0.39	98.95	bd
3	5.80	2.43	4.52	3.46	18.42	1.19		0.88	0.10	61.46	0.03	0.25	98.52	48
4	5.81	4.69	2.42	4.36	17.76	0.36		1.56	0.23	65.09	bd	0.33	102.56	91
5	1.21	12.26	19.31	2.38	7.63	6.98		1.84	1.04	42.74	0.13	5.33	100.61	bd
AVG	**3.75**	**6.99**	**6.98**	**4.51**	**14.47**	**3.18**		**1.48**	**0.36**	**56.78**	**0.06**	**1.39**	**99.88**	**73**
SD	**1.14**	**2.13**	**3.16**	**0.91**	**2.15**	**1.33**		**0.23**	**0.17**	**4.17**	**0.03**	**0.99**	**0.76**	**14**
JH-B13														
1	0.62	16.24	16.71	0.09	5.29	10.52	0.03	3.71	bd	45.76	0.41	0.22	99.59	bd
2	0.72	14.61	18.48	0.12	6.38	10.05	bd	3.48	bd	45.16	0.28	0.26	99.56	bd
3	1.28	11.87	17.41	0.29	6.04	9.79	bd	2.93	bd	43.37	0.24	0.26	93.50	bd
4	0.75	12.29	18.67	0.34	7.45	9.37	0.03	3.45	bd	48.20	0.24	0.41	101.19	bd
AVG	**0.84**	**13.75**	**17.82**	**0.21**	**6.29**	**9.93**	**0.01**	**3.39**	**bd**	**45.62**	**0.29**	**0.29**	**98.46**	**bd**
SD	**0.15**	**1.03**	**0.46**	**0.06**	**0.45**	**0.24**	**0.01**	**0.17**	**bd**	**1.00**	**0.04**	**0.04**	**1.70**	**bd**
JH-B16														
1	4.66	6.39	7.44	2.89	14.57	2.58		1.95	bd	55.77	0.12	0.39	96.76	86

	Na_2O	FeO	CaO	K_2O	Al_2O_3	MgO	Cr_2O_3	TiO_2	Cl	SiO_2	MnO	P_2O_5	Total	In (ppm)
2	4.19	3.06	2.73	4.84	15.99	0.49		1.69	0.07	54.56	0.08	0.95	88.63	45
3	3.57	7.93	10.47	0.88	14.37	6.21		1.39	bd	52.22	0.16	0.28	97.46	bd
4	4.80	2.18	1.05	8.33	17.93	0.15		0.89	0.02	60.82	bd	0.23	96.38	bd
5	0.58	23.60	5.47	3.74	12.69	6.37		6.11	0.10	31.72	0.32	2.66	93.35	bd
AVG	**3.56**	**8.63**	**5.43**	**4.14**	**15.11**	**3.16**		**2.40**	**0.04**	**51.02**	**0.14**	**0.90**	**94.52**	**34**
SD	**0.77**	**3.89**	**1.67**	**1.23**	**0.88**	**1.34**		**0.94**	**0.02**	**5.02**	**0.05**	**0.46**	**1.63**	**15**

Table 20. Major and trace element data for Region 3 in the starting basalt and run products. SD is the standard deviation of the mean (1σ) of the concentrations in a given experiment. Indium concentrations listed as bd indicate the analysis was below the detection limit (25 ppm) and so the concentration was set at one half the detection limit (12.5 ppm).

	Na_2O	FeO	CaO	K_2O	Al_2O_3	MgO	Cr_2O_3	TiO_2	Cl	SiO_2	MnO	P_2O_5	Total	In (ppm)
Starting Basalt														
1	2.11	17.92	5.23	1.16	12.03	3.92	bd	1.57	0.03	50.52	0.20	3.43	98.13	
2	1.88	31.94	1.31	2.28	9.96	5.42	bd	3.34	0.04	43.20	0.54	0.40	100.31	
3	4.39	16.33	2.80	1.96	16.86	1.10	bd	3.21	0.03	55.88	0.17	0.37	103.10	
4	3.84	21.17	1.47	2.51	11.48	6.41	bd	2.44	0.04	52.15	0.22	0.39	102.13	
5	2.56	7.56	5.84	2.13	18.59	1.88	bd	1.33	0.04	52.82	0.13	1.40	94.28	
6	0.50	34.89	0.88	0.56	17.03	7.63	bd	2.31	0.02	32.04	0.64	0.78	97.27	
7	4.85	8.13	5.73	2.02	17.66	0.81	bd	1.71	0.03	56.64	0.09	0.26	97.93	
8	4.67	3.25	4.96	2.36	18.55	0.68	bd	0.96	0.02	59.60	0.07	0.54	95.65	
9	1.38	22.36	6.01	1.82	10.70	5.58	bd	3.58	0.05	48.81	0.33	0.41	101.02	
AVG	**2.91**	**18.17**	**3.81**	**1.87**	**14.76**	**3.71**	**bd**	**2.27**	**0.03**	**50.19**	**0.27**	**0.89**	**98.87**	
SD	**0.53**	**3.60**	**0.72**	**0.21**	**1.21**	**0.89**	**bd**	**0.32**	**0.00**	**2.77**	**0.07**	**0.34**	**0.99**	
JH-B1														
1	3.18	13.99	6.18	0.46	14.43	0.49		5.27	0.33	57.85	0.05	0.81	102.96	45
2	1.69	17.20	5.21	1.95	12.40	4.17		4.21	0.76	53.49	0.10	1.40	102.41	84
3	4.46	10.07	6.91	0.79	17.96	0.87		2.50	0.31	57.02	bd	0.54	101.37	63
4	2.65	16.71	9.50	0.82	14.02	2.84		3.53	0.50	48.71	0.17	0.50	99.84	43
5	2.53	21.75	4.38	1.12	13.20	1.50		5.73	0.43	44.04	0.07	0.17	94.84	126
AVG	**2.90**	**15.95**	**6.44**	**1.03**	**14.40**	**1.97**		**4.25**	**0.47**	**52.22**	**0.08**	**0.68**	**100.28**	**72**
SD	**0.46**	**1.93**	**0.88**	**0.25**	**0.96**	**0.68**		**0.58**	**0.08**	**2.60**	**0.03**	**0.21**	**1.46**	**15**
JH-B2														
1	3.29	11.94	6.68	1.21	15.57	2.58		3.26	0.27	55.67	0.07	1.43	101.91	bd
2	2.05	9.97	6.28	0.52	18.44	0.68		3.23	0.74	55.37	0.07	0.61	97.79	31
3	0.65	14.25	6.90	1.00	9.66	4.54		3.63	0.46	49.15	0.09	1.06	91.29	bd
4	3.54	5.65	6.46	1.00	14.63	1.20		1.23	0.41	63.68	bd	1.24	98.98	55
5	4.01	5.33	6.59	1.36	17.79	1.71		1.46	0.42	60.76	bd	0.52	99.94	61
AVG	**2.71**	**9.43**	**6.58**	**1.02**	**15.22**	**2.14**		**2.56**	**0.46**	**56.93**	**0.06**	**0.97**	**97.98**	**35**
SD	**0.61**	**1.75**	**0.11**	**0.14**	**1.55**	**0.68**		**0.50**	**0.08**	**2.50**	**0.02**	**0.18**	**1.80**	**10**
JH-B4														
1	2.34	2.16	5.51	0.48	14.82	0.05		0.94	0.11	69.78	bd	0.05	96.22	bd
2	2.00	12.00	7.13	0.38	12.83	0.88		3.31	0.35	61.96	0.04	1.75	102.54	26
3	2.71	4.03	6.83	0.53	13.66	0.79		1.17	0.24	61.34	0.04	1.37	92.64	169

	Na_2O	FeO	CaO	K_2O	Al_2O_3	MgO	Cr_2O_3	TiO_2	Cl	SiO_2	MnO	P_2O_5	Total	In (ppm)
4	3.57	6.55	6.48	0.62	16.99	0.71		1.86	0.47	59.11	0.08	0.43	96.77	190
5	0.82	27.54	2.76	2.35	8.89	8.00		14.01	0.65	29.51	0.16	1.12	95.67	555
AVG	**2.29**	**10.46**	**5.74**	**0.87**	**13.44**	**2.09**		**4.26**	**0.36**	**56.34**	**0.06**	**0.94**	**96.77**	**191**
SD	**0.45**	**4.58**	**0.79**	**0.37**	**1.34**	**1.49**		**2.47**	**0.09**	**6.95**	**0.03**	**0.31**	**1.61**	**98**
JH-B7														
1	0.62	26.67	0.57	3.48	2.29	1.02		10.23	1.37	57.31	0.07	0.00	103.32	256
2	5.94	4.70	1.93	5.51	16.72	0.75		1.46	0.64	58.88	0.07	0.12	96.58	189
3	1.19	11.54	1.94	9.77	14.70	2.87		2.61	0.40	52.34	0.03	1.02	98.34	102
4	3.73	10.28	1.35	7.46	14.19	0.35		3.09	0.98	53.24	bd	0.42	94.90	136
5	3.81	29.32	2.91	3.69	14.15	0.49		6.98	1.12	43.47	0.09	0.79	106.56	155
AVG	**3.06**	**16.50**	**1.74**	**5.98**	**12.41**	**1.10**		**4.87**	**0.90**	**53.05**	**0.05**	**0.47**	**99.94**	**168**
SD	**0.97**	**4.85**	**0.38**	**1.19**	**2.57**	**0.46**		**1.63**	**0.17**	**2.69**	**0.02**	**0.19**	**2.17**	**26**
JH-B10														
1	0.71	8.17	1.84	10.10	12.65	2.35		2.19	0.53	54.14	0.07	1.38	94.01	106
2	1.11	8.90	19.52	0.10	4.49	13.70		1.78	0.06	50.88	0.21	0.24	100.99	146
3	6.31	1.05	7.44	1.05	23.83	0.12		0.16	0.03	59.33	bd	bd	99.31	47
4	6.24	15.37	4.05	1.82	19.35	0.29		4.47	0.13	51.86	bd	0.15	103.72	100
5	4.03	2.50	1.43	8.14	17.94	0.48		1.15	0.25	62.95	bd	0.27	99.11	121
AVG	**3.68**	**7.20**	**6.85**	**4.24**	**15.65**	**3.39**		**1.95**	**0.20**	**55.83**	**0.06**	**0.41**	**99.43**	**104**
SD	**1.20**	**2.55**	**3.34**	**2.03**	**3.31**	**2.61**		**0.72**	**0.09**	**2.30**	**0.04**	**0.25**	**1.59**	**16**
JH-B13														
1	1.48	42.64	5.05	1.90	7.16	4.42	0.05	8.81	0.02	37.40	0.54	0.65	110.12	77
2	0.50	31.26	12.13	0.31	3.77	7.25	bd	6.85	0.06	34.72	0.62	0.20	97.65	148
3	1.65	32.81	7.89	2.17	6.48	3.79	bd	11.52	0.05	29.61	0.71	0.89	97.57	bd
4	0.83	55.65	4.37	1.31	5.13	4.34	bd	11.52	0.02	23.29	0.64	0.32	107.41	33
AVG	**1.12**	**40.59**	**7.36**	**1.42**	**5.63**	**4.95**	**0.01**	**9.68**	**0.04**	**31.26**	**0.63**	**0.52**	**103.19**	**68**
SD	**0.27**	**5.62**	**1.76**	**0.41**	**0.75**	**0.78**	**0.01**	**1.14**	**0.01**	**3.11**	**0.03**	**0.16**	**3.27**	**30**
JH-B16														
1	1.45	19.71	9.65	3.34	9.40	6.88		3.90	0.04	46.16	0.31	0.83	101.67	60
2	3.96	6.76	6.34	5.53	13.97	2.26		2.26	0.03	54.82	0.17	0.59	96.69	183
3	4.60	2.63	4.36	4.78	18.70	0.19		1.44	0.04	61.01	0.04	0.72	98.49	153

	Na_2O	FeO	CaO	K_2O	Al_2O_3	MgO	Cr_2O_3	TiO_2	Cl	SiO_2	MnO	P_2O_5	Total	In (ppm)
4	0.77	18.54	12.91	0.87	5.42	10.77		3.24	0.01	46.77	0.44	0.32	100.08	83
5	6.02	0.91	8.90	0.71	25.55	0.15		0.22	bd	58.70	bd	bd	101.16	84
AVG	**3.36**	**9.71**	**8.43**	**3.05**	**14.61**	**4.05**		**2.21**	**0.02**	**53.49**	**0.19**	**0.49**	**99.62**	**112**
SD	**0.98**	**3.97**	**1.46**	**0.99**	**3.52**	**2.08**		**0.65**	**0.01**	**3.04**	**0.08**	**0.15**	**0.91**	**24**

Appendix G. Data Comparison Between Method 1 and Method 2

Table 21. Data comparison for major elements and indium between Methods 1 and 2. SD is the standard deviation of the mean (1σ) of the concentrations in a given experiment.

	Na_2O	FeO	CaO	K_2O	Al_2O_3	MgO	TiO_2	SiO_2	P_2O_5	In (ppm)
Starting Basalt										
Method 1 AVG	4.37	9.73	5.97	2.70	14.89	2.85	2.34	54.26	0.57	
Method 1 SD	0.12	0.31	0.29	0.10	0.23	0.25	0.06	0.29	0.02	
Method 2 AVG	3.45	8.66	7.55	2.33	14.04	3.83	2.20	55.54	0.63	
Method 2 SD	0.34	0.90	0.75	0.19	0.98	0.53	0.19	3.23	0.10	
JH-B1										
Method 1 AVG	2.77	10.32	8.61	0.98	13.12	4.77	2.29	52.26	0.70	68
Method 1 SD	0.34	0.84	1.65	0.19	1.32	1.49	0.22	1.22	0.09	23
Method 2 AVG	4.52	5.73	7.89	1.15	15.55	2.45	1.79	58.18	0.35	54
Method 2 SD	0.62	0.78	0.54	0.20	1.45	0.40	0.37	2.64	0.12	16
JH-B2										
Method 1 AVG	2.17	12.35	7.62	0.93	13.49	4.48	2.62	52.30	0.60	22
Method 1 SD	0.32	1.20	1.30	0.30	1.36	1.30	0.13	1.80	0.11	5
Method 2 AVG	4.29	6.32	9.85	0.79	16.41	3.42	1.59	58.09	0.35	47
Method 2 SD	0.48	0.81	0.93	0.13	1.41	0.77	0.22	3.41	0.16	9
JH-B4										
Method 1 AVG	4.15	9.42	5.29	2.19	14.70	2.03	2.50	57.18	0.52	49
Method 1 SD	0.19	0.43	0.49	0.39	0.34	0.35	0.17	0.50	0.05	13
Method 2 AVG	2.90	7.73	5.72	1.74	15.68	4.74	2.18	54.70	0.45	147
Method 2 SD	0.47	1.76	0.79	0.39	2.16	1.12	0.51	5.76	0.12	48
JH-B7										
Method 1 AVG	4.09	8.74	4.87	4.53	13.56	2.53	2.40	57.04	0.51	106
Method 1 SD	0.41	0.46	1.11	0.43	0.89	0.87	0.20	0.88	0.05	20

	Na_2O	FeO	CaO	K_2O	Al_2O_3	MgO	TiO_2	SiO_2	P_2O_5	In (ppm)
Method 2 AVG	3.93	9.15	7.03	4.43	14.01	3.25	2.50	54.12	0.40	101
Method 2 SD	0.59	1.52	1.06	1.08	1.16	0.60	0.44	3.07	0.18	15
JH-B10										
Method 1 AVG	3.12	7.51	3.25	5.83	13.08	3.01	1.83	51.20	0.96	128
Method 1 SD	0.40	0.75	0.72	0.42	0.60	1.18	0.16	1.61	0.19	13
Method 2 AVG	3.01	14.05	6.83	4.14	12.57	3.52	2.32	52.62	1.11	129
Method 2 SD	0.56	3.29	2.10	0.81	1.42	1.14	0.43	3.63	0.44	20

Appendix H. Estimating Volumes of the Interior and Rim

The volumes of the interior and rim are needed in order to calculate the overall bulk partition coefficient of the basalt. In order to estimate the volumes of the interior and rim of the basalt, a BSE image of the altered basalt was uploaded into Adobe Illustrator. The interior and the rim were then traced to form two polygons, one representing each region. These polygons were entered into ImageJ and the method *Fit to Ellipse* (*Edit* → *Selection* → *Fit to Ellipse* → *Draw*) was used to generate an ellipse around each region. In order to determine the lengths of the minima and maxima axes, measurements were made. The volume of each region was then calculated using the formula for an ellipsoid ($V = \frac{4}{3}\pi abc$), where *a* is equal the length of the maximum axis. However, because the image is 2D, both *b* and *c* were set equal to the length of the minimum axis (i.e. $V = \frac{4}{3}\pi ab^2$). The two partition coefficients for the rim and interior were then multiplied by their *volume/overall volume* and added together to find the overall partition coefficient for each experiment.

Appendix I. EPMA Methodology

Operating Conditions and Standards

Samples were analyzed for major and minor elements by using a JEOL 8900R electron probe microanalyzer at the AIMLab (Advanced Imaging and Microscopy Laboratory) at the University of Maryland. Backscatter electron (BSE) images were also collected using the same instrument. Major and trace element analyses were collected in

sequence using two sets of operating conditions optimized for the analyses. Furthermore, probe beam diameter varied depending on whether or not Method 1 or 2 was used and was either 1 or 10 μm. Accelerating voltage was set to 15 kV for major element analyses and 20 kV for trace element analyses. The current was set to $1x10^{-8}$ A for major elements and $2x10^{-7}$ A for trace elements. Spectrometers, crystals, and standards are listed in tables I-1 through I-4. One concern when analyzing low concentrations of indium in silicates is the overlap of the primary analytical peaks with major constituents. For example, the L-value, where $L = n\lambda R/d$ ($n = 1$ for both In and K, $2d = 8.742$, and $R = 140$ mm), of Kα for potassium (119.8632 mm) interferes with the L-value of Lα for indium (120.8465 mm) on the PETH crystal. Additionally, the L-value of Kβ for iron (112.5445 mm when $n = 2$) interferes with the L-value of Lβ for indium (113.8801 mm when $n = 1$) on the PETH crystal. A single channel analyzer is used to filter out the Kβ peaks of iron but will accept the Lβ peaks of indium.

Table 22. EPMA conditions used for major element and trace element analyses in both sets of experiments. Note that S was only analyzed in the high pH, sulfur-bearing seawater experiments.

Spectrometer	Majors (Crystal)	Trace Element (Crystal)
1	Na (TAP) Mg (TAP)	Na (TAP) Mg (TAP) Fe (LIF)
2	Fe (LIFH) Mn (LIFH) Cr (LIFH)	In (PETH)
3	Ca (PETJ) Ti (PETJ)	K (PETJ)
4	K (PETJ) Cl (PETJ) S (PETH)	In (PETJ)
5	Al (TAP) Si (TAP) P (TAP)	Al (TAP) Si (TAP)

Table 23. Standards used in WDS analyses in the low initial pH, HCl-bearing experiments.

Standard Name	Oxide/Element Analyzed
Basalt, Makaopuhi Lava Lake, HI	Na_2O, FeO, CaO, K_2O, Al_2O_3, MgO, TiO_2, SiO_2
Hornblende, Kakanui, New Zealand (trace analyses)	Na_2O, Al_2O_3, K_2O, SiO_2
Apatite, Durango, Mexico	P_2O_5
Bushveld Chromite	Cr_2O_3
Rhodonite, Broken Hill Mine, Australia	MnO
Scapolite (Meionite), Brazil	Cl
NIST 610 (trace) InAs (trace), synthetic	In_2O_3

Table 24. Standards used in WDS analyses of the altered glass in the high initial pH, sulfur-bearing seawater experiments.

Standard Name	Oxide/Element Analyzed
Basalt, Makaopuhi Lava Lake, HI	Na_2O, FeO, CaO, K_2O, Al_2O_3, MgO, TiO_2, SiO_2
Basalt, Makaopuhi Lava Lake, HI (trace analyses)	Na_2O, Al_2O_3, K_2O, SiO_2, FeO, MgO, CaO
Apatite, Durango, Mexico	P_2O_5
Rhodonite, Broken Hill Mine, Australia	MnO
Scapolite (Meionite), Brazil	Cl, SO_3
InAs (trace), synthetic	In_2O_3

Table 25. Standards used in WDS analyses of the plagioclase in the high pH, sulfur-bearing seawater experiments.

Standard Name	Oxide/Element Analyzed
Basalt, Makaopuhi Lava Lake, HI	K_2O, FeO, MgO, TiO_2
Basalt, Makaopuhi Lava Lake, HI (trace analyses)	Na_2O, Al_2O_3, K_2O, SiO_2, FeO, MgO, CaO
Anorthite, Great Sitkin Island, AK	Na_2O, CaO, Al_2O_3, SiO_2
Apatite, Durango, Mexico	P_2O_5
Rhodonite, Broken Hill Mine, Australia	MnO
Scapolite (Meionite), Brazil	Cl, SO_3
InAs (trace), synthetic	In_2O_3

Detection Limit

The detection limit (D.L.) for an element at the 1σ level is calculated by using the following equation (JEOL, 2001):

$$D.L. = \frac{1}{\frac{I_{std}}{wt\%_{std}}} * \sqrt{\frac{2 * I_{bg}}{t_{bg}}}$$

where: I_{std} is equal to the intensity of the x-rays of the standard; $wt\%_{std}$ is the concentration of the element in the standard in wt. %; I_{bg} is the mean background intensity; and t_{bg} is the count time of the background. For indium, the count times used was 300 on peak and 300 on the background. The calculated detection limit is 25 ppm.

Appendix J. Experimental Conditions for the High Initial pH, Sulfur-bearing Seawater Experiments

Table 26. Experimental conditions for seawater experiments. The initial and final masses (m_i and m_f) are the masses of the experimental charge before they were placed in the furnace and after they were taken out of the furnace. Δ mass is the change of the mass of the experimental charge.

	Time (wk)	W/R	In (ppm)	Rock (mg)	$InCl_3$-Water (mg)	Seawater (mg)	$Solution_{total}$ (mg)	$Total_i$ (mg)	$Total_f$ (mg)	Δ mass (mg)
JH-S1	4	0.99	1097	54.16	5.47	48.09	*53.56*	887.76	888.62	0.86
JH-S2	4	2.06	1082	49.95	10.36	92.29	*102.65*	970.49	1003.3	32.81
JH-S3	4	3.05	1021	33.33	9.73	91.9	*101.63*	956.91	912	-44.91
JH-S5	8	3.07	1017	29.89	8.77	83.13	*91.9*	966.78	967.11	0.33
JH-S8	6	9.86	995	11.85	10.93	105.86	*116.79*	1033.88	1157.38	123.5

Appendix K. Major Element and Indium Concentrations in the High Initial pH, Sulfur-bearing Seawater Experiments

Table 27. Major element (wt.%) composition of the Juan de Fuca MORB, reported by Arévalo and McDonough (2008).

Na_2O	CaO	FeO	Al_2O_3	MgO	TiO_2	MnO	SiO_2	P_2O_5	Total
2.68	10.84	11.71	13.73	6.87	1.83	0.23	49.67	0.12	97.70

Table 28. Major element (wt.%) and indium (ppm) concentrations in the interior of the altered basaltic glass. SD is the standard deviation of the mean (1σ) of the concentrations in a given experiment. Indium concentrations listed as bd indicate the analysis was below the detection limit (17 ppm) and so the concentration was set at one half the detection limit (8.5 ppm).

	Na_2O	Cl	CaO	FeO	Al_2O_3	MgO	SO_3	TiO_2	MnO	SiO_2	K_2O	P_2O_5	Total	In (ppm)
JH-S1-1	3.67	0.16	10.21	12.82	10.13	9.64	0.06	1.62	0.11	37.06	0.51	bd	85.99	204
JH-S1-2	4.97	0.46	8.31	11.55	10.10	10.39	0.08	1.68	0.18	37.09	0.81	bd	85.53	178
JH-S1-3	3.45	0.24	9.62	12.49	10.30	9.73	0.05	1.66	0.24	37.59	0.47	bd	85.74	178
JH-S1-4	3.54	0.52	9.71	13.25	10.21	9.31	0.08	1.66	0.26	36.97	0.44	0.08	85.92	194
JH-S1-5	2.58	0.58	11.19	13.57	11.15	8.95	0.03	1.73	0.21	38.15	0.44	bd	88.47	253
JH-S1-6	2.78	0.51	9.09	13.09	9.46	9.75	0.06	1.66	0.19	37.20	0.47	0.05	84.21	438
AVG	**3.50**	**0.41**	**9.69**	**12.80**	**10.22**	**9.63**	**0.06**	**1.67**	**0.20**	**37.34**	**0.52**	**0.02**	**85.98**	**241**
SD	**0.34**	**0.07**	**0.40**	**0.29**	**0.22**	**0.20**	**0.01**	**0.01**	**0.02**	**0.18**	**0.06**	**0.01**	**0.57**	**41**
JH-S2-1	1.25	0.13	10.04	13.30	10.13	9.26	0.09	1.78	0.37	39.43	0.43	0.10	86.28	168
JH-S2-2	4.21	0.23	9.40	12.62	10.23	9.73	0.06	1.64	0.17	36.71	0.40	bd	85.37	169
JH-S2-3	3.10	0.16	10.47	13.96	11.11	8.60	0.11	1.70	0.21	37.36	0.38	0.07	87.19	214
JH-S2-4	2.77	0.16	10.97	12.41	10.39	8.44	0.11	1.63	0.20	37.21	0.27	0.08	84.60	224
JH-S2-5	2.17	0.14	10.24	12.48	9.63	9.09	0.13	1.69	0.16	36.68	0.23	0.05	82.65	373
JH-S2-6	3.65	0.14	9.64	12.30	9.85	9.44	0.08	1.57	0.26	35.48	0.25	bd	82.67	251
AVG	**2.86**	**0.16**	**10.13**	**12.85**	**10.22**	**9.09**	**0.10**	**1.67**	**0.23**	**37.14**	**0.33**	**0.05**	**84.79**	**233**
SD	**0.43**	**0.01**	**0.23**	**0.27**	**0.21**	**0.20**	**0.01**	**0.03**	**0.03**	**0.53**	**0.03**	**0.02**	**0.76**	**31**
JH-S3-1	0.95	0.17	13.83	14.06	11.05	9.13	0.03	1.89	0.28	40.56	0.32	bd	92.25	658
JH-S3-2	1.06	0.19	11.94	14.94	12.10	9.23	0.06	2.10	0.24	40.71	0.42	0.04	92.97	510
JH-S3-3	1.03	0.16	12.27	14.22	11.49	9.34	0.05	1.95	0.19	40.71	0.40	0.04	91.83	510
JH-S3-4	5.76	0.20	8.93	6.61	17.75	**2.41**	0.02	1.99	0.10	53.42	0.09	0.10	97.34	329
JH-S3-5	1.21	0.21	12.01	14.84	12.08	9.51	0.05	1.89	0.27	41.06	0.49	bd	93.59	541
JH-S3-6	0.97	0.22	12.57	14.99	11.18	9.88	0.06	2.05	0.29	40.67	0.35	0.06	93.23	564
AVG	**1.83**	**0.19**	**11.92**	**13.28**	**12.61**	**8.25**	**0.04**	**1.98**	**0.23**	**42.85**	**0.35**	**0.04**	**93.54**	**519**
SD	**0.79**	**0.01**	**0.66**	**1.34**	**1.04**	**1.17**	**0.01**	**0.03**	**0.03**	**2.11**	**0.06**	**0.02**	**0.81**	**44**
JH-S5-1	2.31	0.36	7.57	10.58	10.00	13.28	0.04	2.14	0.17	38.16	0.25	0.17	84.94	390
JH-S5-2	1.97	0.29	9.01	12.08	10.77	12.40	0.03	2.17	0.18	39.94	0.24	0.04	89.04	169
JH-S5-3	2.10	0.34	8.81	11.40	10.24	11.94	0.05	1.85	0.06	38.40	0.22	0.09	85.44	403
JH-S5-4	0.78	0.59	9.74	10.81	6.51	7.94	0.12	2.54	0.10	30.75	0.06	bd	69.81	691
JH-S5-5	0.81	0.83	10.70	10.84	7.59	7.45	0.16	2.30	0.14	32.73	0.08	0.08	73.51	710
JH-S5-6	0.81	0.57	11.50	11.52	7.74	7.60	0.15	2.12	0.15	34.31	0.06	0.19	76.59	707
JH-S5-7	0.79	0.63	10.86	11.25	7.76	7.84	0.17	2.38	0.10	34.29	0.07	bd	76.01	651
JH-S5-8	7.45	0.30	7.53	2.20	19.02	1.38	0.05	1.83	0.03	49.28	0.09	0.05	89.14	388
JH-S5-9	0.81	0.59	11.10	10.99	7.18	8.18	0.16	2.51	0.11	31.09	0.08	0.03	72.69	1085

	Na_2O	Cl	CaO	FeO	Al_2O_3	MgO	SO_3	TiO_2	MnO	SiO_2	K_2O	P_2O_5	Total	In (ppm)
JH-S5-10	0.62	0.67	10.68	10.89	7.13	7.29	0.52	2.81	0.14	32.54	0.05	bd	73.14	948
AVG	**1.84**	**0.52**	**9.75**	**10.25**	**9.40**	**8.53**	**0.15**	**2.26**	**0.12**	**36.15**	**0.12**	**0.07**	**79.03**	**614**
SD	**0.66**	**0.06**	**0.46**	**0.91**	**1.17**	**1.08**	**0.05**	**0.10**	**0.02**	**1.77**	**0.03**	**0.02**	**2.32**	**88**
JH-B8-1	2.05	0.27	11.24	11.84	10.27	10.70	0.16	1.86	0.18	38.55	0.23	0.04	87.33	1178
JH-B8-2	1.26	0.24	10.96	10.52	9.93	10.16	0.14	1.76	0.19	38.43	0.16	0.05	83.75	1654
JH-B8-3	0.78	0.11	6.59	4.31	7.27	7.08	0.07	0.92	0.11	27.53	0.06	bd	54.84	2183
JH-B8-4	1.19	0.32	10.08	10.29	9.71	10.38	0.20	1.83	0.16	38.39	0.16	0.09	82.72	1514
JH-B8-5	2.00	0.20	10.53	11.58	10.35	10.85	0.12	1.87	0.08	38.70	0.20	0.06	86.50	1366
JH-B8-6	0.93	0.16	9.61	8.20	9.79	9.96	0.06	1.91	0.16	38.99	0.16	0.12	80.02	1678
JH-B8-7	0.91	0.18	10.86	9.32	9.60	9.74	0.14	1.92	0.22	39.02	0.15	0.12	82.15	1791
JH-B8-8	1.05	0.19	13.44	11.96	9.86	9.56	0.19	2.13	0.18	40.24	0.10	0.15	89.01	3086
AVG	**1.27**	**0.21**	**10.41**	**9.75**	**9.60**	**9.80**	**0.13**	**1.78**	**0.16**	**37.48**	**0.15**	**0.08**	**80.79**	**1806**
SD	**0.17**	**0.02**	**0.68**	**0.90**	**0.34**	**0.42**	**0.02**	**0.13**	**0.02**	**1.44**	**0.02**	**0.02**	**3.85**	**211**

Table 29. Major element (wt.%) and indium (ppm) concentrations in the rim of the altered basaltic glass. Note that the light regions in JH-S8 are not considered in the averages of this experiment. SD is the standard deviation of the mean (1σ) of the concentrations in a given experiment. Indium concentrations listed as bd indicate the analysis was below the detection limit (17 ppm) and so the concentration was set at one half the detection limit (8.5 ppm).

	Na_2O	Cl	CaO	FeO	Al_2O_3	MgO	SO_3	TiO_2	MnO	SiO_2	K_2O	P_2O_5	Total	In (ppm)
JH-S1-1	0.55	0.36	10.08	10.78	5.47	6.21	0.35	2.12	0.13	32.00	0.06	0.12	68.16	384
JH-S1-2	0.35	0.35	7.35	7.63	4.07	5.88	0.75	1.72	0.14	27.12	0.05	0.08	55.39	407
JH-S1-3	0.70	0.45	11.00	13.33	7.56	6.67	0.52	2.01	0.14	33.42	0.06	0.10	75.86	501
JH-S1-4	0.47	0.38	10.00	10.66	5.48	6.39	0.55	1.94	0.17	32.01	0.06	0.14	68.17	421
JH-S1-5	0.52	0.46	11.17	11.98	6.69	6.15	0.29	2.10	0.16	32.93	0.07	bd	72.41	571
JH-S1-6	0.62	0.32	9.57	11.59	8.42	8.77	0.06	1.68	0.16	36.26	0.09	0.07	77.53	419
AVG	**0.54**	**0.39**	**9.86**	**10.99**	**6.28**	**6.68**	**0.42**	**1.93**	**0.15**	**32.29**	**0.07**	**0.09**	**69.59**	**451**
SD	**0.05**	**0.02**	**0.56**	**0.78**	**0.65**	**0.43**	**0.10**	**0.08**	**0.01**	**1.22**	**0.01**	**0.02**	**3.25**	**29**
JH-S2-1	0.64	0.26	14.23	12.56	7.97	7.90	0.20	1.97	0.23	40.52	0.06	0.09	86.57	398
JH-S2-2	2.15	0.17	9.20	12.43	9.06	9.36	0.21	1.70	0.17	36.52	0.22	bd	81.14	197
JH-S2-3	0.94	0.15	10.32	11.31	8.09	8.00	0.07	1.71	0.12	37.06	0.08	0.10	77.91	1325
JH-S2-4	0.61	0.24	11.79	12.76	7.70	8.00	0.22	3.06	0.21	38.07	0.10	0.22	82.93	395
JH-S2-5	0.69	0.20	12.03	14.15	8.89	9.44	0.06	2.23	0.16	40.78	0.10	0.13	88.81	355
AVG	**1.00**	**0.20**	**11.51**	**12.64**	**8.34**	**8.54**	**0.15**	**2.13**	**0.18**	**38.59**	**0.11**	**0.11**	**83.47**	**534**
SD	**0.29**	**0.02**	**0.85**	**0.45**	**0.27**	**0.35**	**0.04**	**0.25**	**0.02**	**0.88**	**0.03**	**0.04**	**1.93**	**201**
JH-S3-1	1.04	0.60	10.70	14.95	10.17	10.13	0.14	3.08	0.15	40.19	0.17	0.23	91.40	788
JH-S3-2	1.15	0.46	14.26	15.89	9.67	8.95	0.10	2.43	0.19	40.88	0.10	0.03	93.98	822
JH-S3-3	1.22	0.48	11.20	15.39	10.28	10.50	0.09	2.62	0.23	41.17	0.16	0.14	93.37	737
JH-S3-4	0.98	0.38	14.85	16.01	10.07	8.32	0.08	2.29	0.20	42.10	0.08	0.15	95.43	745
JH-S3-5	0.88	0.49	12.88	15.59	10.19	9.65	0.07	2.19	0.28	40.97	0.18	0.12	93.38	735
JH-S3-6	0.94	0.67	14.19	16.44	9.69	8.11	0.18	2.61	0.25	41.09	0.09	0.07	94.18	926
AVG	**1.03**	**0.51**	**13.01**	**15.71**	**10.01**	**9.28**	**0.11**	**2.54**	**0.22**	**41.07**	**0.13**	**0.12**	**93.62**	**792**
SD	**0.05**	**0.04**	**0.71**	**0.21**	**0.11**	**0.40**	**0.02**	**0.13**	**0.02**	**0.25**	**0.02**	**0.03**	**0.54**	**30**
JH-S5-1	1.16	0.45	12.08	16.00	10.21	7.58	0.09	1.25	0.17	40.78	0.11	bd	89.73	3561
JH-S5-2	0.88	0.53	12.30	13.19	8.53	7.43	0.22	2.74	0.16	38.52	0.05	0.03	84.44	902
JH-S5-3	0.96	0.42	11.30	11.98	8.50	8.03	0.23	1.67	0.14	36.85	0.07	bd	80.04	1168
AVG	**1.00**	**0.47**	**11.89**	**13.72**	**9.08**	**7.68**	**0.18**	**1.88**	**0.15**	**38.72**	**0.08**	**0.01**	**84.74**	**1877**
SD	**0.08**	**0.03**	**0.30**	**1.19**	**0.57**	**0.18**	**0.04**	**0.44**	**0.01**	**1.14**	**0.02**	**0.01**	**2.80**	**846**
JH-S8-1	1.12	0.19	13.77	12.58	10.05	9.66	0.15	2.10	0.20	40.65	0.11	0.08	90.62	3234
JH-S8-2	0.96	0.20	14.09	11.45	8.12	7.62	0.14	2.12	0.21	37.92	0.06	0.12	82.97	4318
JH-S8-3	1.01	0.24	12.78	12.28	8.36	8.01	0.73	1.97	0.14	37.63	0.06	0.05	83.21	5450
JH-S8-4	1.13	0.22	12.90	12.24	8.57	7.85	0.63	2.02	0.17	37.34	0.06	bd	83.12	3950

	Na_2O	Cl	CaO	FeO	Al_2O_3	MgO	SO_3	TiO_2	MnO	SiO_2	K_2O	P_2O_5	Total	In (ppm)
JH-S8-5	0.98	0.23	13.89	11.38	7.90	7.55	0.13	2.22	0.20	37.07	0.06	0.12	81.68	2770
JH-S8-6	1.05	0.26	13.84	11.82	7.84	7.75	0.30	2.11	0.12	37.61	0.06	bd	82.69	3508
JH-S8-7	1.12	0.24	12.57	11.48	7.76	7.91	0.34	2.23	0.21	35.99	0.08	0.07	79.95	4403
JH-S8-8	1.20	0.22	12.07	12.66	8.12	8.18	0.14	2.08	0.20	37.35	0.09	0.05	82.30	4866
JH-S8-light1	1.37	0.14	13.76	13.37	9.11	9.32	0.20	1.47	0.13	41.99	0.11	bd	90.94	28791
JH-S8-light2	1.34	0.14	13.10	13.64	9.13	9.39	0.20	1.50	0.15	41.74	0.10	bd	90.35	23104
JH-S8-light3	1.26	0.13	13.75	13.57	9.09	9.02	0.15	1.56	0.17	42.21	0.11	bd	90.99	22857
JH-S8-light4	1.30	0.16	13.48	14.03	9.08	9.32	0.20	1.69	0.26	42.84	0.11	bd	92.47	21115
AVG	**1.07**	**0.23**	**13.24**	**11.99**	**8.34**	**8.07**	**0.32**	**2.11**	**0.18**	**37.69**	**0.07**	**0.06**	**83.32**	**4062**
SD	**0.03**	**0.01**	**0.27**	**0.18**	**0.26**	**0.24**	**0.08**	**0.03**	**0.01**	**0.47**	**0.01**	**0.02**	**1.11**	**311**

Table 30. Major element (wt.%) and indium (ppm) concentrations in the plagioclase veins and crystals. * denotes experiments that were filtered out based on the criteria detailed within section 4.3. † denotes these analyses were of plagioclase crystals. SD is the standard deviation of the mean (1σ) of the concentrations in a given experiment. Indium concentrations listed as bd indicate the analysis was below the detection limit (17 ppm) and so the concentration was set at one half the detection limit (8.5 ppm). Plagioclase from experiments JH-S3 and JH-S5 did not use a plagioclase standard, as this phase was not identified as plagioclase at time of analysis.

	Na_2O	Cl	CaO	FeO	Al_2O_3	MgO	SO_3	TiO_2	MnO	SiO_2	K_2O	P_2O_5	Total	In (ppm)
JH-S1-1	7.98	0.04	6.84	0.77	21.97	0.13	0.01	1.89	bd	62.24	0.08	0.09	102.00	bd
JH-S1-2	7.85	0.06	6.59	1.06	20.88	0.27	bd	1.92	0.04	61.53	0.09	0.05	100.33	35
JH-S1-3	7.66	0.08	6.97	2.02	20.34	0.58	0.02	1.88	bd	61.17	0.08	bd	100.78	66
JH-S1-4	8.38	0.05	5.72	0.81	20.17	0.22	0.03	1.70	bd	62.65	0.05	0.13	99.90	50
JH-S1-5	8.04	0.08	6.61	1.36	20.56	0.32	bd	1.76	bd	61.53	0.06	0.08	100.37	47
JH-S1-6†	7.96	0.05	6.84	1.11	20.59	0.31	bd	2.41	bd	61.06	0.05	bd	100.42	41
JH-S1-7†	8.57	0.04	5.22	0.86	21.89	0.07	0.03	1.59	0.07	62.12	0.07	bd	100.51	54
AVG	**8.06**	**0.06**	**6.40**	**1.14**	**20.91**	**0.27**	**0.01**	**1.88**	**0.02**	**61.76**	**0.07**	**0.05**	**100.62**	**43**
SD	**0.12**	**0.01**	**0.25**	**0.17**	**0.28**	**0.06**	**0.00**	**0.10**	**0.01**	**0.22**	**0.01**	**0.02**	**0.25**	**7**
JH-S2-1*	6.47	0.11	8.27	5.13	18.74	1.86	0.01	1.63	0.08	56.78	0.11	bd	99.17	146
JH-S2-2	8.21	0.08	5.89	1.29	20.21	0.52	0.01	1.67	0.08	60.78	0.07	bd	98.77	bd
JH-S2-3*	7.07	0.11	7.64	3.91	19.15	1.78	0.02	2.00	0.06	57.68	0.08	0.06	99.54	154
JH-S2-4	7.38	0.09	7.28	2.53	19.98	0.75	0.02	1.73	0.09	59.47	0.07	0.04	99.40	101
JH-S2-5	7.93	0.05	6.30	0.87	21.19	0.10	bd	1.81	0.10	62.63	0.05	0.04	101.06	bd
JH-S2-6	8.69	0.03	5.88	0.59	20.28	0.12	bd	1.76	bd	62.77	0.07	0.04	100.19	26
AVG	**8.05**	**0.06**	**6.34**	**1.32**	**20.41**	**0.38**	**0.01**	**1.74**	**0.07**	**61.41**	**0.07**	**0.03**	**99.86**	**36**
SD	**0.27**	**0.02**	**0.33**	**0.43**	**0.27**	**0.16**	**0.00**	**0.03**	**0.02**	**0.79**	**0.01**	**0.01**	**0.50**	**28**
JH-S3-1	7.84	0.13	6.21	1.51	20.93	1.07	0.01	1.29	0.03	59.71	0.06	bd	98.76	118
JH-S3-2	7.94	0.24	4.87	1.98	20.95	1.20	0.03	1.61	0.07	59.80	0.09	bd	98.71	212
JH-S3-3	7.50	0.11	6.52	2.94	19.80	1.88	0.02	1.30	0.04	59.86	0.08	bd	99.97	210
JH-S3-4	7.34	0.11	6.86	2.37	19.79	1.66	0.01	1.81	0.03	58.56	0.05	0.04	98.60	156
JH-S3-5	7.85	0.16	6.51	1.62	21.06	1.06	0.02	1.27	bd	59.34	0.06	bd	98.94	169
AVG	**7.69**	**0.15**	**6.19**	**2.08**	**20.51**	**1.37**	**0.02**	**1.45**	**0.03**	**59.45**	**0.07**	**0.01**	**98.99**	**173**
SD	**0.12**	**0.02**	**0.35**	**0.26**	**0.29**	**0.17**	**0.00**	**0.11**	**0.01**	**0.24**	**0.01**	**0.01**	**0.25**	**18**
JH-S5-1	9.12	0.01	4.56	0.33	22.16	bd	bd	0.07	bd	62.39	0.08	bd	98.63	bd
JH-S5-2	8.11	0.29	6.63	0.95	20.30	0.46	0.02	1.40	0.04	57.42	0.06	bd	95.62	122
JH-S5-3	8.39	0.24	6.14	0.75	21.54	0.69	0.03	1.68	bd	59.98	0.09	bd	99.45	182
JH-S5-4	7.65	0.43	7.03	2.05	20.49	1.22	0.01	1.41	0.08	58.58	0.07	bd	98.89	582
JH-S5-5*	5.89	0.16	9.52	5.43	17.73	2.60	0.02	1.82	0.06	53.23	0.10	bd	96.51	387
JH-S5-6	7.65	0.12	6.57	2.19	18.64	1.56	0.01	2.07	0.04	56.17	0.06	bd	95.04	127
AVG	**8.18**	**0.22**	**6.18**	**1.25**	**20.63**	**0.78**	**0.02**	**1.32**	**0.03**	**58.91**	**0.07**	**bd**	**97.53**	**205**
SD	**0.27**	**0.07**	**0.43**	**0.37**	**0.60**	**0.28**	**0.01**	**0.34**	**0.02**	**1.08**	**0.00**	**bd**	**0.91**	**99**

	Na_2O	Cl	CaO	FeO	Al_2O_3	MgO	SO_3	TiO_2	MnO	SiO_2	K_2O	P_2O_5	Total	In (ppm)
JH-B8-1*	5.52	0.10	9.71	6.99	17.13	3.25	0.01	1.72	0.17	54.69	0.06	bd	99.32	1930
JH-B8-2*	5.17	0.09	10.90	7.52	16.08	3.35	0.02	1.79	0.15	53.60	0.06	0.10	98.82	1238
JH-B8-3*	5.67	0.13	9.96	5.76	17.54	2.50	0.04	1.73	0.06	54.90	0.07	0.08	98.42	1797
JH-B8-4*	4.57	0.11	11.68	7.79	15.90	3.88	0.02	1.81	0.07	52.30	0.08	bd	98.21	4213
JH-B8-5*	5.45	0.10	9.52	6.37	16.22	3.08	0.01	1.73	0.10	53.17	0.06	bd	95.81	864
JH-B8-6	7.62	0.14	6.23	1.96	20.13	1.19	bd	1.91	0.07	60.24	0.09	bd	99.56	639
JH-B8-7*	5.34	0.13	9.71	6.24	17.48	3.29	0.03	1.80	0.15	54.21	0.05	bd	98.40	4194
JH-B8-8	7.57	0.09	5.71	0.75	21.52	0.73	0.02	1.44	bd	59.97	0.08	bd	97.84	329
JH-B8-9	7.22	0.08	6.45	1.15	21.00	0.80	0.03	1.95	bd	58.31	0.07	bd	97.03	1316
JH-B8-10	8.30	0.14	5.09	0.70	21.60	0.72	0.02	0.97	bd	61.44	0.07	bd	98.97	347
AVG	**7.68**	**0.11**	**5.87**	**1.14**	**21.06**	**0.86**	**0.02**	**1.57**	**0.02**	**59.99**	**0.08**	**bd**	**98.35**	**658**
SD	**0.23**	**0.02**	**0.30**	**0.29**	**0.34**	**0.11**	**0.01**	**0.23**	**0.02**	**0.64**	**0.00**	**bd**	**0.57**	**231**

Appendix L. Method for Calculating Area of Plagioclase and Altered Glass

In order to estimate the areas of the altered basaltic glass and the plagioclase veins, a mosaic of BSE images of the altered basalt was uploaded into Adobe Illustrator. The plagioclase veins and crystals were painted over (see Figure 16) to form a polygon. The altered glass was then traced over to form a polygon. These polygons were entered into ImageJ in order to calculate the areas of each polygon. The two partition coefficients for the glass and plagioclase ($D_{In}^{glass/aqueous}$ and $D_{In}^{plagioclase}$) were then multiplied by their area fraction (*area/total area)* and added together to determine the bulk partition coefficient (bulk D) for each experiment. In the case of JH-S8, where the area of the rim and interior were calculated, two separate polygons were drawn and areas were subsequently calculated. The area fractions were then multiplied by the concentration of indium in their respective region (i.e. rim and interior) in order to determine a representative indium concentration of the entire altered glass. By doing so, the partition coefficient of the glass takes into account the proportions of the rim and the interior as well as the distribution of indium concentrations in these two regions. The bulk D was then calculated using the same method as described above.

Appendix M. Mosaics of BSE Images

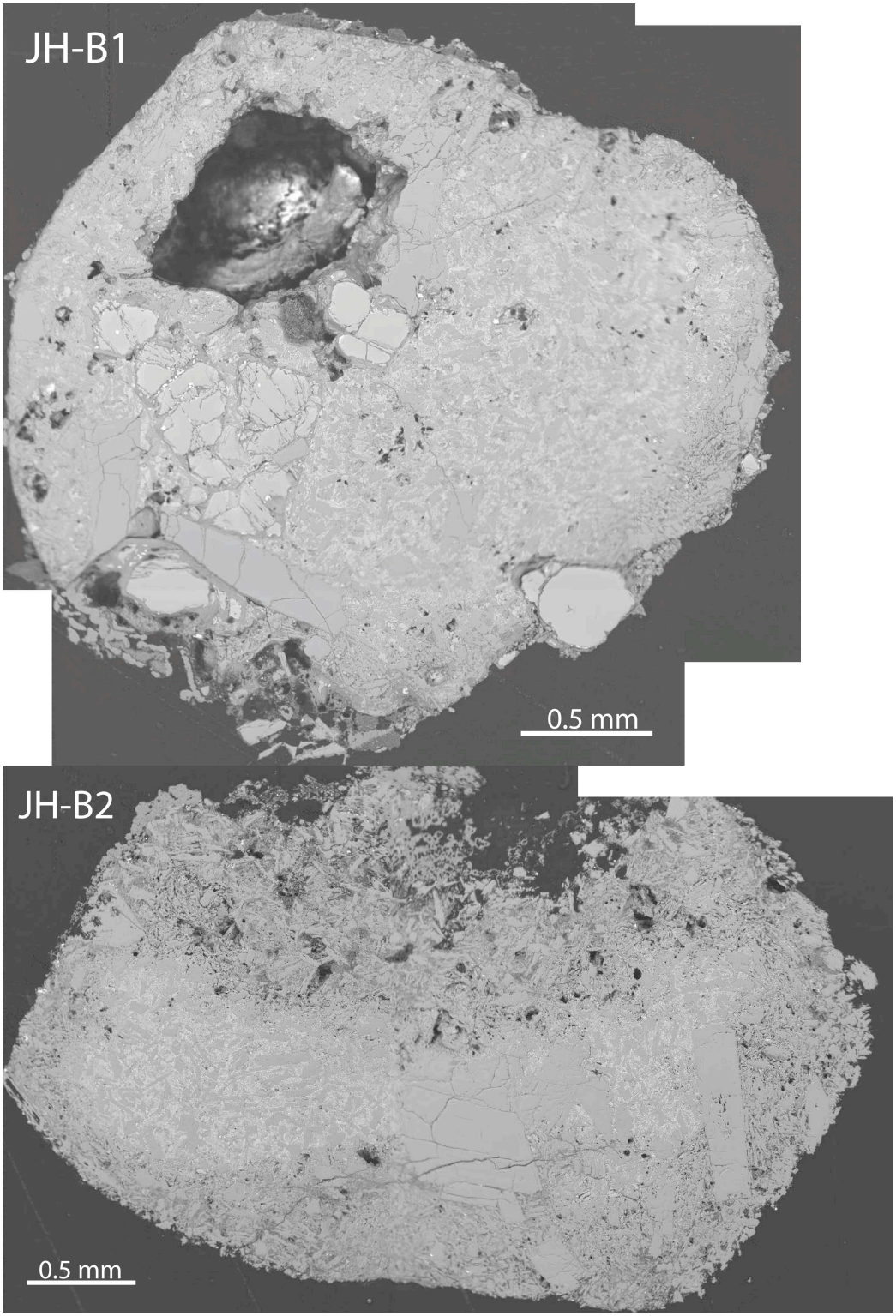

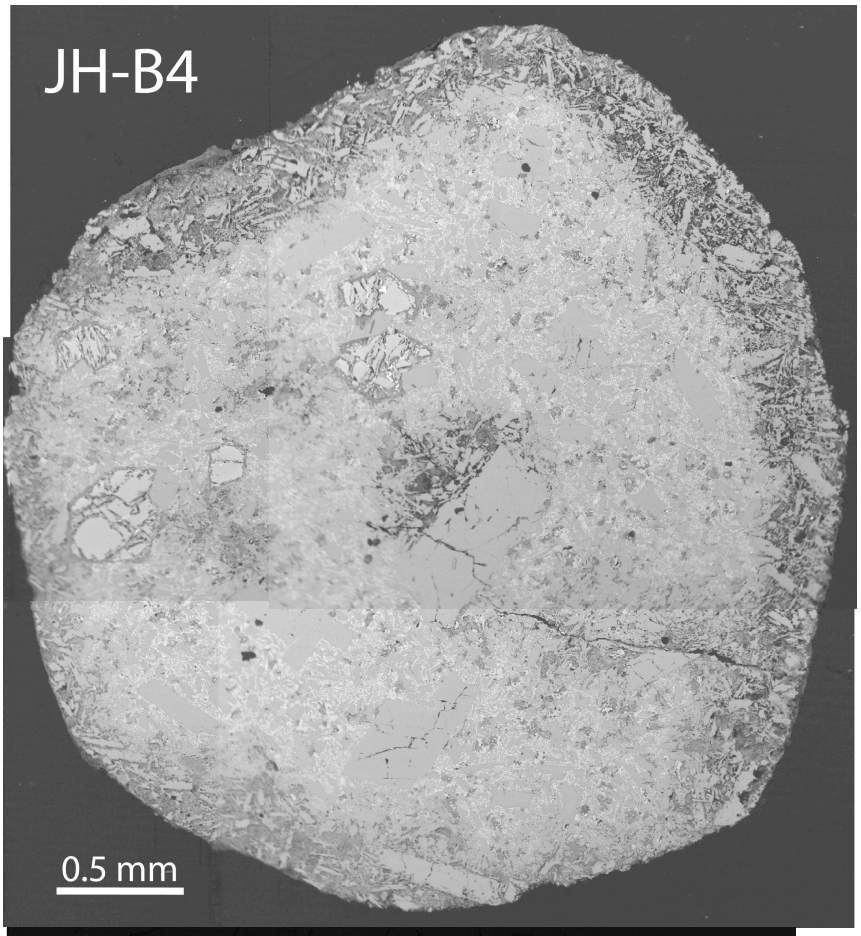
JH-B4
0.5 mm

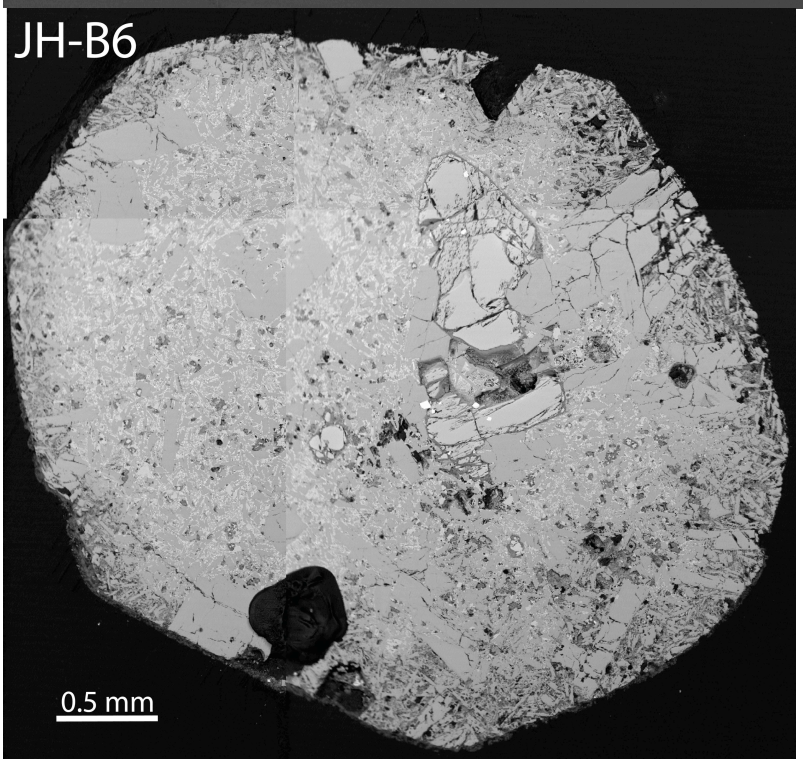
JH-B6
0.5 mm

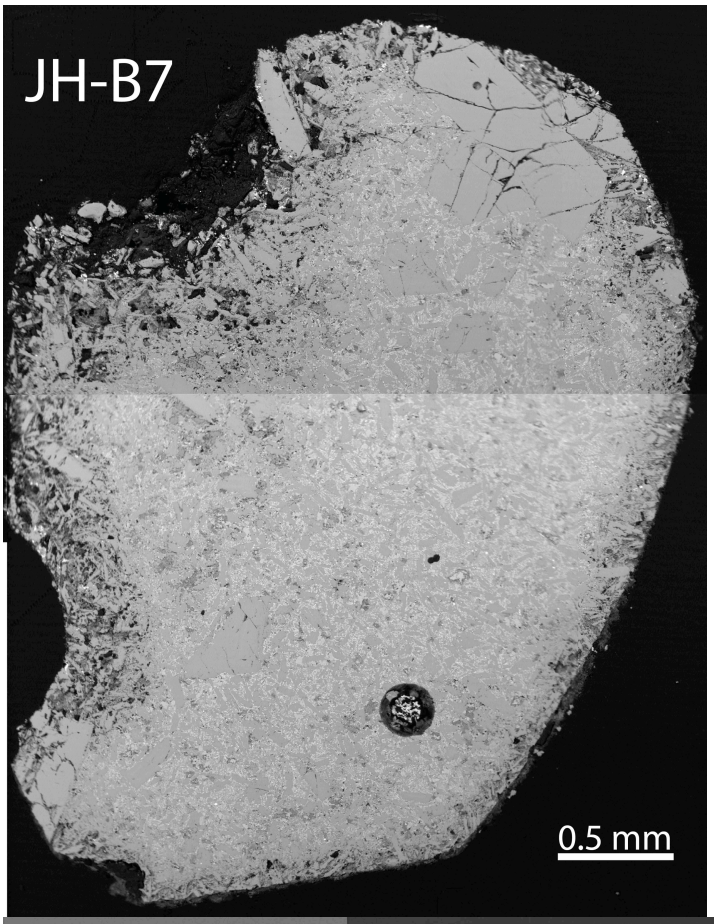
JH-B7
0.5 mm

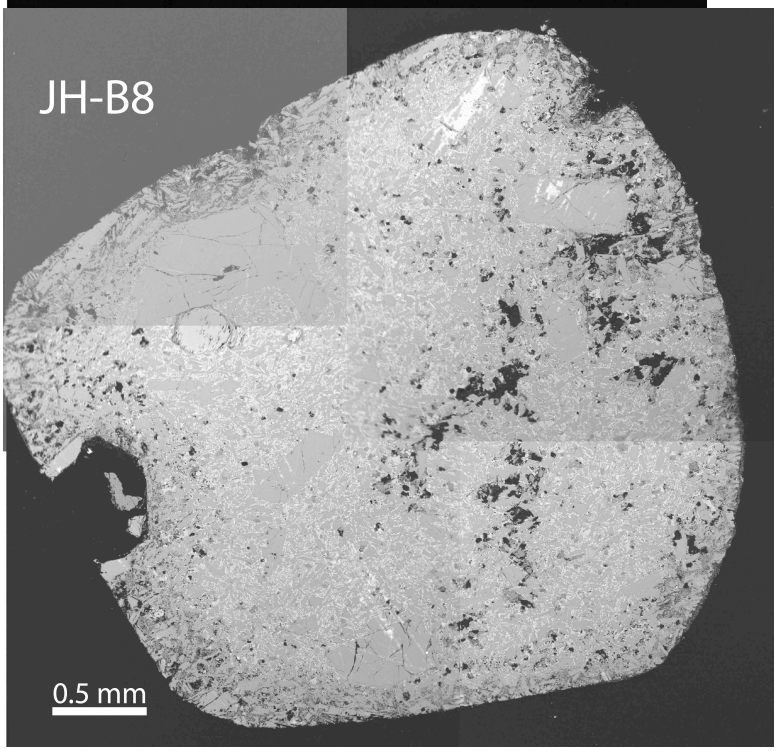
JH-B8
0.5 mm

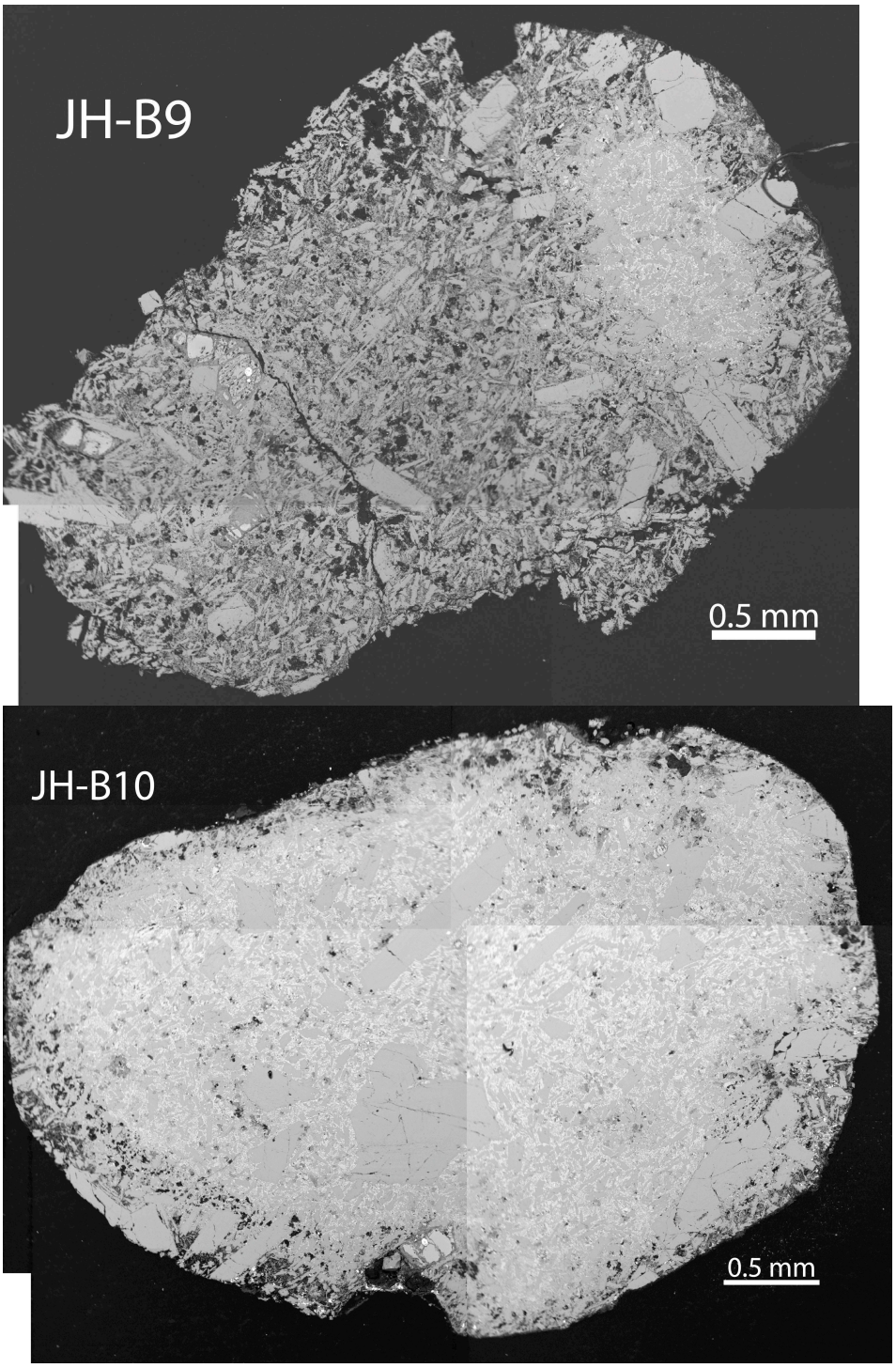
JH-B9
0.5 mm
JH-B10
0.5 mm

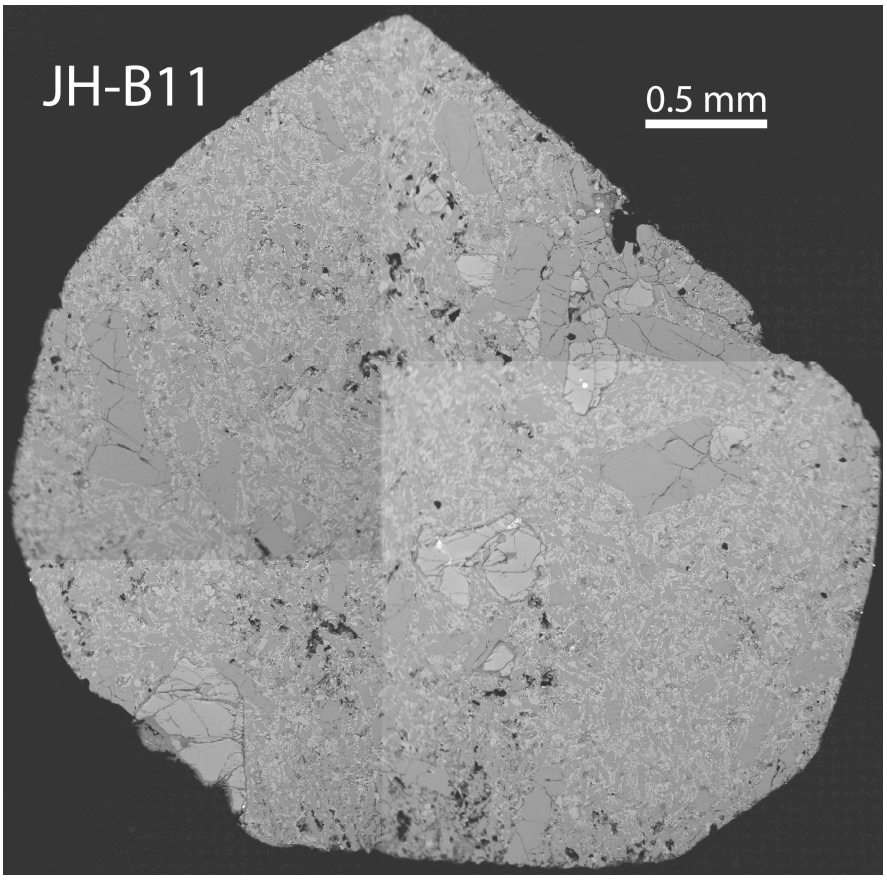
JH-B11
0.5 mm

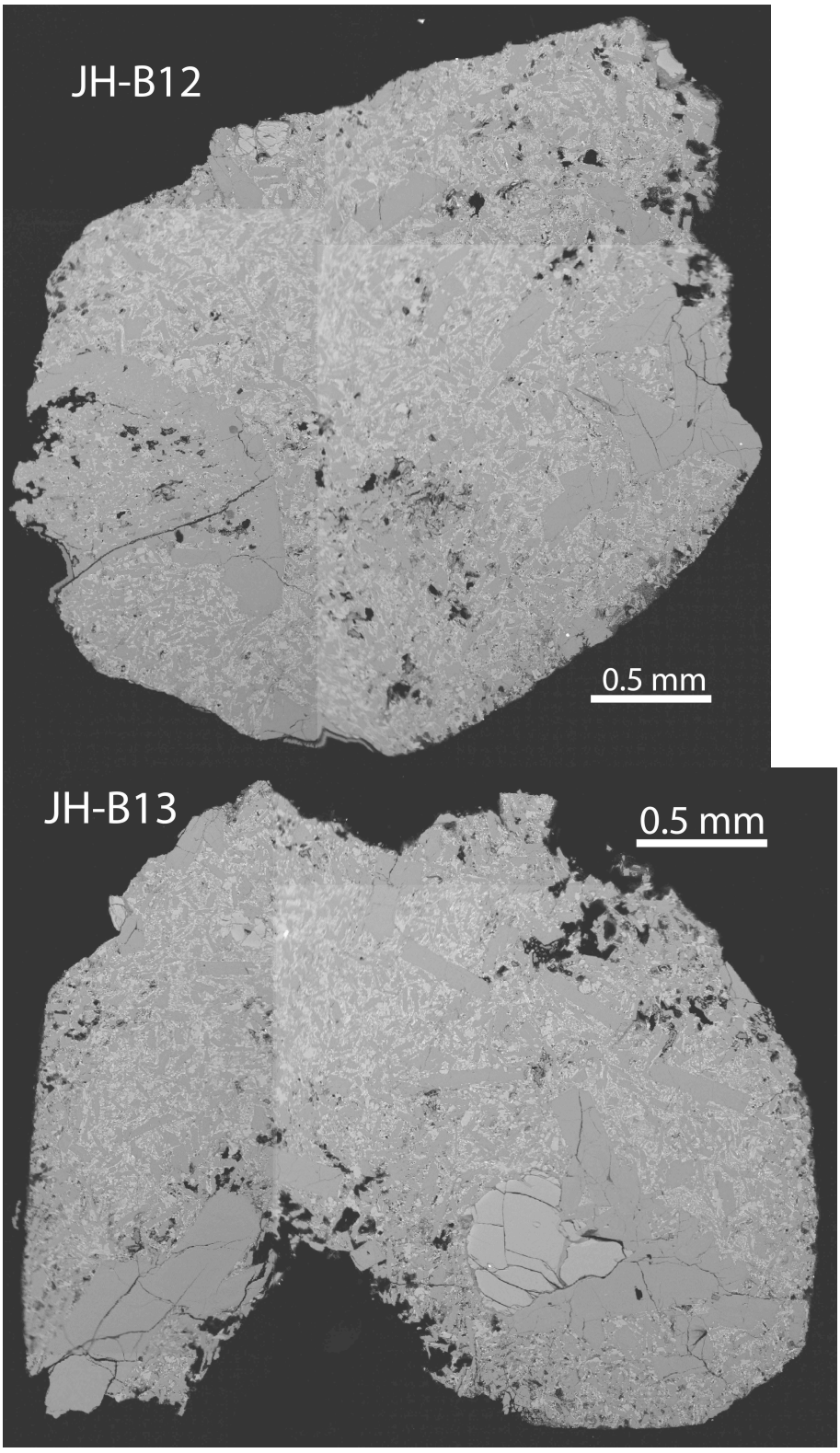
JH-B12
0.5 mm
JH-B13
0.5 mm

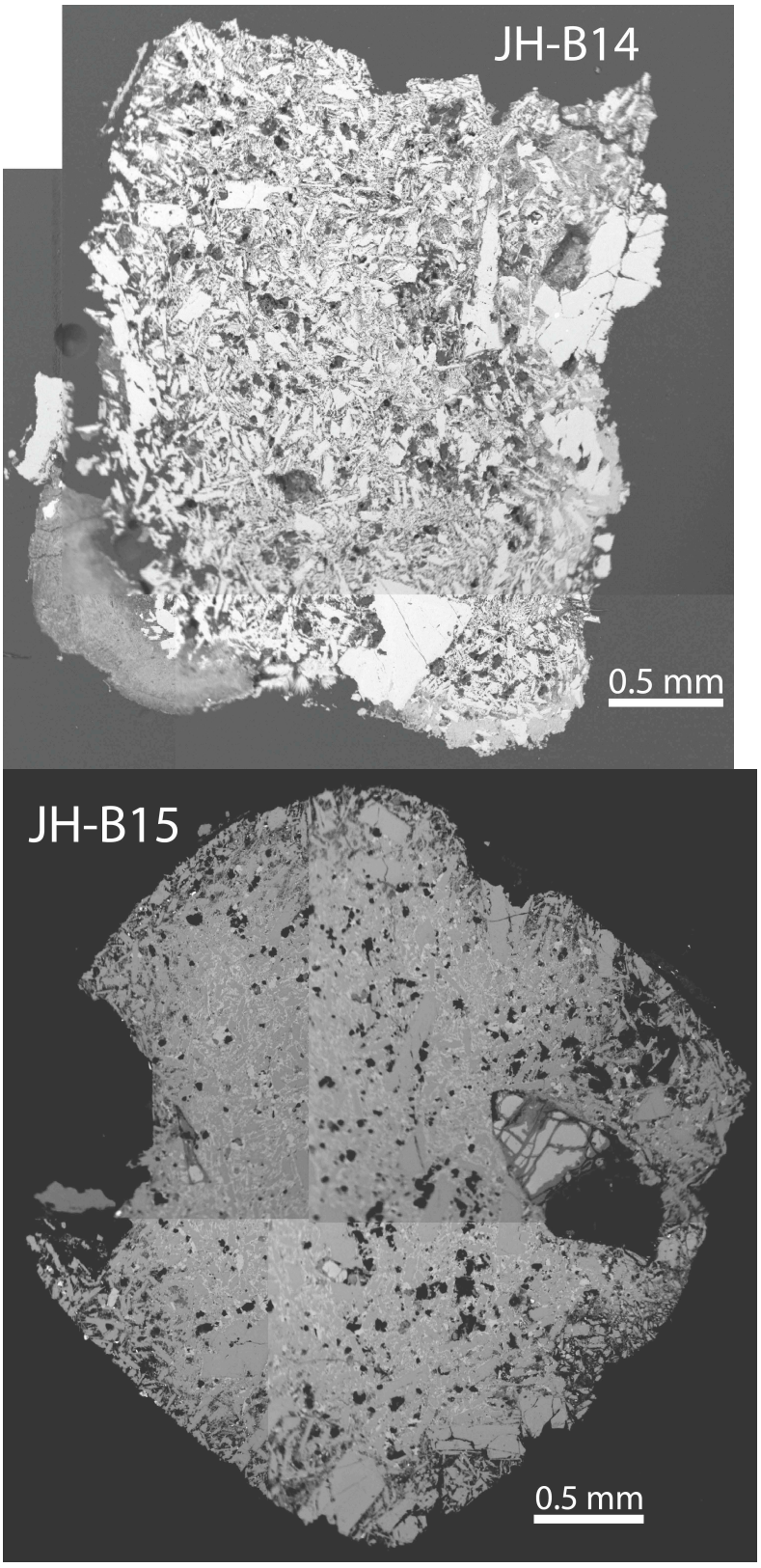
JH-B14
0.5 mm
JH-B15
0.5 mm

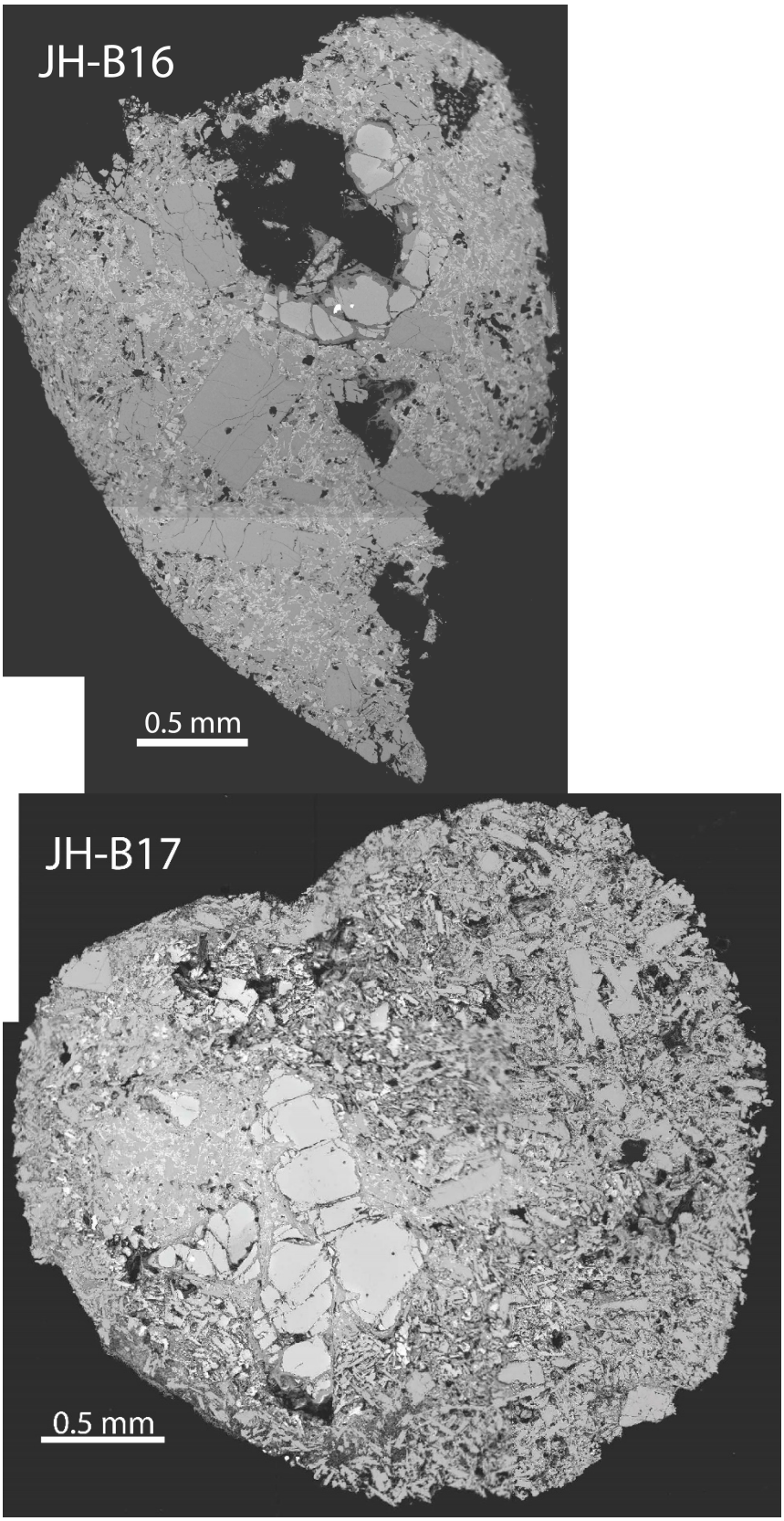
JH-B16
0.5 mm
JH-B17
0.5 mm

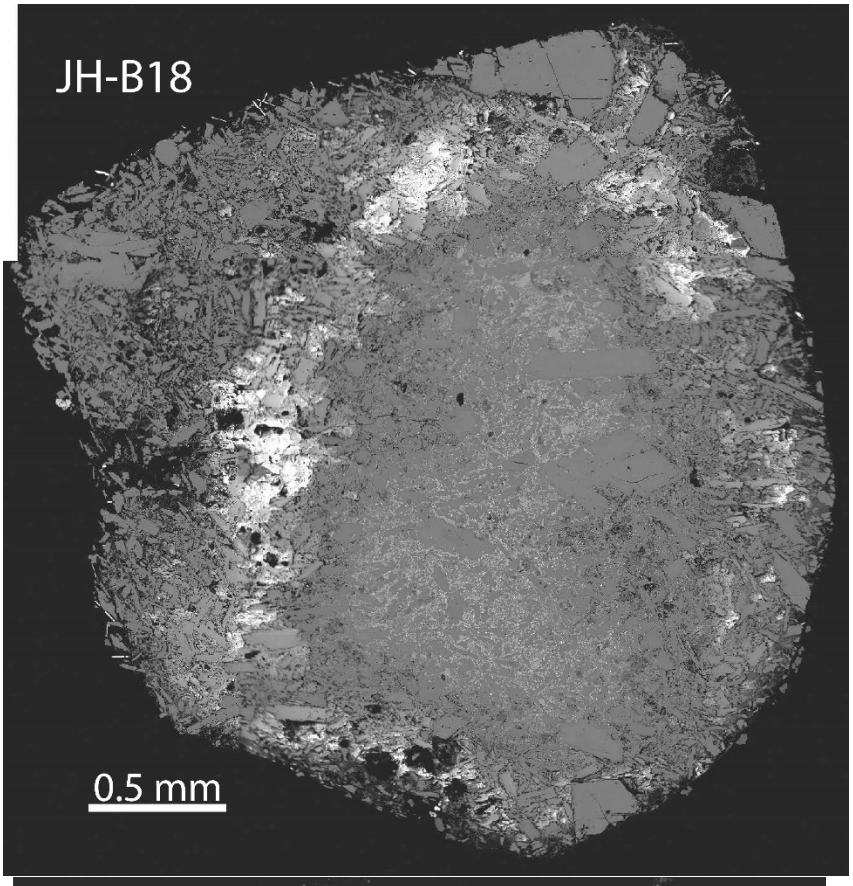
JH-B18
0.5 mm

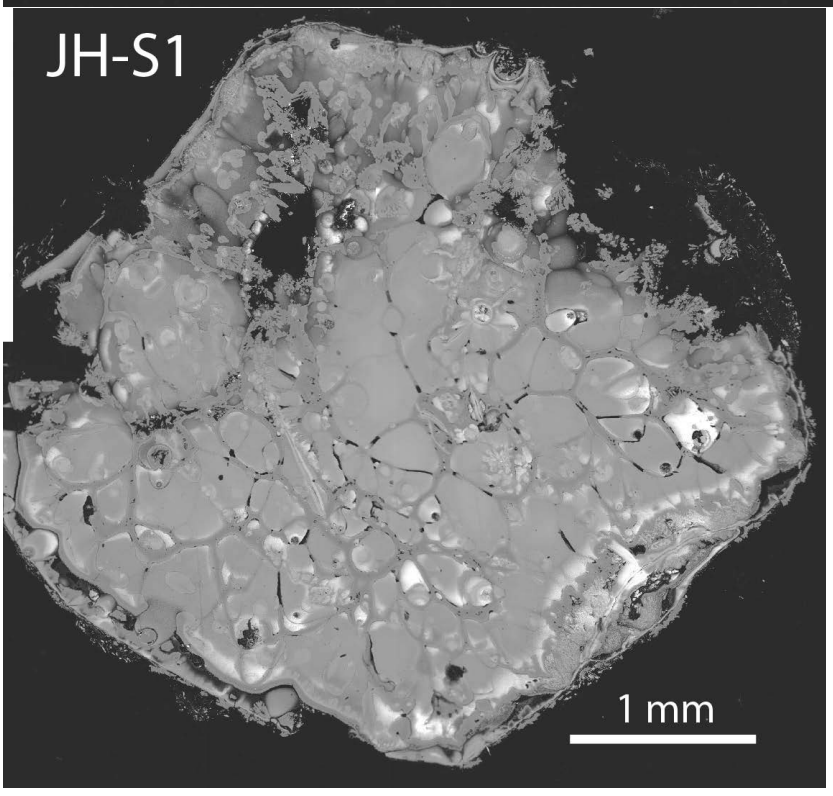
JH-S1
1 mm

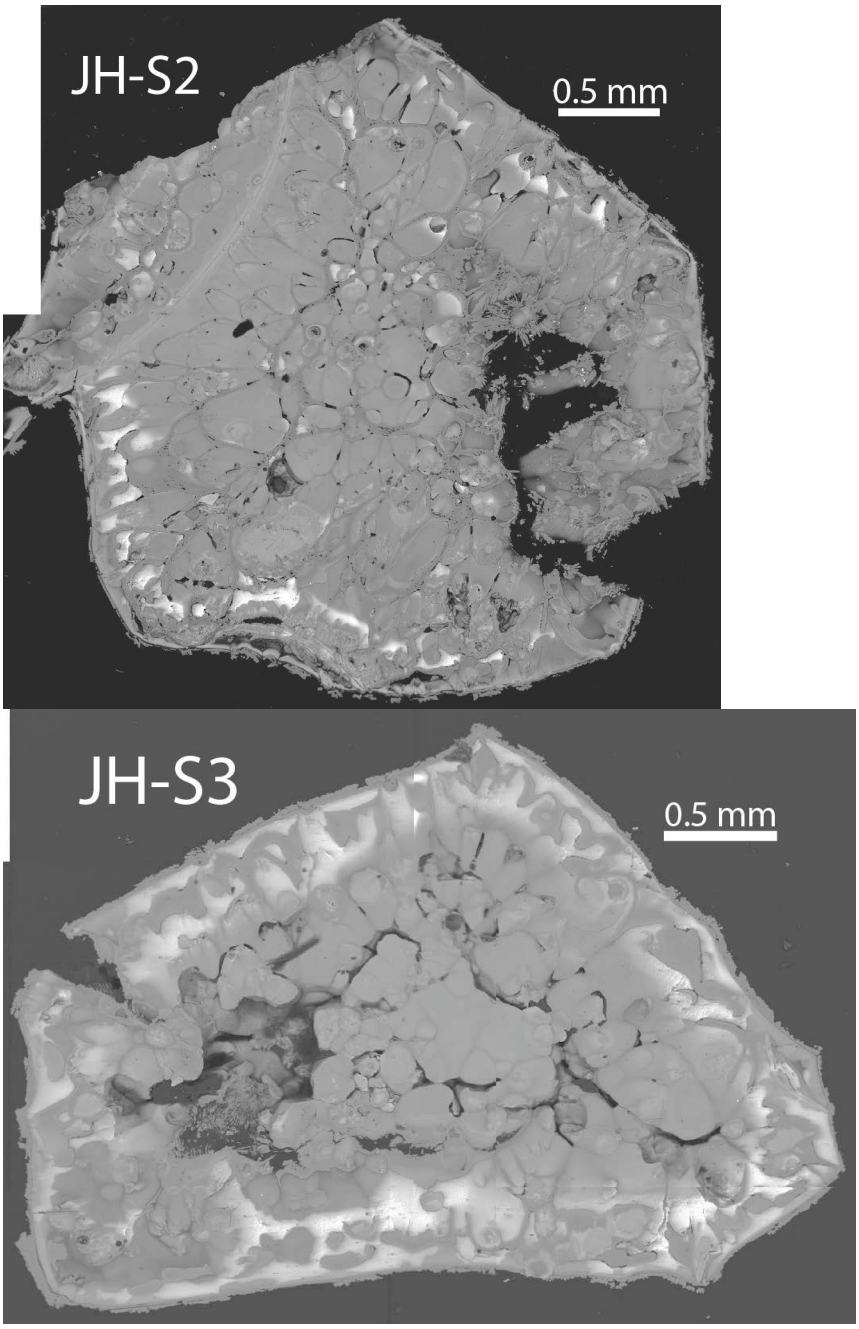
JH-S2
0.5 mm
JH-S3
0.5 mm

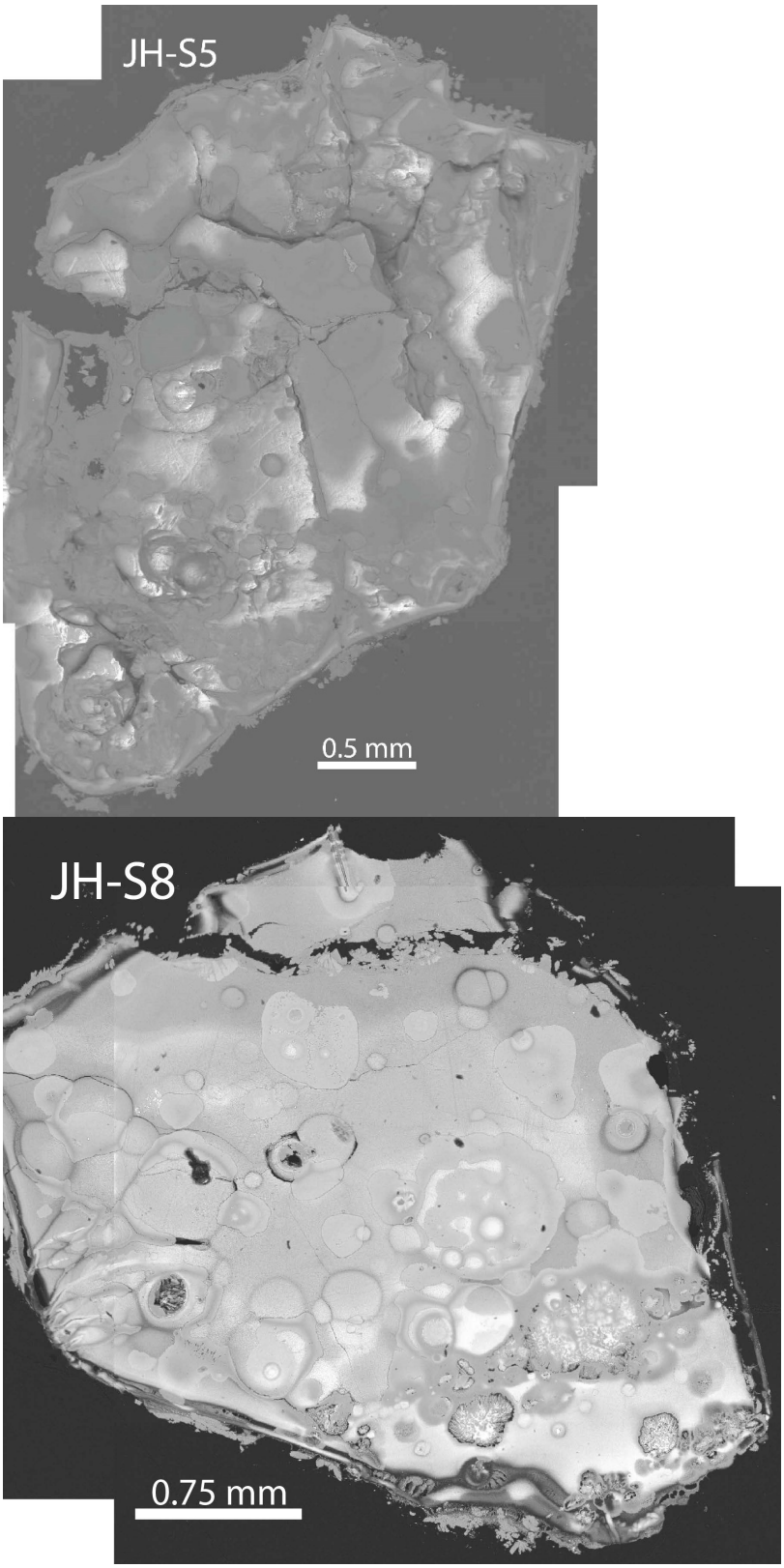
JH-S5
0.5 mm
JH-S8
0.75 mm

7. References

Arévalo, R., and McDonough, W.F., 2008, Tungsten geochemistry and implications for understanding the Earth's interior: Earth and Planetary Science Letters, v. 272, p. 656-665.

Barker, D.S., 1983, Igneous Rocks: Englewood Cliffs, Prentice-Hall, p. 114.

Barnes, H.L., 2015, Hydrothermal Processes: Geochemical Perspectives, v. 4, 93 p.

Barrett, T.J., MacLean, W.H., Cattalani, S., and Hoy, L., 1993, Massive sulfide deposits of the Noranda area, Quebec. V. The Corbet Mine: Canadian Journal of Earth Sciences, v. 30, p. 1934-1954.

Beaty, D.W., and Taylor, H.P., 1982, Some petrologic and oxygen isotopic relationships in the Amulet Mine, Noranda, Quebec, and their bearing on the origin of Archean massive sulfide deposits: Economic Geology, v. 77, p. 95-108.

Beaudoin, G., Mercier-Langevin, P., Dubé, B., and Taylor, B.E., 2014, Low-temperature alteration at the world-class LaRonde Penna Archean Au-rich volcanogenic massive sulfide deposit, Abitibi Subprovince, Quebec, Canada: Evidence from whole-rock oxygen isotopes: Economic Geology, v. 109, p. 167-182.

Berger, G., Schott, J., and Loubet, M., 1987, Fundamental processes controlling the first stage of alteration of a basalt glass by seawater: an experimental study between 200° and 320°C: Earth and Planetary Science Letters, v. 84, p. 431-445.

Berger, B.R, Tingley, J.V., and Drew, L.J., 2003, Structural localization and origin of compartmentalized fluid flow, Comstock Lode, Virginia City, Nevada: Economic Geology, v. 98, p. 387-408.

Bischoff, J.L., and Dickson, F.W., 1975, Seawater-basalt interaction at 200°C and 500 bars: implications for the origin of sea-floor heavy-metal deposits and regulation of seawater chemistry: Earth and Planetary Science Letters, v. 25, p. 385-397.

Clayton, R.N., O'Neil, J.R., and Mayeda, T.K., 1972, Oxygen isotope exchange between quartz and water: Journal of Geophysical Research, v. 77, p. 3057-3067.

Cook, N.J., Ciobanu, C.L., Pring, A., Skinner, W., Danyushevsky, L., Shimizu, M., Saini-Eidukat, B., and Melcher, F., 2009, Trace and minor elements in sphalerite: a LA-ICP-MS study: Geochimica et Cosmochimica Acta, v. 73, p. 4761-4791.

Cook, N.J., Sundblad, K., Valkama, M., Nygård, R., Ciobanu, C.L., and Danyushevsky, L., 2011, Indium mineralization in A-type granites in southeastern Finland: Insights into mineralogy and partitioning between coexisting minerals: Chemical Geology, v. 284, p. 62-73.

Eichelberger, J.C., Vogel, T.A., Younker, L.W., Miller, C.D., Heiken, G.H., and Wohletz, K.H., 1988, Structure and stratigraphy beneath a young phreatic vent: South Inyo Crater, Long Valley Caldera, California: Journal of Geophysical Research, v. 93, p. 13,208-13,220.

Emsbo, P., Hofstra, A.H., Lauha, E.A., Griffin, G.L., and Hutchinson, R.W., 2003, Origin of high-grade gold ore, source of ore fluid components, and genesis of the Meikle and neighboring Carlin-type deposits, northern Carlin trend, Nevada: Economic Geology, v. 98, p. 1069-1105.

Faure, K., Matsuhisa, Y, Metsugi, H., Mizota, C., and Hayashi, S., 2002, The Hishikari Au-Ag epithermal deposit, Japan: Oxygen and hydrogen isotope evidence in

determining the source of paleohydrothermal fluids: Economic Geology, v. 97, p. 481-498.

Fisher, R.V., and Schmincke, H.-U., 1984, Pyroclastic Rocks: Berlin, Springer Berlin Heidelberg, 472 p.

Fernández-Nieto, C., Torres-Ruiz, J., Subías Pérez, I., Fanlo González, I., and González López, J.M., 2003, Genesis of Mg-Fe carbonates from the Sierra Menera magnesite-siderite deposits, northeast Spain: Evidence from fluid inclusions, trace elements, rare earth elements, and stable isotope data: Economic Geology, v. 98, p. 1413-1426.

Gion, A.M., Piccoli, P.M., Candela, P.A., and Nance, J.R., 2016, Indium in ferromagnesian minerals: An experimental study: Geological Society of America Abstracts with Programs, v. 48, no. 7.

Green, G.R., Ohmoto, H., Date, J., and Takahashi, T., 1983, Whole-rock oxygen isotope distribution in the Fukazawa-Kosaka area, Hokuroku district, Japan, and its potential application to mineral exploration: Economic Geology, Monograph 5, p. 395-411.

Green, G.R., and Taheri, J., 1992, Stable isotopes and geochemistry as exploration indicators: Geological Survey Bulletin 70, p. 84-91.

Hajash, A., 1975, Hydrothermal processes along mid-ocean ridges: An experimental investigation, *in* Rona, P.A., and Lowell, R.P., eds., 1980, Seafloor Spreading Centers: Hydrothermal Systems: Benchmark Papers in Geology, v. 56, p. 44-65.

Heaton, T.H.E., and Sheppard, S.M.F., 1976, Hydrogen and oxygen isotope evidence for sea-water-hydrothermal alteration and ore deposition, Troodos complex, Cyprus,

in Proceedings, Volcanic Processes in Ore Genesis, London, England: joint meeting of the Volcanic Studies Group of the Geological Society of London and the Institution of Mining and Metallurgy, p. 42-57.

Hemley, J.J., and Hunt, J.P., 1992, Hydrothermal ore-forming processes in the light of studies in rock-buffered systems: II. Some general geologic applications: Economic Geology, v. 87, p. 23-43.

Hertogen, J., Janssens, M.-J., and Palme, H., 1980, Trace elements in ocean ridge basalt glasses: implications for fractionations during mantle evolution and petrogenesis: Geochimica et Cosmochimica Acta, v. 44, p. 2,125-2,143.

Hoy, L.D., 1993, Regional evolution of hydrothermal fluids in the Noranda District, Quebec: Evidence from $\delta^{18}O$ values from volcanogenic massive sulfide deposits: Economic geology v. 88, p. 1526-1541.

Humphris, S.E., and Thompson, G., 1978a, Hydrothermal alteration of oceanic basalts by seawater: Geochimica et Cosmochimica Acta, v. 42, p. 107-125.

Humphris, S.E., and Thompson, G., 1978b, Trace element mobility during hydrothermal alteration of oceanic basalts: Geochimica et Cosmochimica Acta, v. 42, p. 127-136.

Huston, D.L., Taylor, B.E., Bleeker, W., Stewart, B., Cook, R., and Koopman, E.R., 1995, Isotope mapping around the Kidd Creek deposit, Ontario: Application to exploration and comparison with other geochemical indicators: Exploration and Mining Geology v. 4, p. 175-185.

Huston, D.L. and Taylor, B.E., 1999, Genetic significance of oxygen and hydrogen isotope variations at the Kidd Creek volcanic-hosted massive sulfide deposit, Ontario, Canada: Economic Geology, Monograph 10, p. 335-350.

James, R.H., Allen, D.E., and Seyfried, W.E., 2003, An experimental study of alteration of oceanic crust and terrigenous sediments at moderate temperatures (51 to 350°C): Insights as to chemical processes in near-shore ridge-flank hydrothermal systems: Geochmica et Cosmochimica Acta, v. 67, p. 681-691.

JEOL, 2001, XM-17330/27330 Basic Software/ Quantitative Analysis Program, Japan, JEOL, 101 p.

John, D.A., Hofstra, A.H., Fleck, R.J., Brummer, J.E., and Saderholm, E.C., 2003, Geologic setting and genesis of the Mule Canyon low-sulfidation epithermal gold-silver deposit, north-central Nevada: Economic Geology, v. 98, 425-463.

Johnson, J.W., Oelkers, E.H., Helgeson, H.C., 1992, SUPCRT92: A software package for calculating the standard molal thermodynamic properties of minerals, gases, aqueous species, and reactions from 1 to 5000 bar and 0 to 1000°C: Computers and Geosciences, v. 18, p. 899-947.

Kelly, T.D., and Matos, G.R., comps., 2014, Historical statistics for mineral and material commodities in the United States (2016 version): U.S. Geological Survey Data Series 140, accessed [Feb., 2017], at https://minerals.usgs.gov/minerals/pubs/historical-statistics/.

Kondziela, P., and Biernat, J., 1975, Determination of stability constants of indium halogenide complexes by polarography: Electroanalytical Chemistry and Interfacial Electrochemistry, v. 61, p. 281-288.

Kreiner, D.C., and Barton, M.D., 2017, Sulfur-poor intense acid hydrothermal alteration: A distinctive hydrothermal environment: Ore Geology Reviews, v. 88, p. 174-187.

MacLean, W.H., and Hoy, L.D., 1991, Geochemistry of hydrothermally altered rocks at the Horne Mine, Noranda, Quebec: Economic Geology, v. 86, p. 506-528.

MacLean, W.H., and Kranidiotis, P., 1987, Immobile elements as monitors of mass transfer in hydrothermal alteration: Phelps Dodge massive sulfide deposit, Matagami, Quebec: Economic Geology, v. 82, p. 951-962.

McCanta, M.C., Dyar, M.D., and Dobosh, P.A., 2017, Extracting bulk rock properties from microscale measurements: Subsampling and analytical guidelines: GSA Today, v. 27, p. 4-9.

McDonough, W.F., and Sun, S., 1995, The composition of the Earth: Chemical Geology, v. 120, p. 223-253.

Miller, J.A., and Cartwright, I., 2006, Albite vein formation during exhumation of high-pressure terranes: a case study from alpine Corsica: Journal of Metamorphic Geology, v. 24, p. 409-428.

Miller, C., Halley, S., Green, G., and Jones, M., 2001, Discovery of the West 45 volcanic-hosted massive sulfide deposit using oxygen isotopes and REE geochemistry: Economic Geology, v. 96, p. 1227-1237.

Mottl, M.J., 1983, Metabasalts, axial hot springs, and the structure of hydrothermal systems at mid-ocean ridges: Geological Society of America Bulletin, v. 94, p. 161-180.

Mottl, M.J., and Holland, H.D., 1978, Chemical exchange during hydrothermal alteration of basalt by seawater–I. Experimental results for major and minor components of seawater: Geochimica et Cosmochimica Acta, v. 42, p. 1,103-1,115.

Mottl, M.J., Holland, H.D., and Corr, R.F., 1979, Chemical exchange during hydrothermal alteration of basalt by seawater–II. Experimental results for Fe, Mn, and sulfur species: Geochimica et Cosmochimica Acta, v. 43, p. 869-884.

Mottl, M.J., and Seyfried, W.E., 1980, Sub-seafloor hydrothermal systems: Rock- vs. seawater dominated, *in* Rona, P.A., and Lowell, R.P., eds., 1980, Seafloor Spreading Centers: Hydrothermal Systems: Benchmark Papers in Geology, v. 56, p. 66-82.

Nakamura, K., Kato, Y., Tamaki, K., and Ishii, T., 2007, Geochemistry of hydrothermally altered basaltic rocks from the Southwest Indian Ridge near the Rodriguez Triple Junction: Marine Geology, v. 239, p. 125-141.

Ohmoto, H., and Rye, R.O., 1974, Hydrogen and oxygen isotopic compositions of fluid inclusions in the Kuroko deposits, Japan: Economic Geology, v. 69, p. 947-953.

O'Neil, J.R. and Taylor, H.P., 1967, The oxygen isotope and cation exchange chemistry of feldspars: The American Mineralogist, v. 52, p. 1414-1437.

O'Neil, J.R., and Taylor, H.P., 1969, Oxygen isotope equilibrium between muscovite and water: Journal of Geophysical Research, v. 74, p. 6012-6022.

Paradis, S., 2015, Indium, germanium and gallium in volcanic- and sediment-hosted base-metal sulphide deposits: Symposium on critical and strategic materials, British Columbia Geological Survey Paper 2015-3, p. 23-29.

Pearson, R.G., 1963, Hard and soft acids and bases: Journal of the American Chemical Society, v. 85, p. 3533–3539.

Reed, M.H., 1983, Seawater-basalt reaction and the origin of greenstones and related ore deposits: Economic Geology, v. 78, p. 466-485.

Rockwell, B.W., 2000, The Goldfield mining district, Nevada: an acid-sulfate bonanza gold deposit, *in* Sabins, F.F., ed., Guidebook for field trip to the Basin and Range, Fourteenth International Conference for Applied Geologic Remote Sensing: Las Vegas Nevada, USA, November 6-8, 2000.

Rudnick, R., and Gao, S., 2003, Composition of the continental crust: Treatise on Geochemistry, p. 1–64.

Saunders, F.T, 1984, Summary report of the exploration potential of Tenneco minerals holdings in the Tonopah mining district Nye-Esmeralda counties, Nevada unpublished report, 11 p.

Schardt, C., Large, R., and Yang, J., 2006, Controls on heat flow, fluid migration, and massive sulfide formation of an off-axis hydrothermal system—the Lau Basin perspective: American Journal of Science, v. 306, p. 103-134.

Schufle, J.A., Stubbs, M.F., and Witman, R.E., 1951, A study of indium(III) chloride complexes by polarographic methods: Journal of the American Chemical Society, v. 73, p. 1013-1015.

Schwarz-Schampera, U., and Herzig, P.M., 1997, Geochemistry of indium in VMS deposits: Implications from active hydrothermal vents in the Southern Lau Basin (SW-Pacific), *in* Proceedings, Fourth Biennial Society for Geology Applied to Mineral Deposits Meeting: Turku, Finland, p. 379-382.

Seewald, J.S., and Seyfried, W.E., 1990, The effect of temperature on metal mobility in subseafloor hydrothermal systems: constraints from basalt alteration experiments: Earth and Planetary Science Letters, v. 101, p. 388-403.

Seward, T.M., Henderson, C.M.B, and Charnock, J.M., 2000, Indium(III) chloride complexing and solvation in hydrothermal solutions to 350°C: an EXAFS study: Chemical Geology, v. 167, p. 117-127.

Seyfried, W.E., and Bischoff, J.L., 1977, Hydrothermal transport of heavy metals by seawater: the role of seawater/basalt ratio: Earth and Planetary Science Letters, v. 34, p. 71-77.

Seyfried, W.E., and Janecky, D.R., 1985, Heavy metal and sulfur transport during subcritical and supercritical hydrothermal alteration of basalt: Influence of fluid pressure and basalt composition and crystallinity: Geochmica et Cosmochimica Acta, v. 49, p. 2,545-2,560.

Seyfried, W.E., Mottl, M.J., and Bischoff, J.L., 1978, Seawater/basalt ratio effects on the chemistry and mineralogy of spilites from the ocean floor: Nature, v. 275, p. 211-213.

Seyfried, W.E., and Mottl, M.J., 1982, Hydrothermal alteration of basalt by seawater under seawater-dominated conditions: Geochimica et Cosmochimica Acta, v. 46, p. 985-1,002.

Shannon, R.D., 1976, Revised ionic radii and systematic studies of interatomic distances in halides and chalcogenides: Acta Crystallographica, A32, p. 751-767.

Shaw, D.M., 1952, The geochemistry of indium: Geochimica et Cosmochimica Acta, v. 2, p. 185-206.

Shikazono, N., Utada, M., and Shimizu, M., 1995, Mineralogical and geochemical characteristics of hydrothermal alteration of basalt in the Kuroko mine area, Japan: implications for the evolution of a Back Arc Basin hydrothermal system: Applied Geochemistry, v. 10, p. 621-642.

Silberglitt, R., Bartis, J.T., Chow, B.G., An, D.L., and Brady, K., 2013, Critical Materials: Present Danger to U.S. Manufacturing: National Defense Research Institute, 46 p.

Simon, L., Lécuyer, C., and Putelat, T., 2017, The calculation of water-rock ratios using trace element (Li, B) stable isotopes: Annales Universitatis Mariae Curie-Sklodowska, section AAA-Physica 71, p. 79-89.

Staudigel, H., and Hart, S.R., 1982, Alteration of basaltic glass: Mechanisms and significance for the oceanic crust-seawater budget: Geochimica et Cosmochimica Acta, v. 47, p. 337-350.

Taylor, H.P., 1968, The oxygen isotope geochemistry of igneous rocks: Contributions to Mineralogy and Petrology, v. 19, 71 p.

Taylor, H.P., 1978, Oxygen and hydrogen isotope studies of plutonic granitic studies: Earth and Planetary Science Letters, v. 38, p. 177-210.

U.S. Department of Energy, 2011, Critical Materials Strategy, 190 p.

Vogel, T.A., Woodburne, T.B., Eichelberger, J.C., and Layer, P.W., 1994, Chemical evolution and periodic eruption of mafic lava flows in the west moat of Long Valley Caldera, California: Journal of Geophysical Research, v. 99, p. 19,829-19,842.

Von Damm, K.L., J.L. Bischoff, and Rosenbauer, R.J., 1991, Quartz solubility in hydrothermal seawater: An experimental study and equation describing quartz solubility for up to 0.5 M NaCl solutions: American Journal of Science, v. 291, p. 977-1007.

Wager, L.R., Smit, J. van R., and Irving, H., 1958, Indium content of rocks and minerals from the Skaergaard intrusion, East Greenland: Geochimica et Cosmochimica Acta, v. 13, p. 81-86.

Wenner, D.B., and Taylor, H.P., 1971, Temperatures of serpentinization of ultramafic rocks based on O^{18}/O^{16} fractionation between coexisting serpentine and magnetite: Contributions to Mineralogy and Petrology, v. 32, p. 165-185.

Werner, T.T., Mudd, G.M., and Jowitt, S.M., 2017, The world's by-product and critical metal resources part III: A global assessment of indium: Ore Geology Reviews, v. 86, p. 939-958.

Wilkinson, J.F.G., 1986, Classification and average chemical compositions of common basalts and andesites: Journal of Petrology, v. 27, p. 31-62.

Wolery, T.J., 1978, Some chemical aspects of hydrothermal processes at mid-oceanic ridges—A theoretical study [Ph.D. thesis]: Evanston, Illinois, Northwestern University, 263 p.

Wood, S.A., and Samson, I.M., 1998, Solubility of ore minerals and complexation of ore metals in hydrothermal solutions, *in* Richards, J.P., and Larson, P.B., eds., Techniques in hydrothermal ore deposits geology, Reviews in Economic Geology, Volume 10: Society of Economic Geologists, p. 33-81.

Wood, S.A., and Samson, I.M., 2006, The aqueous geochemistry of gallium, germanium, indium and scandium: Ore Geology Reviews, v. 28, p. 57-102.

Yi, W., Halliday, A.N., Alt, J.C., Lee, D., Rehämper, M., Garcia, M.O., Langmuir, C.H., and Su, Y., 2000, Cadmium, indium, tin, tellurium, and sulfur in oceanic basalts: Implications for chalcophile element fractionation in the Earth: Journal of Geophysical Research, v. 105, p. 18,927-18,948.

Zeng, Z.G., Qi, H.Y., Chen, S., Yin, X., and Li, Z., 2014, Hydrothermal alteration of plagioclase microphenocrysts and glass in basalts from the East Pacific Rise near 13°N: An SEM-EDS study: Science China: Earth Sciences v. 57, p. 1,427-1,437.

Zhang, X., and Spry, P.G., 1994, Petrological, mineralogical, fluid inclusion, and stable isotope studies of the Gies gold-silver telluride deposit, Judith Mountains, Montana: Economic Geology, v. 89, p. 602-627.